University of Benghazi
Faculty of Science
Department of Earth Sciences

Mineralogy and Geochemistry of the Sabkha Sediments Along the Mediterranean Coast from Surman to Ras Jdeir, Jifarah Plain, NW Libya

A thesis
Submitted to Department of Earth Sciences
University of Benghazi in Partial Fulfillment of the
Requirements for the Degree of Master of Science in Geology

By
Mohamed Mahmud Musa
B.Sc. Geology 2009

Supervised by
Assist. Prof. Osama Shaltami

Academic Year (2016)

Content

2. Mineralogy and Petrography

3. Geochemistry

4. Summary and Conclusions

Acknowledgments

I would like to express my sincere gratitude to my supervisor Dr. Osama Shaltami, for his help and advice in the preparation of this thesis**.**

Special thanks must go to all staff members of the Department of the Earth Sciences for their help during the academic years of my study at this department .

Also, thanks to the Nuclear Materials Authority and the Central Laboratories of the Geological Survey of Egypt in Cairo.

ABSTRACT

The present work attempts to characterize the mineralogy and geochemistry of the sabkha brines and sediments along the Mediterranean Coast from Surman to Ras Jdeir, Jifarah Plain, NW Libya. the shuttle radar topography mission (SRTM) data were principally used in topographic analysis of the study area, to delineate the slope area, complete drainage network, watershed and cross section profile to identify morphology in the Jifarah Plain digitizing by computers programs by Arc GIS, Remote sensing data uses by landsat 8 operational land imager (OLI) is the new product from NASA under Landsat open source series which has been launched in February 2013, uses for interpretation of surface features and produce new geology mapping (determined location of all sabkha) in the study area.

The studied sabkha sediments are composed essentially of gypsum, halite, calcareous sands, soil and algal limestone. The mineral composition for the studied sabkha sediments is chiefly composed of variable proportions of calcite, aragonite, quartz, microcline, orthoclase, gypsum and halite, clay minerals and heavy minerals such as ilmenite, magnetite, hematite, goethite, zircon, augite, tourmaline, rutile, biotite, garnet, monazite, hornblende, staurolite and pistachite. The Cl^-/Na^+ ratios in the studied waters range from 1.66 to 1.85, all slightly higher than the average seawater value (Cl^-/Na^+=1.17), suggesting that the studied brines may have not only marine but also terrigenic and anthropogenic origins.

The studied brine water samples show high concentration of K^+. This may be attributed to partial dissolution of detrital illite which constitutes part of the clay mineral assemblages of the studied sabkha. In the studied sediments, the major oxides CaO and MgO are the main constituents of the carbonate minerals. SiO_2 is mainly in the form of quartz. Sometimes a high quotient of SiO_2 together with the oxides Al_2O_3, K_2O and partly of Na_2O, TiO_2 and Fe_2O_3 are essentially allocated within the structure of the feldspars and clay minerals. Part of Na_2O and the content of Cl belong mainly to halite. Part of Fe_2O_3 and TiO_2 may be accommodated as iron oxyhydroxides. Part of CaO and the content of SO_3 are allotted within the gypsum structure. Ba, Sr, Pb and Cd are basically controlled by the carbonate fraction, while Br, Ni, Co, Cu, Zn, V and Cr are strongly correlated with Na_2O and Cl. The studied sabkha sediments show

low Cu/Zn, V/Cr, V/Ni and Ni/Co and U/Th ratios which suggest that these sediments were deposited in a well oxygenated environment.

List of Figures

List of Tables

Table No. **Page**

CHAPTER ONE
INTRODUCTION

Northwestern Libya is marked by three main geomorphic units, which include Jifarah plain, scarp and plateau. The Jifarah plain is a roughly triangular region bounded to the north by the Mediterranean Sea and to the south by a prominent escarpment of the Jabal Nafusah. From the east the escarpment drops to meet the coast near Al Khums. The plain widens westward until Libyan-Tunisian borders, for about 20.000 km^2. It is covered by Pleistocene and Holocene deposits. The the Jabal, as known by the native, is one of the common morphological features of northwestern Libya. It runs approximately in an east-west direction, from Al Khums and westwards to beyond the Libyan border. In places, the scarp was given different local names as Jabal Tarhuna (Tarhuna-Gharyan strip), that followed westwards by Jabal Gharyan (Gharyan-Yafrin strip) and Jabal Nafusah (Yafrin and Nalut strip). The name of Jabal Nafusah is more popular and was frequently applied for all scarps. Jabal Nafusah overlooks the Jifarah plain and has elevation that ranges from 400 to more than 700 m, especially in Gharyan-Yafrin area. The scarp is capped by hard and resistant dolomitic limestone of Upper Cretaceous age, where its slopes are made of Triassic and Jurassic clastic and nonclastic rocks. The plateau is made of hard and resistant limestone, which belongs to the Cretaceous. It is characterized by gentle dip angles and the elevation ranges from 500-800 m; the low laying areas of the plateau are mainly covered by relative thick sequence of reddish brown Quaternary silts of terra-rossa type, which are mostly cultivated by olives, almond and other vegetations. In the areas to the southeast of Gharyan, the plateau is covered by volcanic sheets forming flat and broad plains. The northern part of the plateau is highly undulated and is dissected by deep wadies. Conspicuous black phonolitic hills are noticed on the plateau, they have an average elevation ranging from 500-800 m. The plateau is poorly inhabited and relative small towns are present (e.g., Tarhuna, Gharyan, Mizda, Yafrin, Giado and Nalut).

The present work attempts to characterize the mineralogy and geochemistry of the sabkha brines and sediments along the Mediterranean Coast from Surman to Ras Jdeir, Jifarah plain, NW Libya (Figure 1.1).

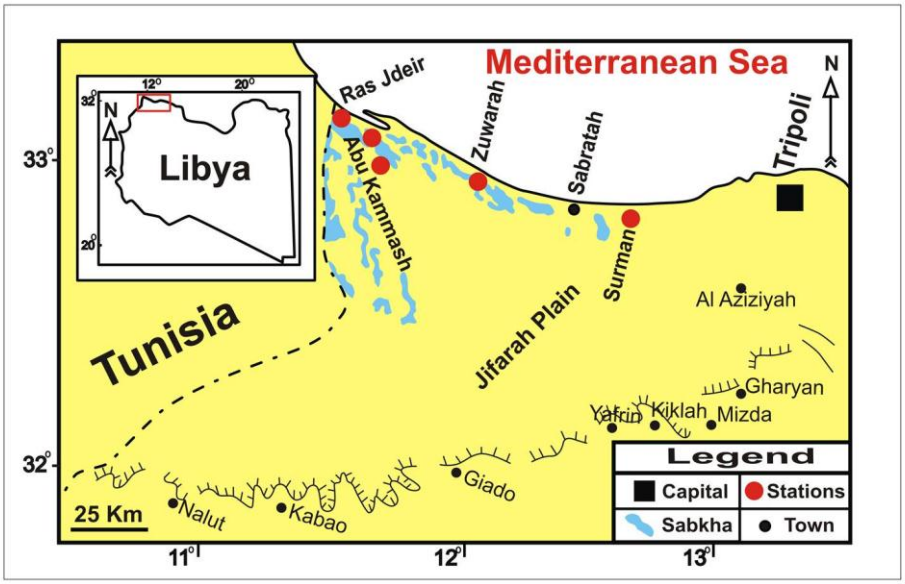

Fig. 1.1: Location map showing the study area and location of the sampled stations.

1.1. General geology and geomorphology of the study area

1.1.1. Regional Geology

The generally flat and fertile though somewhat undulating coastal plain, known as the Jifarah Plain, rises towards the south into an impressive escarpment forming hill range known as Jabal Nafusah. The trend of the Jabal is proximately ENE-WSW extending from near Misratah in the east where it is closer to the Mediterranean coast to Nalut and beyond the international border into Tunisia in the west

The central part of the Jabel is located approximately 70 Km south of Tripoli. The escarpment is irregularly distributed in its east-west extent due to dissection by wadies cut in the Mesozoic rocks. To the south of the escarpment lies the broad dissected plateau AI Hammadah al Hamra extending towards Mizdah and Ghadamis exposing mainly Upper Cretaceous rocks with some Paleocene cover.

1.1.1.1. Precambrian

Precambrian rocks under the Jifarah Arch are exposed in several scattered outcrops in the Jabal Fezzan area in the middle of the Gargaf arch. These rocks, covering considerably less than 100 sq km, are schists and biotite granites cut by rhyolite and pegmatite dikes. The granites are gray and develop an irregular

weathered surface. They are exposed only in the eroded areas in the wadi beds..

1.1.1.2. Paleozoic

The Paleozoic rocks, as reported from exploration wells in the area, represent sequences of epi-continental environments alternating with shallow marine and continental deposits.

The Cambro-Ordovician rocks include non-fossiliferous burrowed quartzitic sandstones and quartzites which directly overlie the crystalline basement. The sandstones may contain *Tigillites.*

The Lower Silurian is represented by a transgressive sequence of the Tanezzuft graptolitic silty shales. These shales are widespread in other basins and form the source beds for most Paleozoic basins. However, the Upper Silurian Acacus Sandstone is missing on the crest of the arch but is found in Ghadames Basin up to the margin of the arch.

The Devonian is also missing in the Jifarah Arch, which is due either to erosion or non-deposition on the Caledonian paleohigh.

The Carboniferous sediments are marked by a transgressive sequence from the north where shallow marine shales, sandstones, dolomites, and evaporates predominate. These beds on the Jifarah Arch cover unconformably the Cambro-Ordovician or Lower Silurian deposits. Most of the Carboniferous sediments were stripped from parts of the Jifarah Arch and from the Gharyan high during the Hercynian movement.

The Permian seas transgressed from the north where the Permian sedimentary thickness thins over the Jifarah Arch and thickens in the offshore basins. These beds directly overlie the Carboniferous over the Jifarah Arch but are missing in the subsurface of the Western Jabal. On the arch the Upper Permian facies of sandstones, shales and carbonates unconformably overlie the Lower Permian clastics. Since Permian time crustal thinning which accompanied the continental drift between Africa and Eurasia has resulted in active subsidence of the offshore basin along the margin of the African land mass. In this offshore basin Permian, Triassic, and Jurassic sediments thickened toward the north (Hammuda, 2000).

1.1.1.3. Mesozoic

During the Mesozoic Era, several hundred meters of sediments was deposited in shallow and deep troughs along the Mediterranean shores. The thickest exposed Mesozoic section is in the Jabal Nefusa escarpment of northwestern Libya. This escarpment exposes Triassic Jurassic and Lower and Upper Cretaceous rocks. A great diversity of sedimentary conditions prevailed in Libya and nearby areas during the Mesozoic Era marine conditions in the northern part produced widespread deposits of limestone, dolomite, marl with estuarine conditions locally caused the deposition of large amounts of gypsum and anhydrite.

The Triassic sediments consist of four formations from non-marine to shallow marine fine- to medium-grained sandstones with minor grey, green and shale. The sandstones contain dolomite dolomitic limestones with occasional marls, claystones and chert bands.

The Jurassic consists of five formations alternating shallow marine, transitional and continental facies gypsum and anhydrite with frequent interbeds of dolomitic limestone and claystone.

The late Jurassic sediments include Sandstone claystone with traces of salt and gypsum, dolomitic sandstones, siltstones and shales.

The Cretaceous consists mudstone, sandstone and conglomerate which were probably deposited in a braided-river system carrying high sediment loads (Hallet, 2002).

1.1.1.4. Cenozoic

The area became a stable platform from the Late Cretaceous to the Miocene. Down warping in the Miocene resulted in the deposition of Miocene sediments.

The Lower Cenozoic sediments include shale and mudstones and chalky limestones with occasional dolomitic limestone beds .

The Middle Cenozoic sediments include limestone containing coquinas and gypsum crystals with conglomerates and sandstones, overlain by gypsiferous marls and chalky limestone.

The Upper Cenozoic sediments include gypsiferous marls with marly limestone and calcareous clays (Hallet, 2002).

1.1.1.5. Pliocene and Quaternary

The volcanic rocks (Tertiary–Quaternary) consist of three types: phonolite and trachyte intrusions, basalt cones, and basalt flows interpreted the age of the basalt sheet as early Eocene to Pliocene (Saadi *et al.,* 2013).

Quaternary erosion surface developed on the northern flank of the regional dome of Jabal Nafusah and on Miocene marine sediments, which are deposited over a distance of about 30 km south of the present coastline, raised beaches, sand dunes and the quaternary alluvial sediments (El-Tantawi, 2005). The Holocene deposits include recent wadi deposits; these deposits consist of loose gravels and loams varying in thickness from 0.5 to 2 m. Beach sands are represented by a narrow strip at the coast and are made up of shell fragments with a small ratio of silica sands. Eolian deposits (sand dunes) are represented by sand dunes and sheets covering large areas in the Jifarah Plain (field dunes) as well as patches of the coastal strip (coastal dunes). The coastal dunes consist of shell fragments with small amounts of silica sands. It is worth mentioning that the eolian material composing both field dunes and coastal dunes contains a large amount of grains of gypsum. In some places, it is composed of nearly pure gypsum (98%) especially in the immediate vicinity of the sabkhas, with a silty gypsum filling. Fluvial–eolian deposits are found on the plateau surface in central Jifarah. They are made up of silt, clay and fine sands with occasional caliche bands (Al Farrah *et al.*, 2011).

Figure 1.2 shows that normal fault extending NW–SE with its downthrown toward west is separating the two shore types. Fault zones in which the component faults are arranged en echelon are one of the most characteristic features of the Jifarah plain. The zones follow two main trends, E-W and NW-SE. Individual faults are again arranged in echelon, trending either NNE-SSW or NNW-SSE. The Al Aziziyah Fault is one of the coastal faults zones which are mentioned by all previous workers dealing with Tripolitania area. It lies 30 to 40 km south of the present shore line. It crosses the Jifarah Plain for a distance of about 100 km extending from Al Aziziyah area to the Tunisian border (Allan, 1989) . Parallel to the Al Aziziyah fault, Allan (1989) maps reported the presence of another fault line extending from west of Bin Ghashir area to the Tunisian border. It lies 10 km to the south of the present shore line and its downthrown side is towards the north.

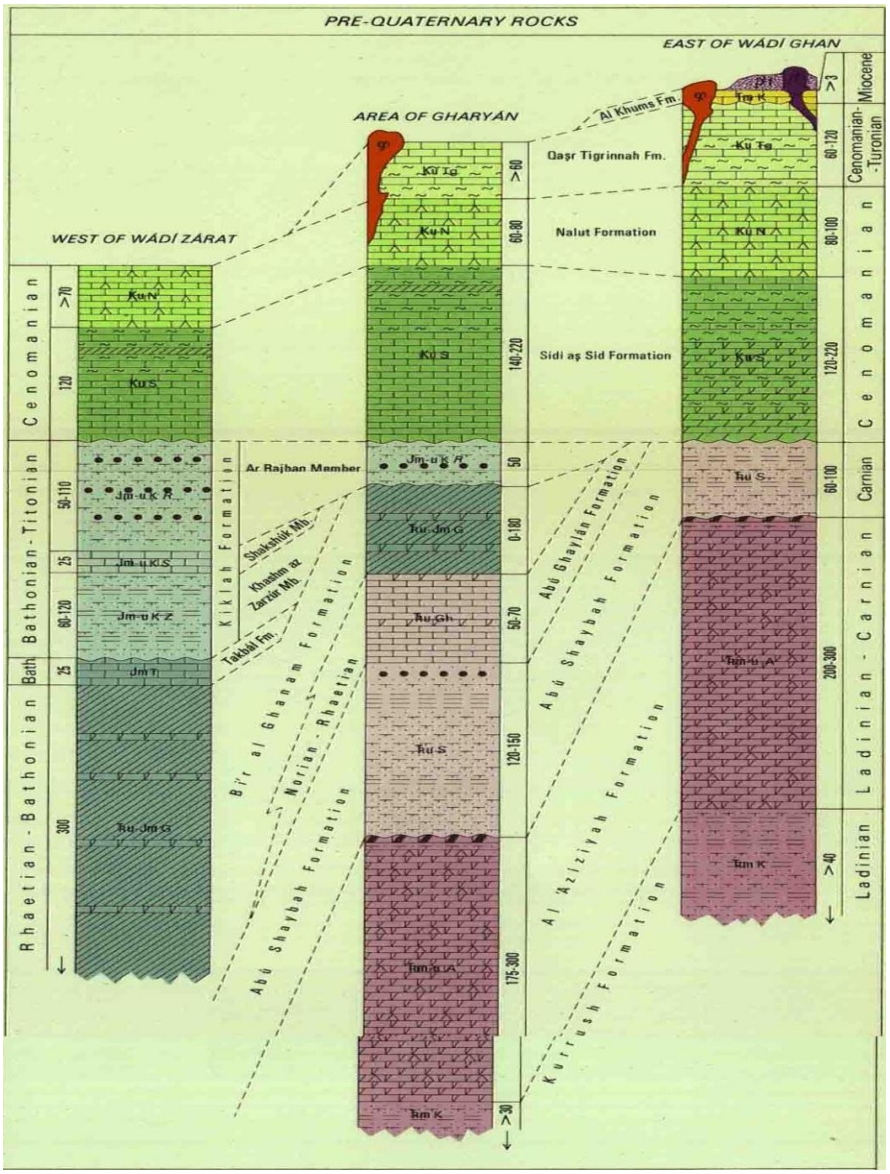

Fig. 1.2: Pre-Quaternary rocks in the area between west of Wadi Zarat and east of Wadi Ghan (after El Hinnawy and Cheshitev 1975).

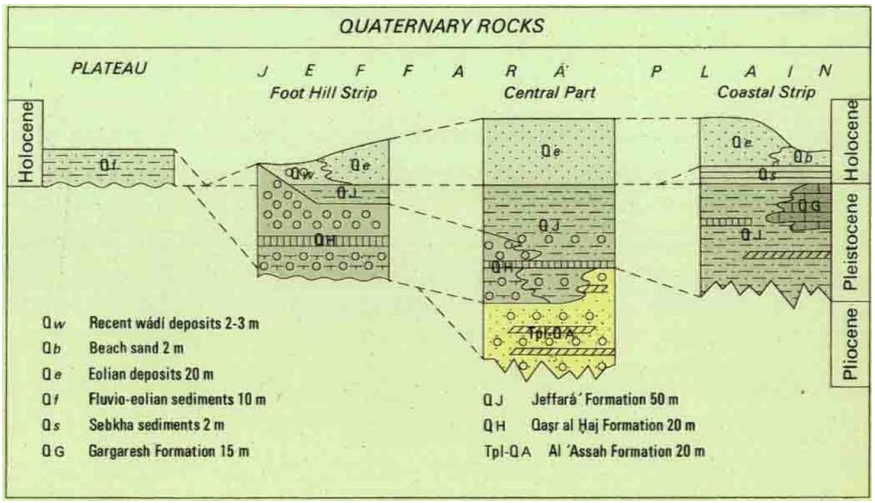

Fig. 1.3: Quaternary rocks in Jifarah plain (after El Hinnawy and Cheshitev 1975).

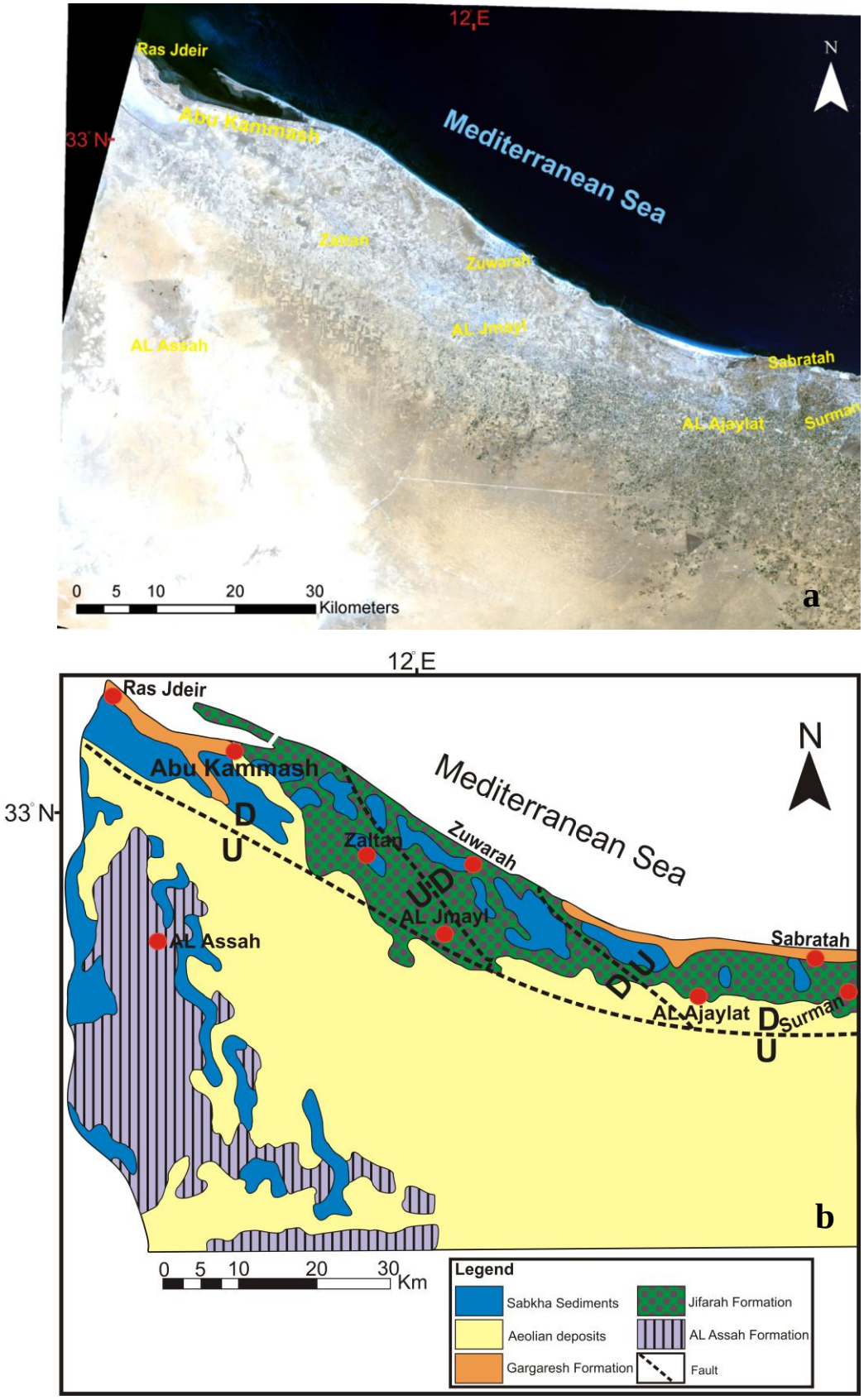

Fig. 1.4: (a) Landsat 8 natural color (b) general geological map of the study area(El Hinnaway and Cheshitev, 1975).

1.1.2. Geomorphology

El Hinnawy and Cheshitev (1975) subdivided the Jifarah Plain into three geomorphic subunits. The first subunit is a coastal strip, which is limited to the north by the Mediterranean Sea cliffs and extends landward to about 10-20 km. These cliffs range in elevation from 5 to 30 m, made of calcrete (Jifarah Formation) and calcarenite (Gargaresh Formation). The low topographic areas in this strip are mostly cultivated especially in the area between Tajoura and Al Ajaylat. The area between Al Ajaylat and westwards toward the Tunisian border is covered occasionally by coastal dunes and sabkhas. The second subunit is a central part that is limited by the southern boundary of the coastal strip and extends to the south for a distance ranges from 60 to 90 km. It rises gradually towards the south to an elevation of 130 m above sea level, where it passes into the foot hills strip. The central part is essentially flat with only minor topographical changes related to active and stabilized dune fields and a number of wadi courses. Some of the wadies which drain the plateau flow over this part of the Jifarah where they fan out before reaching the sea as wadi As Sarat and wadi Al Majinin. The third subunit is a foot hill strip; this part is confined to a narrow strip which stretches from the foot of the scarp and northwards to a distance ranging from 10 to 20 km. The Jifarah Plain is made, here, of a relatively thick sequence of deposits derived from the scarp which further passes gradually due north into the upper part of the Jifarah sands and silts. In some areas these deposits are capped by a hard calcrete band. The foot-hill strip is the highest part of the Jifarah plain assuming elevations range from 130 to 200 m above the sea level. This strip is highly dissected by wadies and displays a more rough topography due to outcrops of the Mesozoic rocks which cut through the Quaternary cover. The study area is a part from the first unit of Jifarah plain which is knows as a coastal strip lying between Surman and the territorial boundary of Tunisia.

Based on the geomorphological characteristics, the coastal area can be subdivided into two main physiographic provinces, namely; emerged and submerged shores (Fig. 1.3). The emerged shore extends for about 108 km long, from 5 km east Tajoura to Marsa Zuwaghah. This area is characterized by irregular shoreline (Fig. 1.4), associated by sea stacks in some places and wave-cut cliffs in others (Fig. 1.5). The wave cut cliffs on the studied area include two formations; Jifarah Formation (calcrete) and Gargaresh Formation (calcarenite).

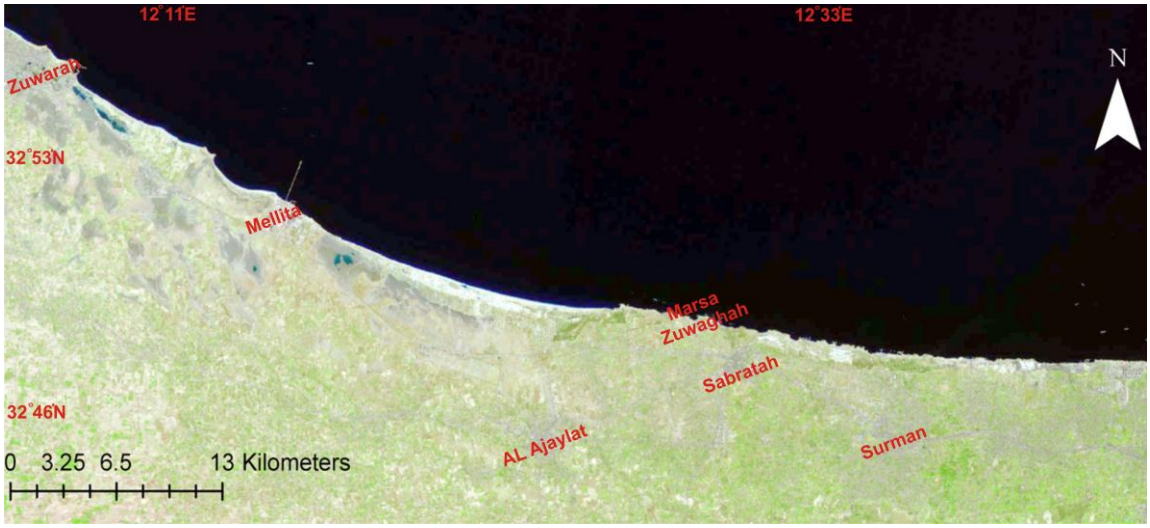

Fig. 1.5: Landsat image shows the difference between the emerged and submerged shores.

Fig. 1.6: Landsat image shows the irregularity of the shoreline which characterizes the emerged shoreline.

Fig. 1.7: High relief shorelines(Jifarah Formation) associated with sea stacks at Al Mayah.

The submerged shore is characterized by its low relief or almost flat coastal area with nearly straight shorelines (Figs. 1.6 to 1.7). It extends from Marsa Zuwaghah to the territorial boundary of Tunisia for about 75 km long. This province is characterized by sandy beach, coastal dunes, thin sand sheets, sabkha deposits and scattered patches of Jifarah and Gargaresh formations.

Fig. 1.8: Landsat image from Zuwarah area between Marsa Zuwaghah and Tunisia border showing the submerged shoreline.

Fig. 1.9: Low relief shoreline at station no. 3 (Abu Kammash).

Sediments of the evaporate environment have commanded increasing attention during recent years. Studies of this environment reveal not only what sediments are initially deposited but also to what extent they are altered and lithified and what new minerals are formed under extreme conditions of temperature, salinity and evaporation. The Arabic word sabkha means salt-encrusted flat land. The original word means cotton flock because sabkhas usually appear white in the horizon compared to the yellowish brown colored deserts. Sabkhas are hydrological regimes developed under arid climatic conditions with shallow water table and characterized by the presence of evaporate minerals such as gypsum, anhydrite and halite (Al-Yafei and AL-Bakri 2014). Deposition and dissolution of the evaporite minerals in the recent deposits are interpreted using the saline pan cycle, which consists of a flood stage (brackish lake), an evaporative concentration stage (saline lake), a desiccation stage (dry saline pan) and return to a flood stage (brackish lake) (fig 1.8). As evaporation and halite crystallization continue, the saline lake shrinks, ultimately drying out (Abdel Galil and El-Fergany, 2011)

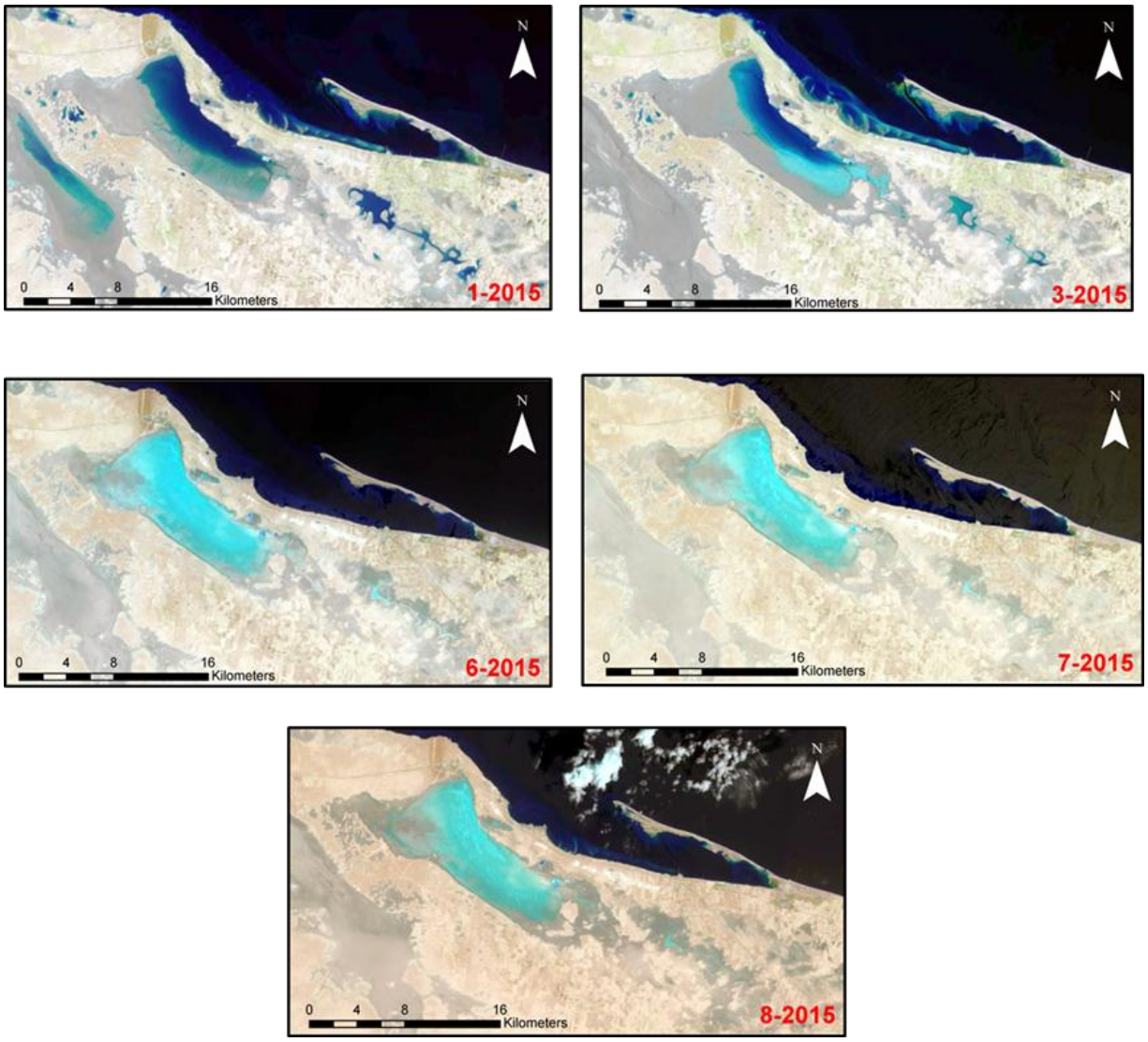

Fig. 1.10: Mellahet el Brega (sabkha), Abu Kammash. Image from January 2015 to Augusts 2015 Alteration from the flooding (brackish lake) to the evaporation (saline lake) (Landsat 7 satellite).

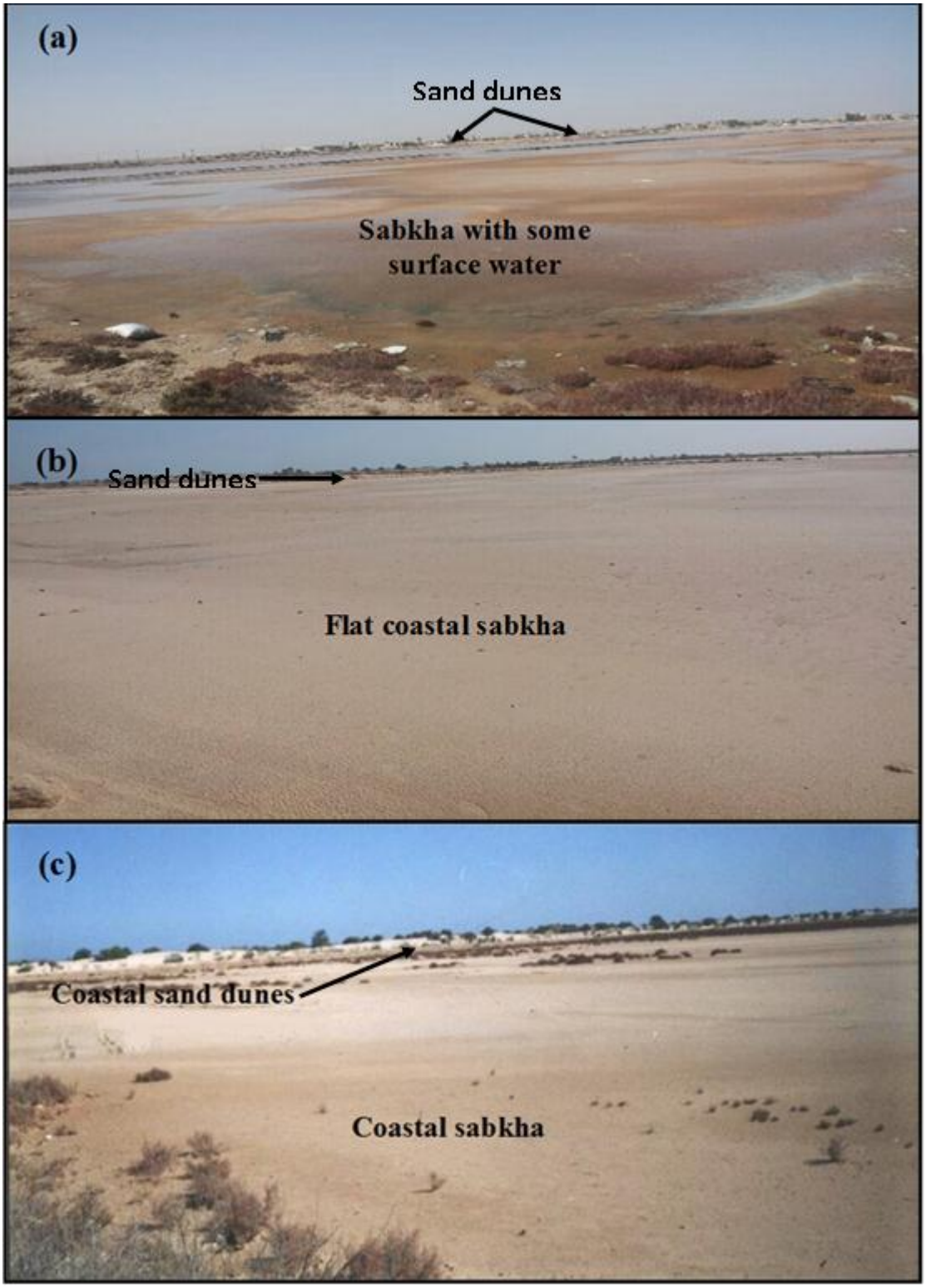

Fig. 1.11: Coastal sabkha and sand dune separated a relatively low area from the sea (a) and (b) Sabkha at Surman in month April 2015 and (c) Sabkha at Abu Kammashin in month August 2013.

1.2. General study area by remote sensing and GIS

1.2.1. Geographic information system (GIS)

GIS-based techniques for land use suitability analysis developed from the practice of manually overlaid maps which were developed in the USA in the last century. GIS capabilities for spatial analysis overcome the drawbacks of the paper map overlay approach. However, GIS has now become a powerful tool for land use planning due to its ability to deal with different functions, which is very useful for land use planning. Of these functions, the most important are database management, cartographic analysis and modeling function. The ability to integrate data in GIS is one of the most important advantages of the system, involving collection of data from different sources, formats, and scales and making them compatible with each other (Mohamed, 2013).

1.2.1.1. Geographic information system data

A- Shuttle radar topography mission (SRTM)

The Shuttle Radar Topography Mission (SRTM) is a NASA mission conducted in 2000 to obtain elevation data for most of the world. It is the current dataset of choice for digital elevation model data (DEM) since it has a fairly high resolution (1 arc-second, or around 25 meters, for the United States, and 3 arc-second, or around 90 meters at the equator, for the rest of the world), has near-global coverage (from 56°S to 60°N), and is in the public domain.

Many Open Street Map-based projects use SRTM data to provide topography information, relief shading, and elevation profiles for trails and routes. An example is the Open Cycle Map rendering which shows contours and relief shading derived from SRTM data (Ghoneim *et al.*, 2012). Publicly available SRTM data (http://srtm.csi.cgiar. org/) at 90 m spatial resolution with 16 m vertical. The SRTM data were principally used in topographic analysis of the study area, to delineate the slope area, complete drainage network, watershed and cross section profile.

B- Computer programs used

All the data used in this study (SRTM, Landsat 7ETM+ and Landsat 8OLI). Illustrations and data analyses contained in this study were achieved using different programs: digitizing by computers programs by Arc GIS (*Arcmap10.1*, *Global Mapper 13, Coreldrawx4* and *Envi 4.7*).

1.2.1.2. Results and discussion

Based on the SRTM-DEM derived The coastal Plain of the study area comprising the flat area is present at low elevation between Elevation line 0 to 20 m in the shoreline it is covered by Quaternary sediments. The altitude rises steadily from the sea coast towards the south. The maximum elevation is found in the south and it amounts to some 116 m above sea level.

A slope is used for the identification of features with topographic expression. Slope is a measure of the steepness of the terrain or the rate of change in elevation at a given part of the topographic surface (Saadi *et al.,* 2013). This slope generates data values in degrees from horizontal. The output image contains slope values that range from 0^o (flat terrain) to 90^o (vertical terrain). The brightness of each pixel in the slope map is related to the slope angle; which gray areas are the slight slopes between 5^o to 15^o degrees and blue areas are the gentlest ones almost flat between 0^o to 5^o degrees.

Fluvial features are developed as a result of denudation of land surface by streams erosion and deposition. The shape of most drainage networks, and especially of the lower order channels, is controlled by regional geological structure the drainage pattern found in the study area is dendritic type.

Watersheds define drainage areas of the land surface that contribute flow to particular edges on the hydro network most of watershed accumulation in Jifarah plain on sabkha.

A traverse profile is a line that displays the amplitude or change in elevation underneath the traverse line. We applied this technique to the DEM to create elevation profiles across topographic anomalies of interest. We selected four profiles three along lines from to the scarp to the costal, one from west to the east width profiles to interpret topographic forms that may have been affected by sabkha.

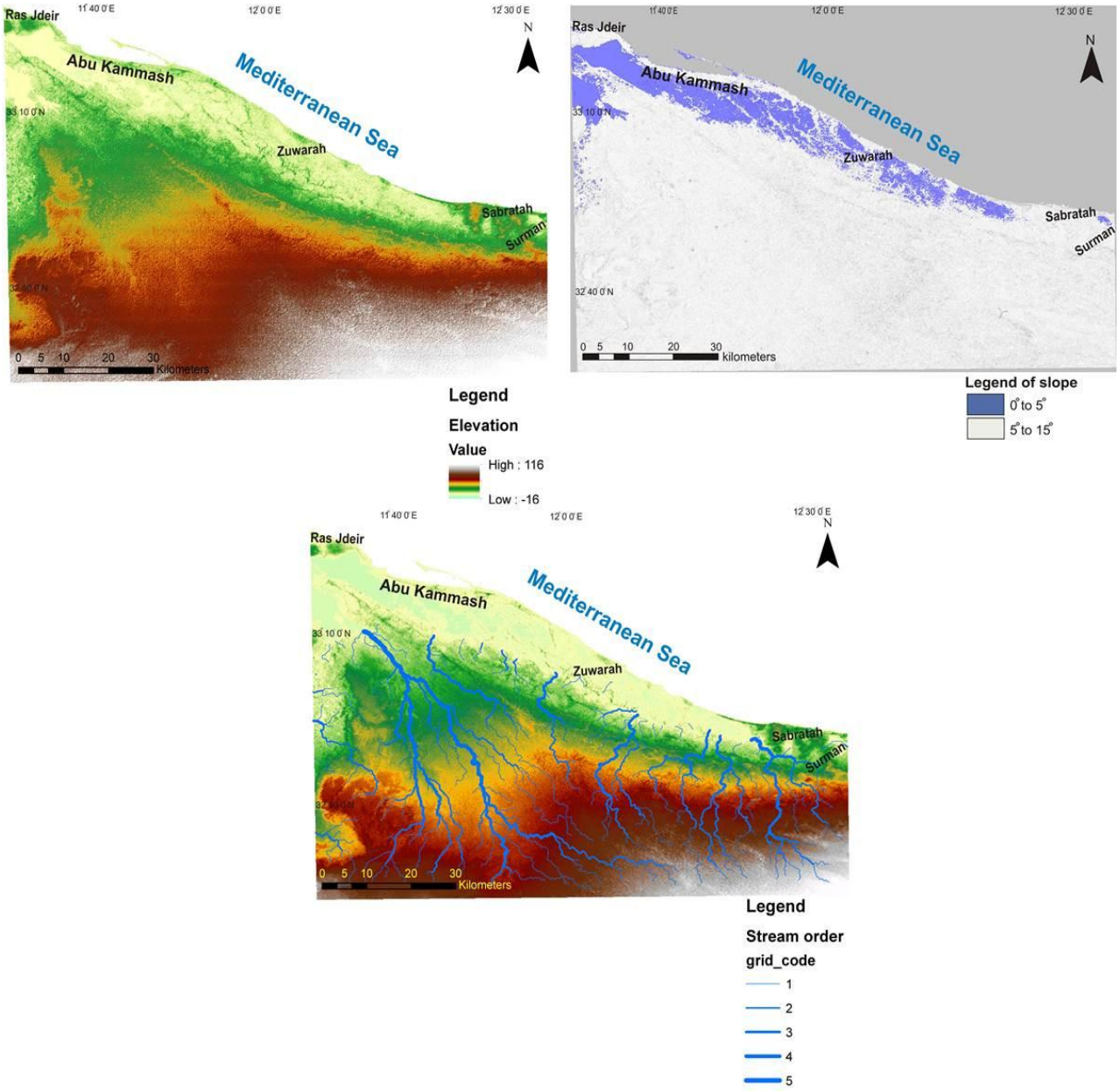

Fig. 1.12: SRTM-DEM (a) Elevation area from 0 to high 116 m. (b) Slope map area within which gray areas are the slight slopes and blue areas are the gentlest ones almost flat area. (c) Area with drainage networks.

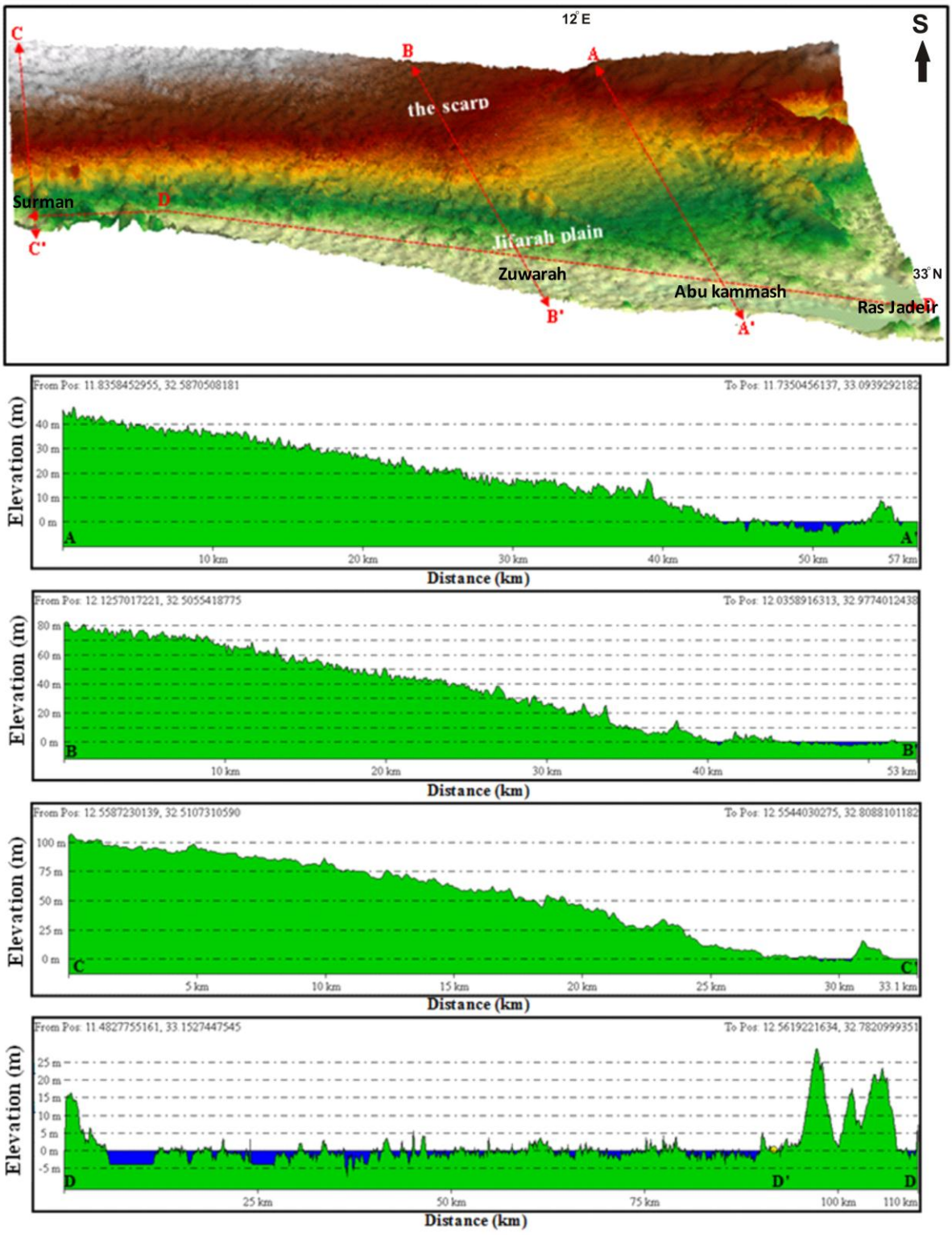

Fig. 1.13: DEM image of the study area with profile lines. Four profiles are shown along the costal sabkha (sabkha in blue color) (AA', BB', CC', DD'D).

1.2.2. Remote Sensing

Remote sensing can be defined as any process whereby information is gathered about an object, area or phenomenon without being in contact with it. Our eyes are an excellent example of a remote sensing device. We are able to gather information about our surroundings by gauging the amount and nature of the reflectance of visible light energy from some external source (such as the sun or a light bulb) as it reflects off objects in our field of view. Contrast this with a thermometer, which must be in contact with the phenomenon it measures, and thus is not a remote sensing device. Another meaning remote sensing has come to be associated more specifically with the gauging of interactions between earth surface materials and electromagnetic energy (Eastman, 2001). Remote sensing can contribute to each of these types of maps through analysis of imagery from one or more system or instrument. The most revealing feature of sedimentary rocks is depositional layering. Sedimentary rocks are characterized by alternating weak and resistant layers of varying thickness and color. The recognition of layering depends on contrasts in grain size, color, resistance to erosion, and composition, which are in turn influenced by the weathering environment, erosion, and vegetation cover (Prost, 2014).

1.2.2.1. Mapping sabkha, landsat 8, NW Libya

Evaporites such as halite and gypsum/anhydrite exist at the surface only in arid climates because they are water soluble. They are recognized because they are generally very bright, and can be nearly white in color. Evaporites accumulate as recent or ancient deposits in dry lake beds and evaporating, shallow seas. They occur as layered beds, diapirs, and, rarely, as sand dunes (Prost, 2014). Libya is home the many concentrations of sabkhas both coastal and inland. The coastal areas of NW Libya include the sabkha sediments along the Mediterranean Coast from Surman to Ras Jdeir, Jifarah plain, NW Libya (*see* Fig. 1.2). The primary to develop a new technique for mapping sabkha using multispectral remotely sensed data. Identifying sabkha pixels in remotely sensed some difficult in study area (Allbed and Kumar, 2013). This is primarily due to the confusion of sabkha pixels with saline soils and the mixture of sabkhas with sand dunes making spectral separation a challenging process. This research uses the multispectral information provided by Landsat 8 data in addition to a set of multispectral data to accurately identify sabkha pixels from other land cover pixel types.

1.2.2.1.1. Classification of remotely sensed imagery

Classification is the process of developing interpreted maps from remotely sensed images. As a consequence, classification is perhaps the most important aspect of image processing to GIS. Traditionally, classification was achieved by visual interpretation of features and the manual delineation of their boundaries. However, with the advent of computers and digital imagery, attention has focused on the use of computer-assisted interpretation. Although the human eye still brings a superior set of capabilities to the classification process, the speed and consistency of digital ocedures make them veryattractive. As a consequence, the majority of classification projects today make use of digital classification procedures, guided by human interpretation (Eastman, 2001). There are two general approaches to image classification: supervised and unsupervised. They differ in how the classification is performed. In the case of supervised classification, the software system delineates specific land cover types based on statistical characterization data drawn from known examples in the image (known as training sites). With unsupervised classification, however, clustering software is used to uncover the commonly occurring land cover types, with the analyst providing interpretations of those cover types at a later stage (Eastman, 2001).

The first step in supervised classification is to identify examples of the information classes (i.e., land cover types) of interest in the image. These are called training sites. Once a statistical characterization has been achieved for each information class, the image is then classified by examining the reflectances for each pixel and making a decision about which of the signatures it resembles most (Eastman, 2001). Using the new dataset for classification resulted in significantly improved identification and separation of sabkha areas from other land cover types. Using the Landsat 8 dataset it was able to separate the sabkha areas from the desert surface .The addition of the transformed components and incorporation of the sabkha index proved to be useful in separating sabkha pixels from others. Compared with the geological map (*see* Fig. 1.2) we can see the decline in the size and spread of the sabkha in the coast (Fig. 1.12). The decrease of the salt affected areas (sabkhas) in the study area could be explained as a result of eolian sand movement and coverage on the surface which prevents sabkhas detection using remote sensing. These thicknesses of the sand material range from 20 – 30 cm (Nwer *et al.,* 2013).

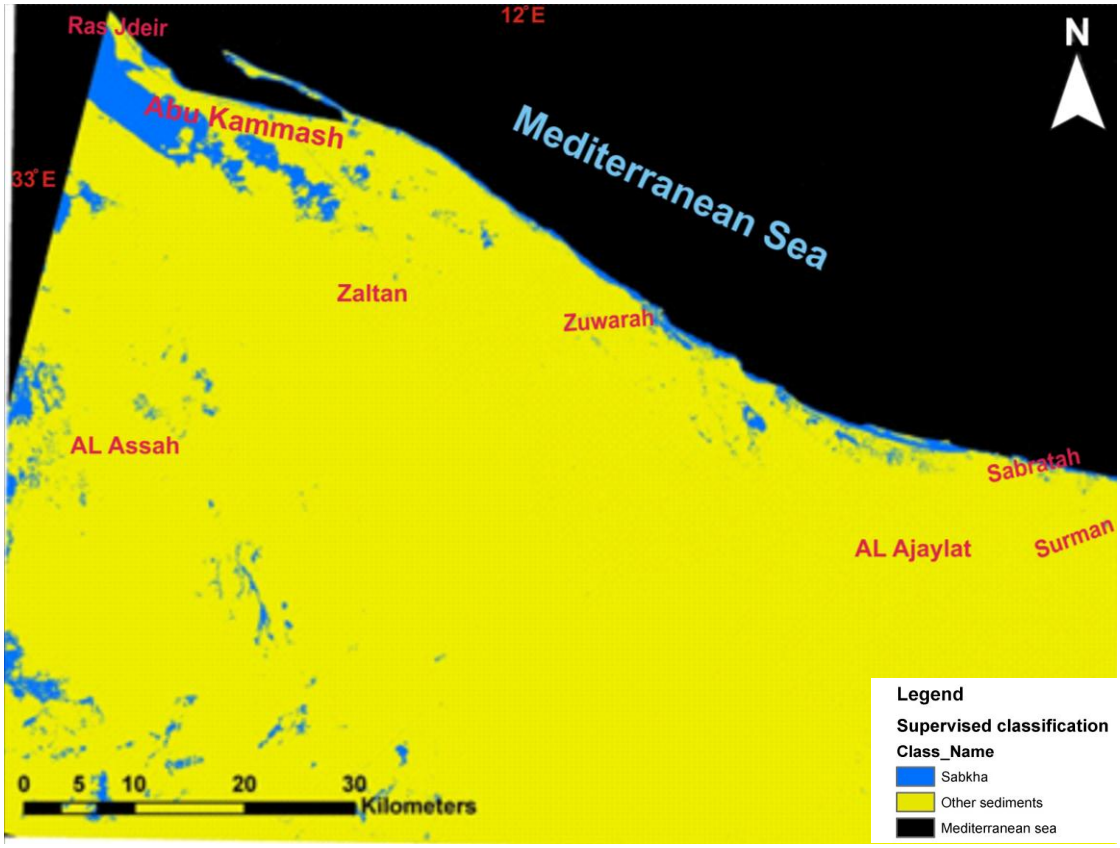

Fig. 1.14: Landsat 8 land covers classification using supervised classification and index dataset for sabkha.

1.3. Previous Work

Quaternary studies in the Jifarah Plain are less numerous than those on Mesozoic rocks to the south. Few attentions have been directed towards the northwest Libyan coast. The present thesis attempts to contribute to the available knowledge on the mineralogy and geochemistry of the sabkha brines and sediments along the Mediterranean Coast from Surman to Ras Jdeir, Jifarah plain, NW Libya.

Stivaletta *et al* (2009), studied the Astrobiological significance of the sabkha life and environments of southern Tunisia. The studied investigates the continental sabkha environments of southern Tunisia, in which ecological niches (i.e. water and salt precipitates, including halite, gypsum, and dolomite) host microbial life. Halophilic microorganisms can be trapped in the extensive saline crusts of halite and gypsum, which can be regarded as the first step of their delivery to the fossil record.

Kloss and Roy (2010), studied the evaporite mineralogy and major element geochemistry as tools for palaeoclimatic investigations in arid regions: A synthesis. The studied presents a synthesis of the applications of evaporite mineralogy and the relationship between major elements for the palaeoclimatological research of arid regions, with examples from Playa Oum el Krialate in Tunisia, Wadi Natron in Egypt, East African Rift Valley. The numerous evaporite minerals serving as indicators of palaeo-drylands (salinity and evaporation) include carbonates, sulfates, and Na, K, Ca, and Mg chlorides.

Abdel Galil and El-Fergany (2011), studied the sedimentological significance and brine Chemistry of Recent coastal sabkha, at Zuwarah, Northwest Libya. They found that sabkha deposits occupy the relatively low topographic areas and are separated from the sea by coastal sand dunes. The sabkha sediments are relatively finer compared to those of the coastal sand dunes and beach. Grain size grading with improvement in sorting occurs in the direction of sediment drift landward. The brines of the saline pans are of recent marine water origin.

The salinities increase from the sea landward (46.9 g/l, up to 180.4 g/l and up to 323.8 g/l for the seawater, coastal sand dunes pans, and the sabkha brines respectively). Accompanying the increase in salinities is the very high concentration of Na^+ and Cl^- ions. The brines are highly saturated with NaCl, which favors a

dominant halite precipitation (65.02- 78.12%), while bicarbonate salts are traces (0.13-0.79 %).

El-Omla and Aboulela (2012), studied the environmental and mineralogical studies of the sabkhas soil at Ismailia-Suez Roadbed, Southern of Suez Canal District, Egypt. Sedimentological and mineralogical analyses were conducted using grain size; for study the physiographic features of sabkha deposites and their distribution pattern at the southwestern of Suez Canal district. Grain size analyses, mineralogical analyses using Scanning Electron Microscopy (SEM), EDAX, and X-ray diffraction techniques.

Nesrine *et al* (2015),studied the multivariate statistical analysis of saline water - A Case Study: Sabkha Oum LeKhialate (Tunisia). The studied Hydrochemical data of 80 wells from the catchment area of sabkha Oum leKhialate, southern Tunisia and 9 parameters (pH, TDS, Na^{+}, Ca^{2+}, $SO4^{2-}$, Mg^{2+}, K+, Cl^{-}, HCO^{3-}) show that the abundance of major ions from the sabkha is as follows: Na>Ca>Mg>K and SO4>Cl> HCO^{3-}. Multivariate statistical analysis methods such us correlation analysis, principal component analysis (PCA) and hierarchical cluster analysis (HCA) were used to identify the geochemical processes controlling the chemistry of saline water in the catchment area of the sabkha. Results of statistical analysis reveal that the major source of sulfate sodium deposit is the process of evaporation, cationic exchange between Ca and Na in clay formation and mineral precipitation.

1.4. Objective and plan of work

The work is done to achieve the following:

1) To study the mineralogy of the sabkha sediments.
2) To discuss the geochemical characteristics of the sabkha brines and sediments.

The work is done according to the following plan:

1) Sampling of the sabkha brines from the field and sediments from the core samples.
2) Mineralogical analysis using petrographic microscope, X-ray diffraction (XRD) and Scanning-Electron Microscope (SEM-EDX) investigations.

3) Chemical analysis of major ions, major oxides and trace elements using Inductively Coupled Plasma-Association Emission Spectrometer (ICP-AES) and Inductively Coupled Plasma Mass Spectrometry (ICP-MS) techniques.
4) Summary and conclusions.

1.5. Methodology

1.5.1. Sampling

The studied 31 samples have been obtained from five cores provided by the chemical complex of Abu Kammash (GCCI), in which the thickness of the most cores is one meter and representing as much as possible apparent variation in lithic nature, color and grain size. These samples were collected from the sabkha sediments along the Mediterranean Coast from Surman to Ras Jdeir, Jifarah Plain, NW Libya, from 5 stations (Fig. 1.1). The traverse is parallel to the studied coast. The core samples were separately air dried, their carbonate-sand-mud contents were determined and analyzed textural composition according to Carver (1971) and Folk (1980).

Five samples from the sabkha brines from the field were collected and chemically analyzed for Ca^{2+}, Na^{+}, K^{+}, Mg^{2+}, Cl^{-}, $SO4^{2-}$ and HCO^{3-}.

1.5.2. Analytical techniques

1.5.2.1. Petrographic analysis

This analysis was done in the Central Laboratories of the Geological Survey of Egypt in Cairo (Fig. 1.14). Petrographic analysis involves taking a sample from cores, fixing it to a glass slides, grinding the sample to 0.003 mm or 25 µm , thick (thin section) and observing to polarizing microscope with attached camera, where it used to identify minerals and textures in the rock. moreover Dunham classification (1962) has been applied to classifying the rocks.

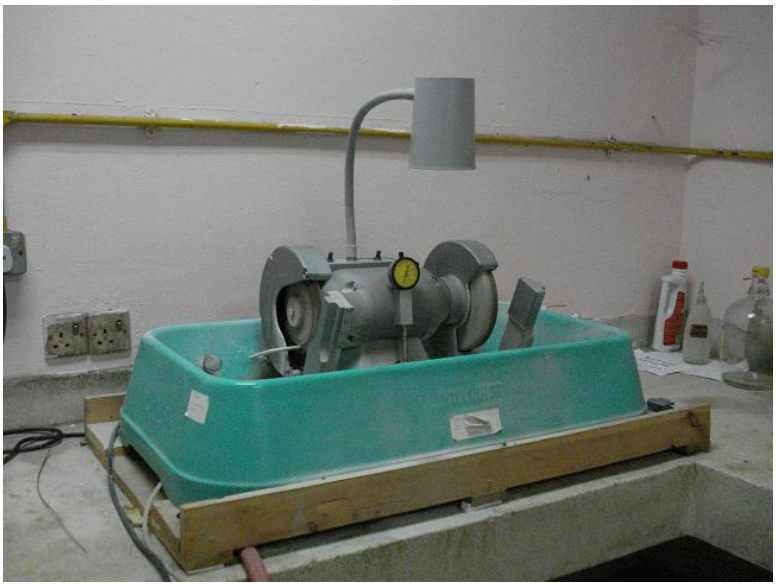

Fig. 1.15: Thin section instrument.

1.5.2.2. X-ray diffraction (XRD)

This analysis was done in the Central Laboratories of the Geological Survey of Egypt in Cairo . XRD analysis has become the more accurate and quick method for estimation of whole rock minerals and especially in the identification of clay minerals. A Phillips Norelco diffractometer with Ni filter and Cu-Kα radiation at kV and 20 mA is used. The working conditions are kept the same to maintain equal base for comparison of peak intensities as relative measure of mineral abundance. Diagnostic and interference-free peaks have been considered for the identified minerals. The measured area under the selected peak designates the relative abundance of a mineral and does not represent its quantitative concentration (Fig. 1.15).

Fig. 1.16: X-ray diffraction instrument.

1.5.2.3. Scanning Electron Microscopey (SEM)

A scanning-electron microscope, housed at the Nuclear Materials Authority of Egypt, has been used in the present study. The scanning electron microscope (SEM) uses a focused beam of high-energy electrons to generate a variety of signals at the surface of solid specimens. The signals that derive from electron-sample interactions reveal information about the sample including external morphology (texture), chemical composition, and crystalline structure and orientation of materials making up the sample. The SEM is also capable of performing analyses of selected point locations on the sample (Fig 1.16).

Fig. 1.17: Scanning electron microscope instrument.

1.5.2.4. Loss on Ignition (LOI)

Loss on Ignition (LOI) analysis is used to determine the organic matter content (OM %) of the studied samples. It does not involve the use of any chemicals, only the use of a muffle furnace. LOI calculates OM % by comparing the weight of a sample before and after the soil has been ignited. Before ignition, the sample contains OM, but after ignition all that remains is the mineral portion of the soil. The difference in weight before and after ignition represents the amount of the OM that was present in the sample (Fig 1.17). The analysis was done in the Nuclear Materials Authority of Egypt. The following is, however summary of the preparation:

1) Weigh the crucible empty…….A.

2) Weigh the crucible + sample ……B.

3) Install B into oven and heated up to 1000° for an hour.

4) Weigh the crucible after heating …….C.

5) B – A = weigh of sample…….D.

6) Weight loss = B – C = E.

7) LOI (%) = E / D *100.

Fig. 1.18: Loss on Ignition instrument.

1.5.2.5. Inductively Coupled Plasma-Association Emission Spectrometer (ICP-AES)

About 7 major ions are analyzed by the ICP-AES technique (Fig. 1.18). It is a reproducible and very accurate analysis technique, suitable for all types of watery and solid samples . Water samples were filtered and acid stabilized soon after collection. A 200 ml aliquot of a well-mixed, acid preserved sample was transferred to a beaker. 20 ml of concentrated HCl was added to the sample. The sample was heated (not boiled) on a steam bath until it was evaporated to near dryness. The beaker was rinsed thoroughly with 10% HCl solution and the contents were transferred to a 20 mL volumetric flask, and made up to the mark with 10% HCl solution. The analysis was done in the Nuclear Materials Authority of Egypt. The obtained data are given in table (3.1).

Fig. 1.19: Inductively Coupled Plasma-Association Emission Spectrometer instrument.

1.5.2.6. Inductively Coupled Plasma-Mass Spectrometry technique (ICP-MS)

About 12 major oxides and 15 trace elements are analyzed by the ICP-MS technique (Fig. 1.19), which is widely used, at present, for determination of elements in various materials with high precision. The analytical procedure depends on the decomposition of exact weight of 0.2 g powdered fine sand size sample in 50 ml Teflon beaker. Decomposition was done by 4 ml HNO_3, 3 ml $HClO_4$ and 5 ml HF, and evaporated to dryness under 200^{o}C. The residue was dissolved with 5 ml (1:1) HNO_3 by heating and 5 ml of 4 ppm indium solution was added as an internal standard. The sample, as well as reference, solutions were introduced by peristaltic pump with 0.18 rpm. Before each measurement, nebulizer and spray chamber were washed by introducing the solution for 3 min with 0.5 rpm and 30 seconds with 0.18 rpm. The analysis was done in the Nuclear Materials Authority of Egypt. The obtained data are given in tables (3.2 to 3.6).

Fig. 1.20: Inductively Coupled Plasma-Mass Spectrometry instrument.

CHAPTER TWO

MINERALOGY AND PETROGRAPHY

2.1. Introduction

About 31 representative samples from the study area were examined for better understanding of their nature, origin and diagenetic history. Petrographic study of limestone, gypsum and halite samples is a detailed investigation of thin sections, while the study of soil and calcareous sand samples is a detailed mineralogical investigation on the very fine size fraction (125-63μm). The studied very fine size fraction is subjected to gravitational heavy mineral separation using Bromoform (specific gravity 2.87). The fractions of both the light and heavy minerals were mounted in Canada balsam for transmitted light microscopy. Scanning electron microscope with an energy dispersive X-ray attachment (SEM-EDX) was applied to shed light on the geochemical characteristics of the mineral composition. X-Ray powder diffraction on clay fraction was used to estimate the relative frequency of clay minerals. The sequence of the Quaternary sediments along the study area is shown in Fig. (2.1).

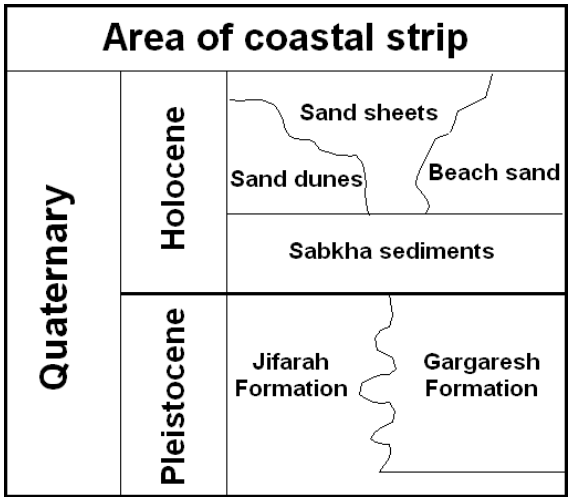

Fig. 2.1: Quaternary sequence along the study area (after El Hinnaway and Cheshitev,1975).

2.2. Holocene deposits

2.2.1. Sabkha deposits

Sabkha is an Arabic word for salt flat area. It represents an equilibrium state controlled by geomorphic surface whose level is dictated by the local water table. Sabkhas are occasionally covered by ephemeral shallow water, but for most of the time they are subaerial mud flats. They were documented first in the Arabian Gulf by Curtis *et al.*, (1963) but were subsequently described along the coast of Baja California, Mexico (Shearman, 1970), the coast of Sinai (Gavish, 1974), and in many other areas of the world. If the word sabkha is used objectively to imply salt flat, there are both coastal and continental sabkhas. The marine portion of the sabkha is characterized by marine sediments with largely marine-derived ground waters and the continental portion by non-marine sediments and ground waters. Kendall (1979) used continental playa as a term equivalent to continental sabkha; other workers use sabkha in a narrower sense to describe marine sabkha exemplified by the Arabian Gulf sabkhas. Warren (1989) defines sabkhas as marine and continental mudflats where displacive and replacive evaporite minerals are forming in the capillary zone above a saline water table. Continental and marine sabkhas often show similar vertical sequences. A marine sabkha is a near coastal salt dominated by marine-derived brines and processes; a continental sabkha is an inland salt flat dominated by continental brines and processes. Both environments receive water via either subsurface or overland (storm-induced) flow and may be associated with aeolian dune fields and intermittently submerged interdunal corridors. Continental sabkhas, like coastal sabkhas, are characterized by the displacive growth of evaporites in the capillary zone (Fig. 3.2) and are associated with the margins of ephemeral saline lakes. In sabkhas the physical processes thought to be most important (besides evaporation) include those operative under the following conditions a) Marine coastal, b) Fluviolacustrine and c) Aeolian dominated. Dominance of one of these processes gives rise to marine coastal sabkhas, or continental sabkhas, or interdune sabkhas, respectively. An aeolian sabkha can be a subfacies of both marine coastal and continental sabkhas. Sedimentary responses to dominant physical processes create sabkhas composed of combinations of a) Terrigenous clastics b) Carbonate-sulfate (anhydrite-gypsum minerals) and c) Soluble salts (halite, sylvite, polyhalite, etc.). Sabkhas form shoaling sequences in both continental and coastal mud flats. Most of the evaporites in a

sabkha are deposited in the capillary zone as intrastratal displacive nodules and crystal (Warren, 1989, *see* Fig. 2.2).

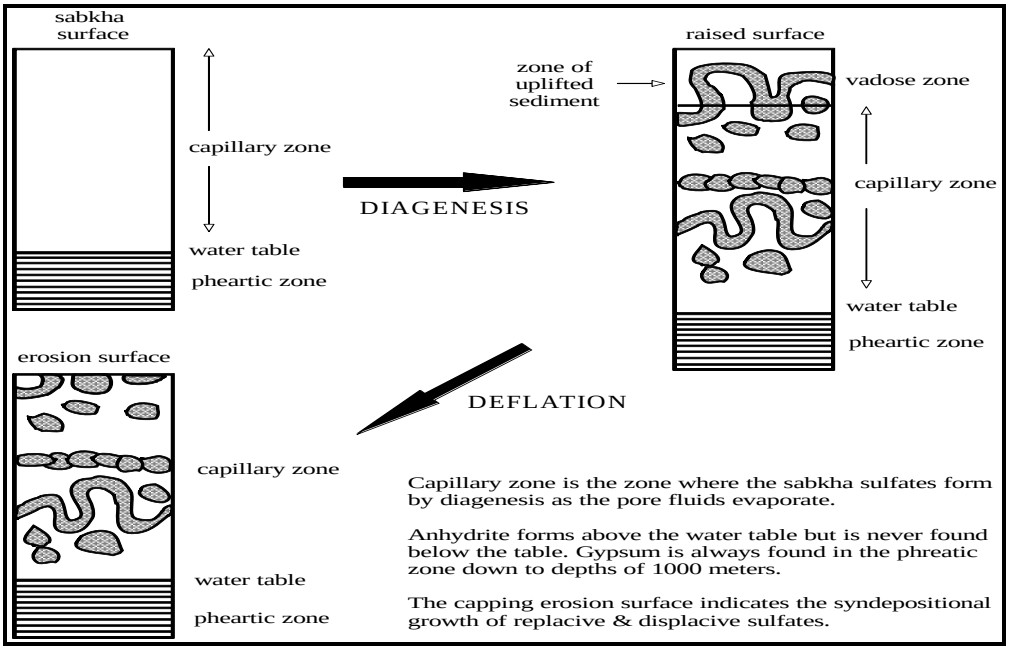

Fig. 2.2: Sabkha hydrology showing the effect of displacive evaporite growth (stippled) within the sedimentary column. The increased volume of evaporites in the column lifts the near-surface sediments into the vadose zone, where they dry and are deflated to create a capping erosion surface (after Warren, 1989).

2.2.1.1. Sabkha sequence

In general, the studied sabkha sediments are composed essentially of gypsum, halite, sands, soil and algal limestone. Sabkhas are best seen along the coastal area between station no. 1 (Surman) and westward to station no. 5 (Ras Jdeir, Fig. 2.12). The sabkhas, in the investigated area, occupy the relatively low topographic areas and are separated from the sea by coastal sand dunes (Fig. 2.13) and by beach ridges, which are mainly made of calcarenite belonging to Gargaresh Formation. Also, sabkha deposits are underlain by Gargaresh Formation in the area near the sea shore and by the calcrete of the Jifarah Formation landwards. Sabkhas surface are marked by the presence of scattered sand islands (sand drift), which are mostly vegetated by wild bushes or flat covered by salt crust and/or associated with sand dunes. All sabkhas share certain characteristics. Although they are restricted and hot being in arid regions, the sabkha surface is always very close to the local water table.

The first core from Surman consists of from base to top of algal limestone dark to brown color, soft to moderately hard, friable of soil grey to dark color and calcareous sand yellowish color with some shell fragments of gastropods and pelecypoda; nodules of gypsum yellow to green color, moderately hard with some of anhydrite, halite whitish to gray color, moderately hard with some of anhydrite (Fig. 2.3).

The second core from Zuwarah consists of from base to top of algal limestone brown color, moderately hard, with dolomite grains, friable calcareous sand yellow color rich shell fragments gastropods and soil brown color, nodules gypsum yellow color, hard with some of anhydrite, friable calcareous sand yellow color, gypsum yellow color with *desert rose* and gastropods (Fig. 2.5). Halite whitish to gray color, moderately hard with some of polyhalite and some anhydrite (Fig. 2.4).

The third and fourth core from Abu Kammash and south Abu Kammash this sabkhas cover area of tens square kilometer all along the coast (Fig. 1.8). The core consists of from base to top first Abu Kammash algal limestone brown to grey color, hard, with dolomite grains, Friable calcareous sand yellow to grey color rich shell fragments and soil brown color, very fine grains, Friable calcareous sand grey color, nodules gypsum yellow color, soft to moderately hard with anhydrite, algal limestone dark to brown color, hard, with dolomite grains, Halite with polyhalite (Fig. 2.6). South Abu Kammash consists of from base to top Friable calcareous sand yellow to grey color rich shell fragments, algal limestone dark brown color, moderately hard, Friable soil brown color, very fine grains, gypsum and top of halite (Fig. 2.8).

The core five, from Ras Jdeir, have a litology similar to the core three, but differs in distribution of sediments from base to top with special white halite in the top of core (Fig. 2.11).

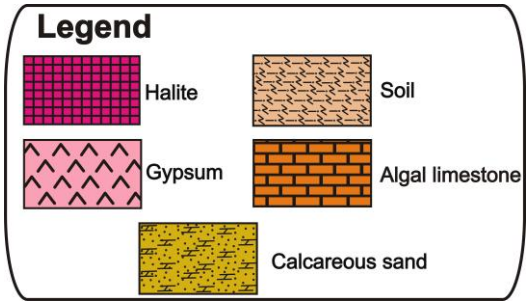

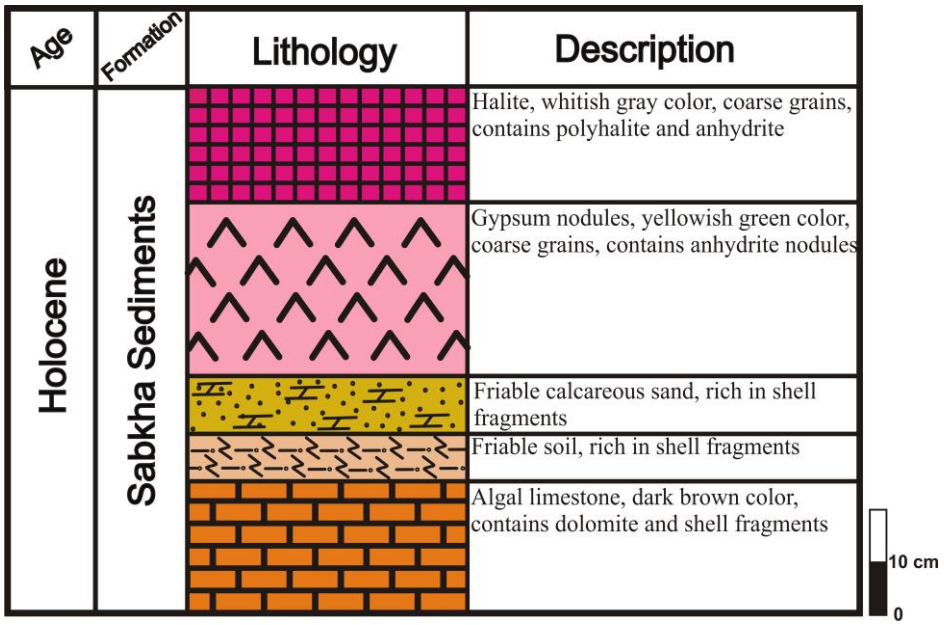

Fig. 2.3: Lithology of core samples profile at the station no. 1 (Surman).

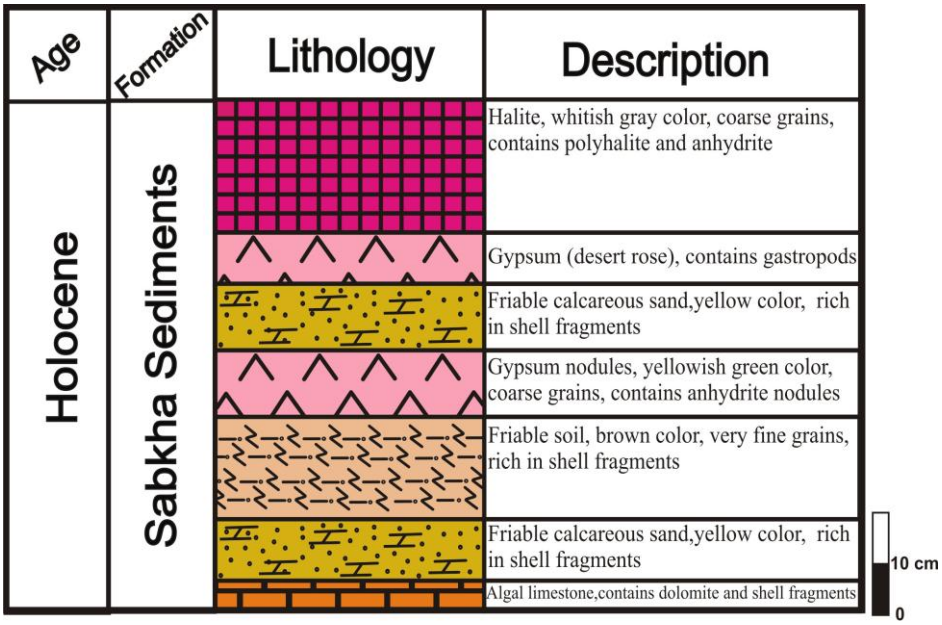

Fig. 2.4: Lithology of core samples profile at the station no. 2 (Zuwarah).

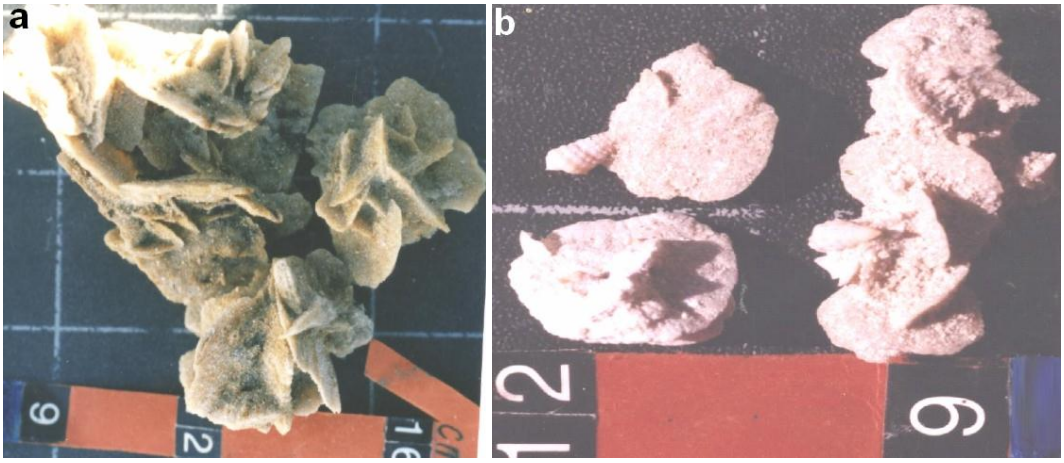

Fig. 2.5: (a) Gypsum (desert rose; sublenticular and flattened at about right angle to the c-axis) and (b) Gastropods associated with these desert rose at the station no. 2 (Zuwarah).

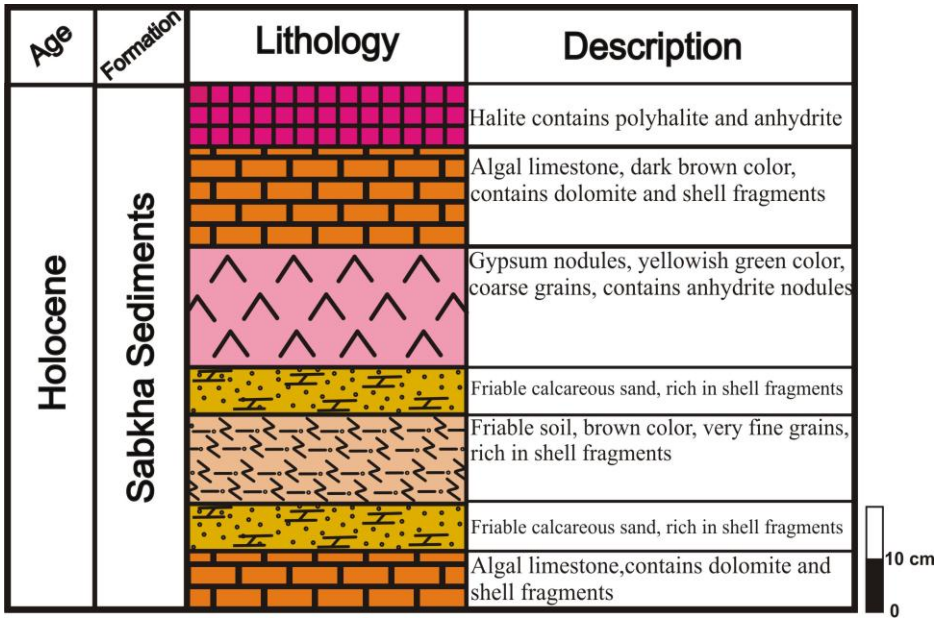

Fig. 2.6: Lithology of core samples profile at the station no. 3 (Abu Kammash).

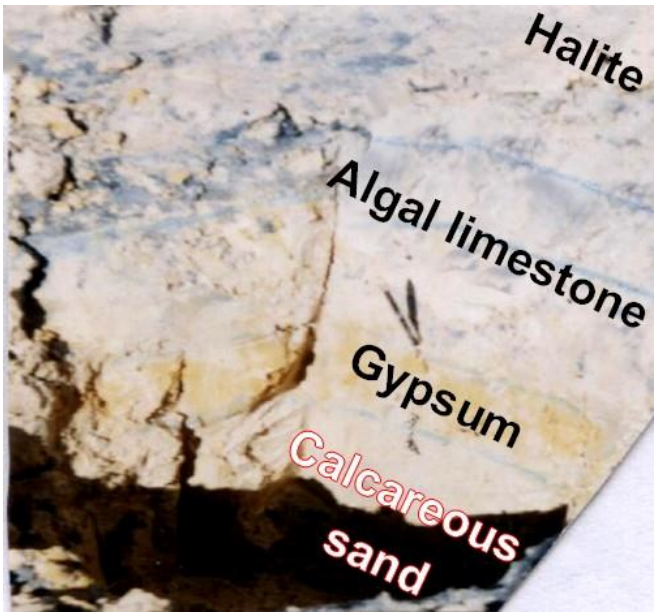

Fig. 2.7: Lithology of sabkha profile at the station no. 3 (Abu Kammash).

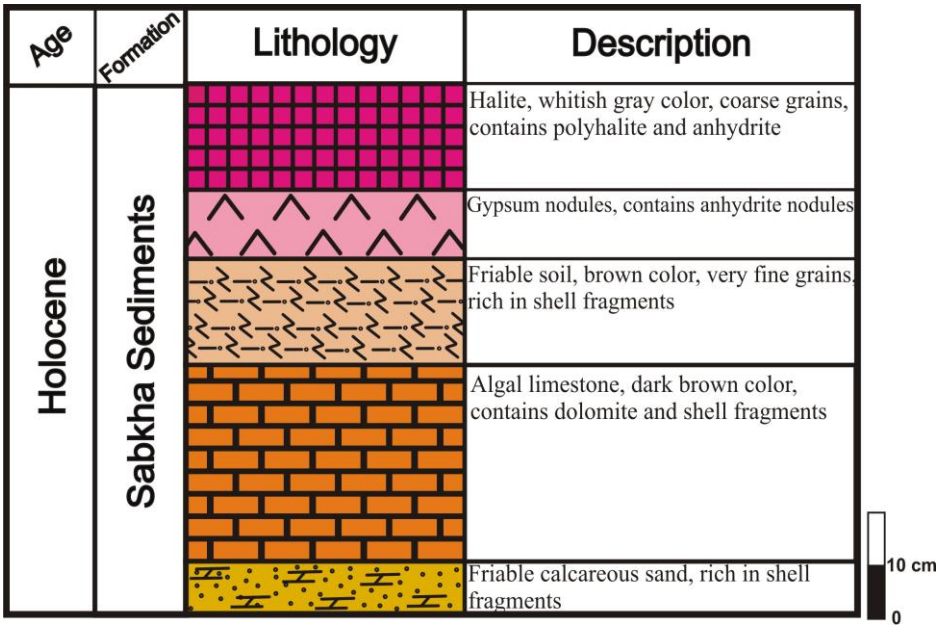

Fig. 2.8: Lithology of core samples profile at the station no. 4 (South Abu Kammash).

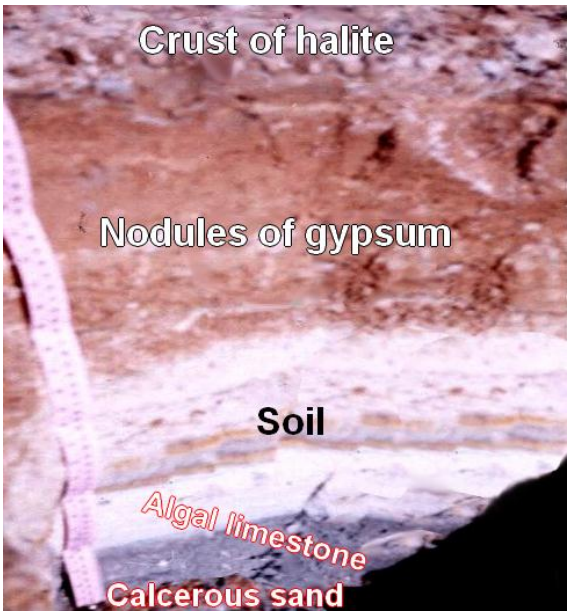

Fig. 2.9: Lithology of sabkha profile at the station no. 4 (South Abu Kammash).

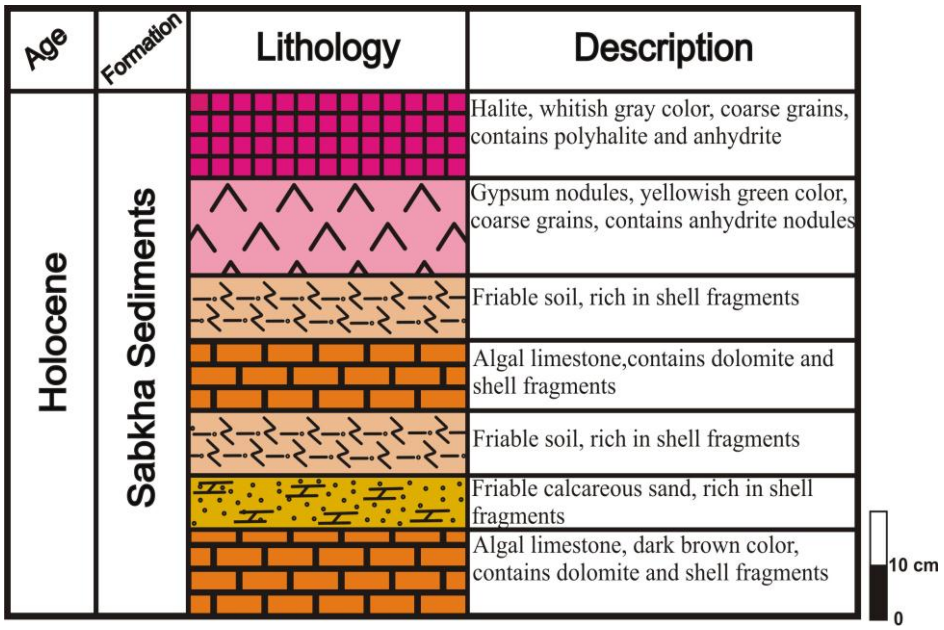

Fig. 2.10: Lithology of core samples profile at the station no. 5 (Ras Jdeir).

Fig. 2.11: Salt crust and nodular gypsum at the station no. 5 (Ras Jdeir).

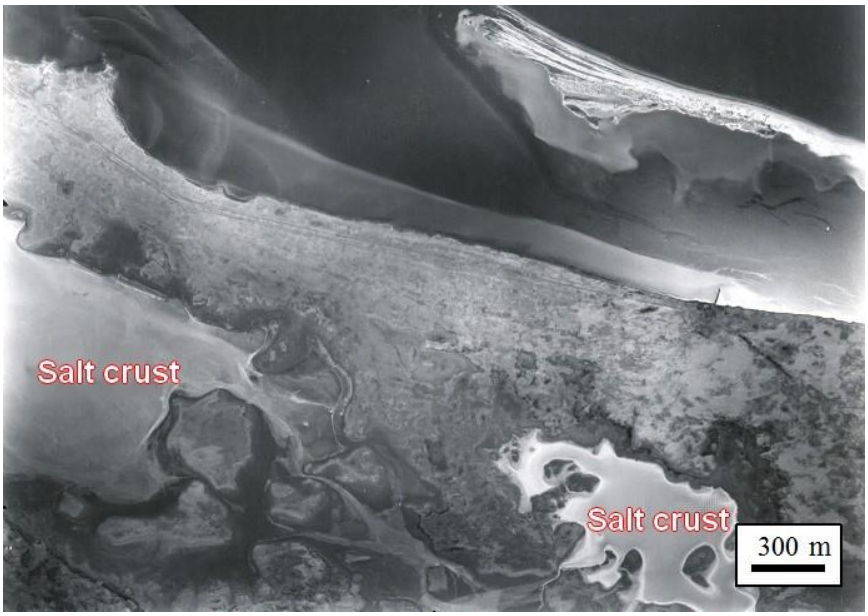

Fig. 2.12: Aerial photograph showing the coastal sabkha at the station no. 3 (Abu Kammash).

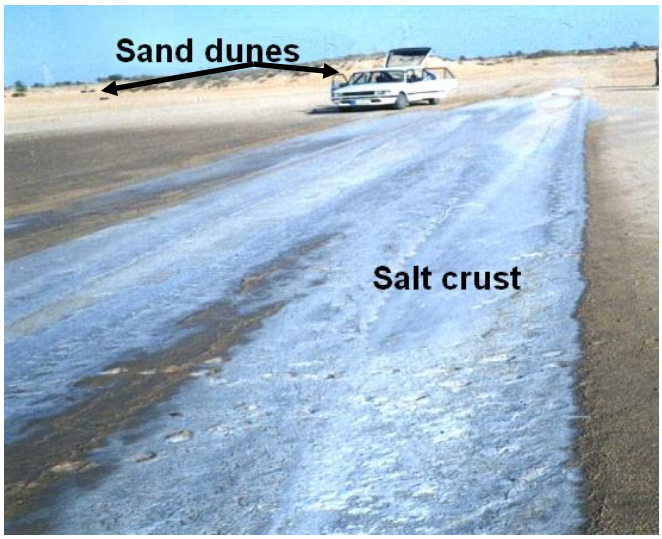

Fig. 2.13: Sand dunes and salt crust at the station no. 3 (Abu Kammash).

In such areas, the minerals including aragonite ($CaCO_3$) and calcite ($CaCO_3$), gypsum ($CaSO_4.2H_2O$) and halite (NaCl) are deposited within sediments by capillary action and evaporation in response to the high temperatures. They are, therefore, diagenetic in origin. These salts create a hard, impermeable crust in a zone about half a meter below the surface, which along with high salinity, discourages all plant growth. The crust also impedes the drainage of surface water, so that after rains the sabkhas flood. The retained water then evaporates over time, leaving behind a white crust of halite. Anhydrite in the modern sabkha is stable only in the capillary zone above the water table; gypsum is the sulfate mineral that occurs below the water table. If ancient sabkhas were stacked one atop the other by a rising relative sea level, then as the capillary zone sediment subsided below the water table, the nodular anhydrite would reconvert to gypsum (Warren, 1989). Displacive nodular gypsum is growing in the carbonate-rich clastics sabkha of the most seaward depression. Landward, there is another larger interdunal depression with halite-encrusted, algal-mat fringed lakes and sabkhas containing lenticular gypsum crystal and some small gypsum nodules.

2.2.1.2. Carbonate-Sand-Mud

The carbonate, sand and mud contents of 20 samples (one sample of each unit) representing the studied sabkha profiles are given in table (2.1). Their petrographic nomenclatures have been assigned in Fig. (2.14). Most samples fall in the carbonate category, where few samples fall in the sand and mud categories. The highest

carbonate content is recorded in sample no. 3f at station no. 3 (Abu Kammash) where it is made up of algal limestone.

Table 2.1: Textural composition (wt %) of the non-evaporite sediments of sabkha profiles in the study area.

Location	Lithology	Sample No.	Carbonate	Sand	Mud
Surman	Algal limestone	1a	65.83	22.29	11.88
	Soil	1b	42.30	20.39	37.31
	Calcareous sand	1c	50.00	15.59	34.41
Zuwarah	Algal limestone	2a	55.50	18.21	26.29
	Calcareous sand	2b	50.10	21.50	28.40
	Soil	2c	48.29	20.40	31.31
	Calcareous sand	2e	51.20	19.00	29.80
Abu Kammash	Algal limestone	3a	65.21	19.50	15.29
	Calcareous sand	3b	52.79	10.00	37.21
	Soil	3c	42.00	22.00	36.00
	Calcareous sand	3d	50.19	15.30	34.51
	Algal limestone	3f	88.80	8.00	3.20
South Abu Kammash	Calcareous sand	4a	50.30	21.39	28.31
	Algal limestone	4b	56.80	3.50	39.70
	Soil	4c	48.40	10.00	41.60
Ras Jdeir	Algal limestone	5a	56.00	9.80	34.20
	Calcareous sand	5b	51.00	15.70	33.30
	Soil	5c	45.00	16.20	38.80
	Algal limestone	5d	54.40	10.00	35.60
	Soil	5e	43.00	21.00	36.00

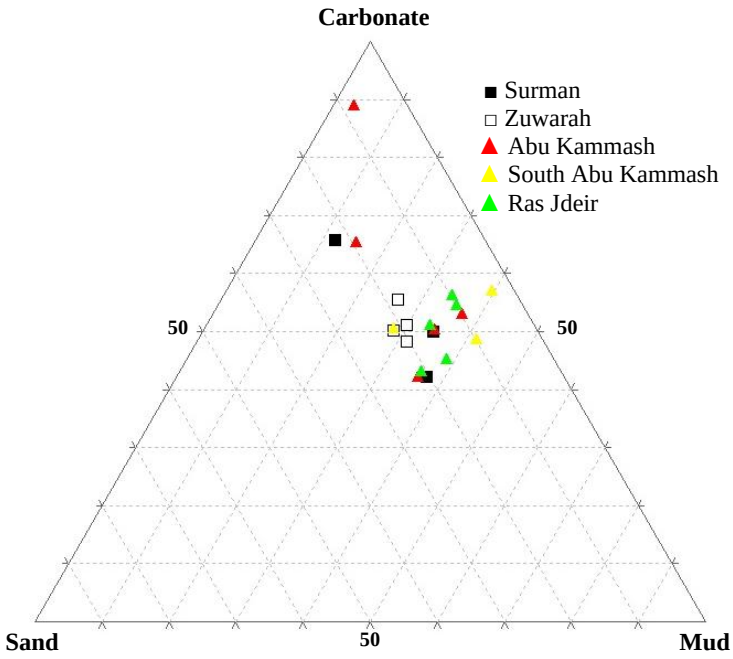

Fig. 2.14: Ternary plots of the carbonate-sand-mud of the non-evaporite sediments of sabkha profiles in the study area (fields after Fuchtbauer and Muller, 1970).

2.3. Mineralogy

The mineralogical composition for the studied sabkha sediments is chiefly composed of variable proportions of carbonates, quartz, feldspars, evaporites, clay minerals and heavy minerals.

2.3.1. Light minerals

2.3.1.1. Carbonates

In the studied samples, the carbonate fraction tends to increase in abundance with increasing grain size, where the medium and fine sand sizes are the most enriched while the very fine sand and silt sizes are markedly impoverished in carbonate (Fig. 3.15). The carbonate minerals are frequent including calcite and aragonite (Fig. 3.16). Aragonite is metastable mineral and it transforms during the diagenesis into calcite, only when aragonite is incorporated in the shells and skeletons of some marine organisms its stability is increased so that it can be preserved for a longer period.

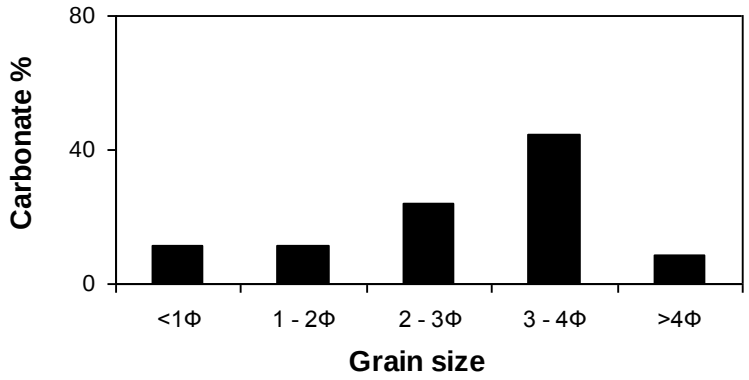

Fig. 2.15: Size distributions of the average carbonate content in the studied sabkha sediments.

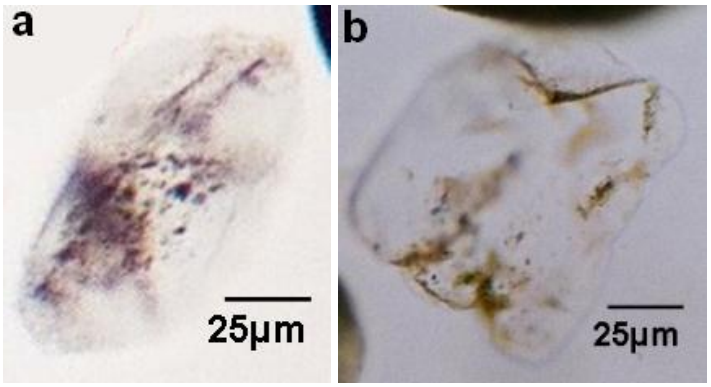

Fig. 2.16: Photomicrographs showing carbonate minerals (a) angular aragonite grai (sample 2a) and (b) colorless calcite grain (sample 1a).

2.3.1.2. Quartz

Quartz is one of the most abundant minerals in igneous, metamorphic and sedimentary rocks that make it useful for roundness and provenance analysis due to its relative durability and diverse varieties (Basu *et al*., 1975; Basu, 1985; Madhavaraju and Ramasamy, 1999; Kasper-Zubillaga *et al*., 2005; Kasper-Zubillaga, 2009). Quartz is mostly monocrystalline with uniform and undulatory extinction (Fig. 2.17). However, polycrystalline quartz grains are observed in some samples. According to Cherian *et al.*, (2004), the reduced percentage of the polycrystalline quartz is probably due to dilution by a fresh supply of monocrystalline quartz. Moreover, polycrystalline quartz grains are expected to disintegrate during the course of transportation from the source.

In the studied samples, quartz occurs either in the form of angular grains or as rounded grains (*see* Fig. 2.17). Roundness is an attribute in quartz that can be used to infer transport and abrasion in different sedimentary environments (Folk, 1978; Sagga, 1993; Kasper-Zubillaga *et al.*, 2005). According to Shine (2006), the rounded and well rounded quartz grains owe their shape largely to a longer distance of transportation and/or the multi-cycle origin of clastic sediments. On the other hand, moderate to high degree of sphericity of the quartz grains are indication of derivation from crystalline and older sedimentary rocks exposed in regions far from the basin of deposition (Rahman *et al.*, 2004). Some quartz grains show cracks, which could either be the feature inherited from the source material or could be due to long distance of transportation.

Fig. 2.17: Photomicrograph showing subrounded quartz grain (sample 2b).

2.3.1.3. Feldspar

In the present study, feldspars are detected in all samples. Microcline and orthoclase are common feldspars (Fig. 2.18). Microcline is mainly colorless and rectangular (*see* Fig. 2.18).

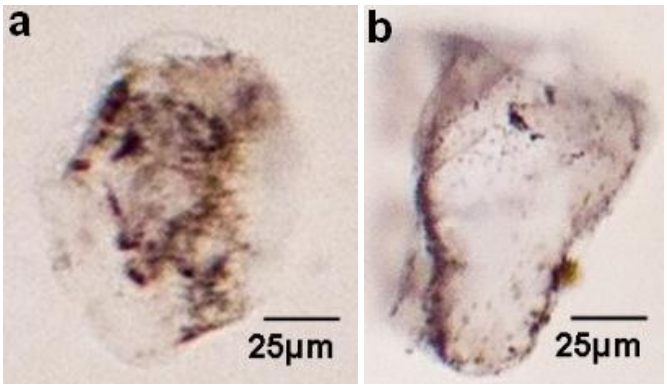

Fig. 2.18: Photomicrographs showing (a) rectangular microcline grain (sample 3c) and (b) colorless orthoclase grain (sample 3b).

2.3.1.4. Evaporites

In the present study, evaporites are detected in all samples. The detected evaporites are gypsum and halite. Microscopically, gypsum occurs as colorless irregular grains, while halite occurs as cubic grains (Fig. 2.19).

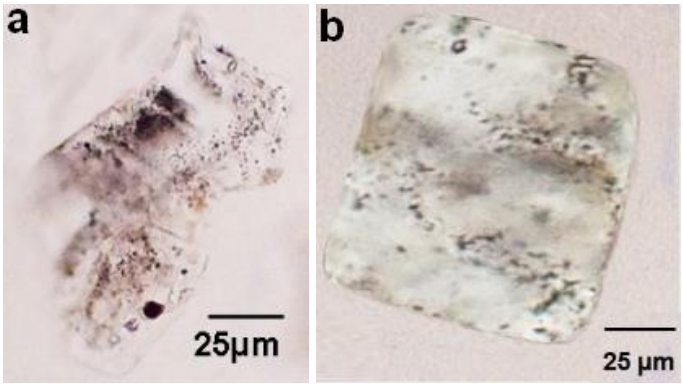

Fig. 2.19: Photomicrographs showing (a) colorless irregular gypsum grain (sample 4a) and (b) cubic halite grain (sample 5a).

2.3.1.5. Clay minerals

The clay size fraction was separated by sedimentation method for one soil sample and examined by XRD in oriented glycolated and heated mounts (Fig. 2.20). Clay minerals were identified by their characteristic basal *d*-spacings using the ASTM tables of the X-ray Powder Diffraction. The identified clay minerals in the studied soil sample are kaolinite and illite. The following is a brief discussion on the identified two minerals.

2.3.1.5.1. Kaolinite

It is detected in the analyzed sample on basis of its characteristic basal reflections at 7.15 Å (001) and 3.57 Å (002). The noticeable asymmetry of the (001) reflection towards the low angle side and of the (002) reflection towards the high angle side of X-ray pattern indicate that the kaolinite is of the disordered type.

2.3.1.5.2. Illite

It is identified by its strong first and third order basal reflections at about 10.0 Å and 3.34 Å, respectively in the untreated mounts, which remain unaffected after glycolation and heated to 550 ºC.

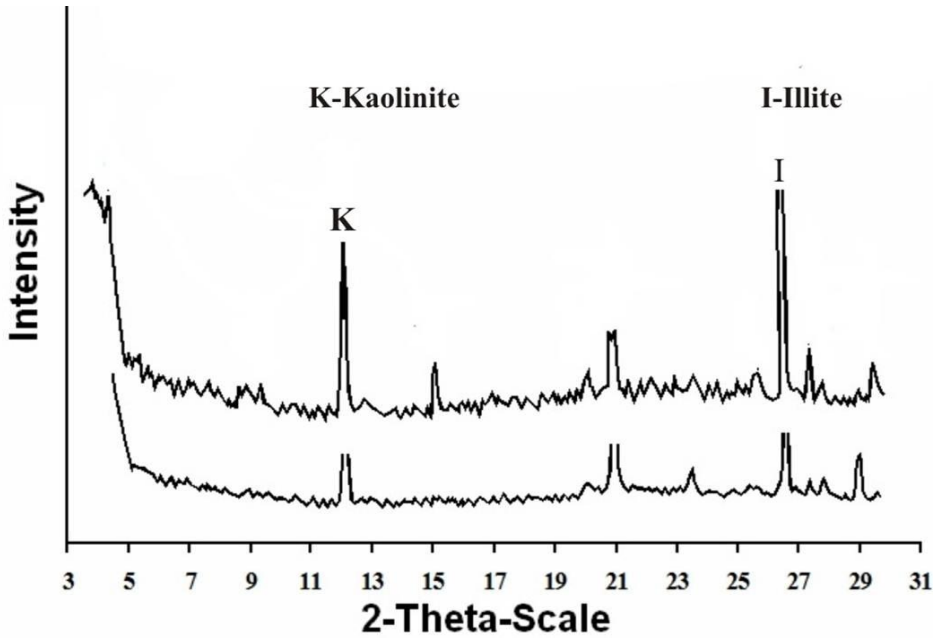

Fig. 2.20: X-Ray diffractograms of oriented clay mounts separated from soil (sample 2c).

2.3.2. Heavy minerals

Heavy minerals have been utilized by numerous authors to define provinces and to identify source rocks (Frihy and Komar, 1993; Pavicic *et al.*, 2000; Nilgun and Betel, 2005; Carranza-Edwards, *et al.*, 2009; Garzanti *et al.*, 2014; among others). Some studies (e.g., Pilkey, 1963; Morton and Hallsworth, 1999) demonstrate that particular association of heavy minerals do not necessarily reflect the mineralogy of the source area, because transport, weathering and post-depositional solution can

appreciably modify them. The formation of heavy mineral placers on beaches is achieved through mineral segregation by entrainment processes as a result of the greater susceptibility of the lighter minerals to fluid shear stress, allowing lighter minerals to be winnowed from more stable, heavier minerals (Peterson *et al.*, 1986). Some heavy minerals are unstable during chemical weathering but stable against physical weathering, thereby influencing the distribution of the heavy minerals. For example, Garnet is less stable to chemical weathering under acidic pH conditions, but more stable to transportation (Polozek and Ehrmann, 1998). Zircon is extremely stable during both chemical and physical weathering, and develops roundness only after substantial recycling. Under most conditions Epidote is stable to moderately stable. Pyroxenes and amphiboles are influenced by most kinds of weathering (Polozek, 2000). At beaches, heavy minerals are often concentrated in rather localized spots usually in the swash zone of the wave run-up or at eroding cliffs. Heavy minerals concentration on a beach can often be recognized from their dark color (red, purple or even black) (de Meijer *et al.*, 2001). Heavy mineral analysis benefits from the general chemical and mechanical stability of the minerals, although variations in properties exist. To be most effective, suites of minerals with similar hydrodynamic behavior (size, shape and density) should be used (Morton and Hallsworth, 1994).

In the present study, the microscopic examination and SEM-EDX show that the detected heavy minerals in the study area are opaques (ilmenite, magnetite, hematite and goethite) and non-opaques (zircon, augite, tourmaline, rutile, biotite, garnet, monazite, hornblende, staurolite and pistachite).

2.3.2.1. Opaque minerals

According to Ozdemir and Dunlop (2000) and Weibel and Friis (2004), the importance of opaque minerals is often neglected when investigating the diagenetic evolution of sediments. The opaque detrital minerals can often be some of the most sensitive minerals to environmental change and, therefore, give detailed information about the diagenetic conditions. In particular, iron-rich detrital minerals, such as hematite and magnetite are sensitive to reducing/oxidizing conditions during alteration (Weibel, 1998).

In the present study, the opaque minerals constitute the major part of the heavy fraction. The detected opaque minerals are ilmenite, magnetite, hematite and goethite (Figs. 2.21-23). Postdepositional weathering overprints include ferruginous mottling. These ferruginous mottles formed under spatially and temporally variable redoximorphic conditions, with Fe being derived from the weathering of Fe-bearing primary minerals, particularly ilmenite (Paine, 2005).

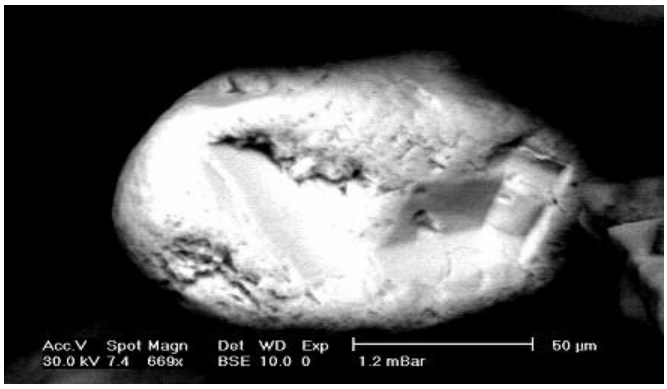

Fig. 2.21: BSE image showing magnetite partially replaced by hematite (sample 3b).

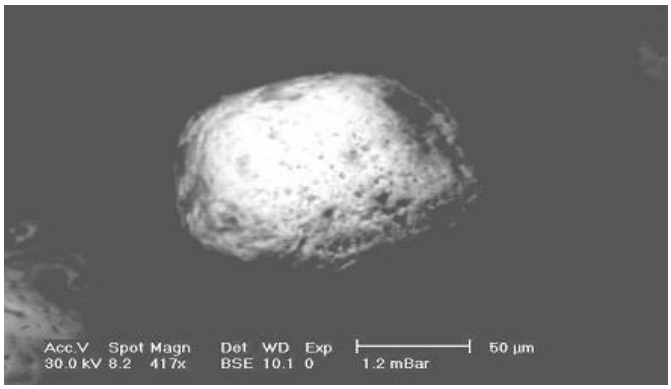

Fig. 2.22: BSE image showing magnetite completely replaced by goethite (sample 5e).

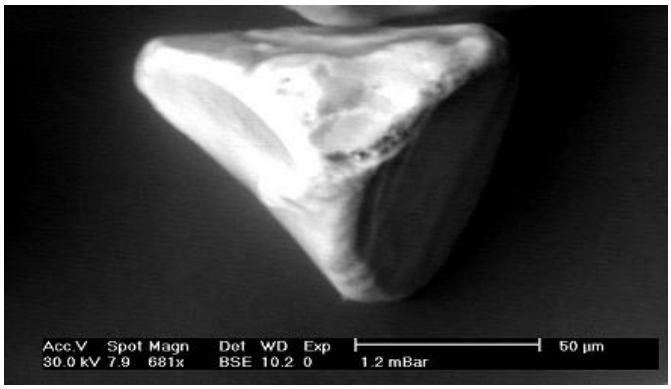

Fig. 2.23: BSE image showing homogeneous ilmenite grain (sample 5e).

2.3.2.2. Non-opaque minerals

2.3.2.2.1. Tourmaline

In the present study, tourmaline is the most abundant non-opaque mineral. It displays pink color (Fig. 2.24). Tourmaline has strong and distinctive pleochrism mainly from pink to brown. Most of the tourmaline grains are subrounded to well rounded (*see* Fig. 3.24). Rounded to well rounded tourmaline grains are polycyclic grains eroded from pre-existing siliciclastic deposits (Mange and Maurer, 1992). The occurrence of rounded to well rounded tourmaline may suggest that the sediments are being reworked from older sediments and the high frequency of tourmaline in the studied sediments may indicate derivation from metasomatized-rich tourmaline source rock.

Fig. 2.24: Photomicrograph of well rounded pink tourmaline grain (sample 3c).

.3.2.2.2. Garnet

Garnet grains display a wide variety of surface textures than other heavy minerals (Al Bakri, 1980). Garnet is fairly resistant to abrasion and to chemical attack (Deer *et al.*, 1997). In the present study, it is the second common non-opaque mineral. It occurs as cubic and rounded grains (Figs. 2.25 to 2.26). The EDX microanalysis data of garnet (Table 2.2) indicates a variety of andradite.

Fig. 2.25: Photomicrograph of cubic garnet grain (sample 2c).

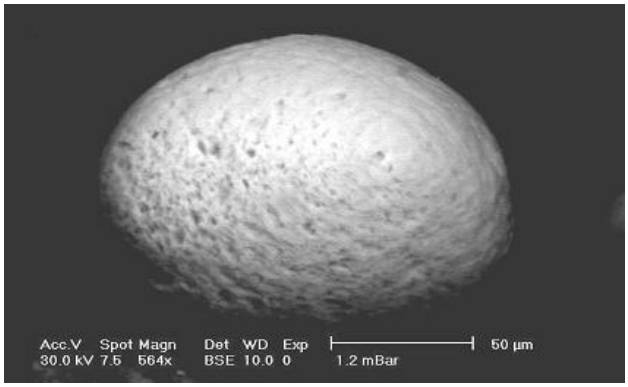

Fig. 2.26: BSE image showing rounded garnet grain (sample 5e).

Table 2.2: EDX microanalysis data (relative wt %) of garnet picked from grain size; 125-63µm (carbon and oxygen are excluded)

Elements	Location
	Ras Jdeir
Si	43.88
Ti	0.98
Al	11.00
Fe	25.00
Mn	0.43
Mg	3.96
Ca	10.65
K	3.12

2.3.2.2.3. Zircon

It is mostly present in the form of elongated prismatic bipyramidal grains (Figs. 2.27 to 2.28). Pinkish zircon is predominant and the colorless variety is occasional. It generally contains different amounts of inclusions as well as vacuoles or bubbles.

Fig. 2.27: Photomicrograph of prismatic bipyramidal zircon grain (sample 3c).

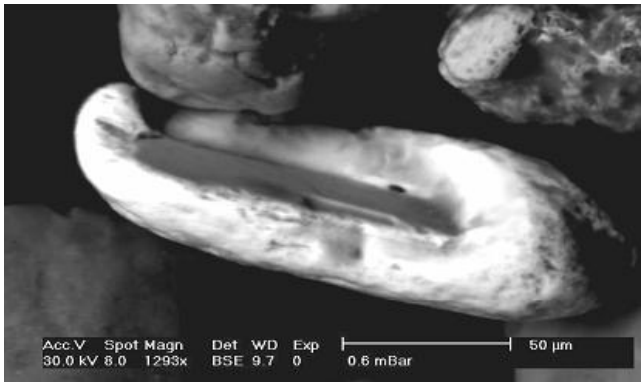

Fig. 2.28: BSE image of prismatic bipyramidal zircon grain (sample 3c).

2.3.2.2.4. Epidote

Pistachite is the only detected epidote mineral. It is characterized by yellowish green color. It forms subrounded to rounded grains (Figs. 2.29).

Fig. 2.29: Photomicrograph of subrounded pistachite grain (sample 3c).

2.3.2.2.5. Rutile

Rutile is among the most stable detrital minerals in sedimentary systems (Force, 1980; Morton, 1984; Margineanu *et al.*, 2014). According to Shaltami (2012) the presence of rutile suggests relative dominance of mafic sources in the hinterland. In the studied samples, it is present as elongated rounded or irregular grains (Figs. 2.30 to 2.31). It is characterized by reddish brown color. The EDX microanalysis data (Table 2.3) indicates that rutile is always impure, where Si, Al, Ca and Fe are common dilutants. The content of Ti represents up to about 83% of the total cations.

Fig. 2.30: Photomicrograph showing reddish brown elongated rounded rutile grain (sample 2b).

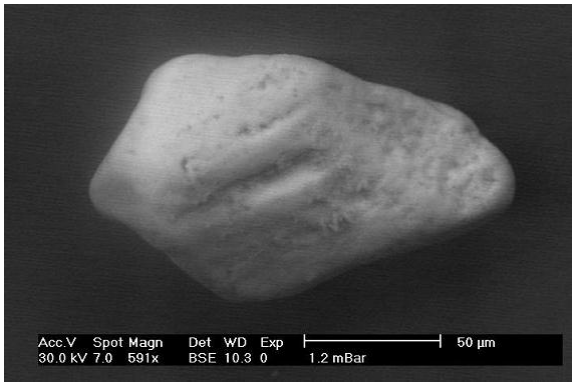

Fig. 2.31: BSE image of irregular rutile grain (sample 3c).

Table 2.3: EDX microanalysis data (relative wt %) of rutile picked from grain size; 125-63µm (carbon and oxygen are excluded)

Elements	Location
	Ras Jdeir
Si	9.25
Ti	83.00
Al	4.80
Fe	1.27
Mn	0.21
Ca	0.90
S	0.26

2.3.2.2.6. Amphibole

Brownish green hornblende is the most common abundant amphibole in the studied sediments (Fig. 2.32). It occurs as rounded to subround. The presence of hornblende in the sediments is often considered as an indication of chemical immaturity of the lithogenic sediments (Blatt *et al.*, 1972; Morton and Hallsworth, 1999; Parra *et la.*, 2012).

Fig. 2.32: Photomicrograph showing subrounded bluish green hornblende grain (sample 4c).

2.3.2.2.7. Mica

It is represented by biotite. It displays platy shape with rounded nature. It is characterized by brown color (Fig. 2.33).

Fig. 2.33: Photomicrograph showing subrounded brown biotite grain (sample 4c).

2.3.2.2.8. Staurolite

In the present study, staurolite occurs in the form of irregular subrounded grains characterized by their orange yellow color, straight extinction and moderate pleochrism (Fig. 2.34). Staurolite occurs in clastic sediments and it is a common constituent of heavy minerals assemblages due to its resistance to chemical weathering and diagenesis (Deer *et al.*, 1997).

Fig. 2.34: Photomicrograph of irregular subrounded staurolite grain (sample 3c).

2.3.2.2.9. Monazite

It is a widespread accessory mineral in felsic igneous rocks and amphibolite and granulite-facies metamorphic rocks, particularly politic schists and gneisses (Overstreet, 1967; Chang *et al.*, 1996; Rasmussen and Muhling, 2007). In the studied samples, it occurs as rounded, pale-yellowish grains (Fig. 2.35).

Fig. 2.35: Photomicrograph of rounded monazite grain (sample 5e).

2.3.2.2.10. Pyroxene

Augite is the only detected pyroxene mineral. It occurs as prismatic grains with pale green color (Fig. 2.36).

Fig. 2.36: Photomicrograph of prismatic augite grain (sample 3c).

2.4. Petrography

Petrographic studies comprise microscopic investigations of thin sections of limestone, gypsum and halite samples. Microfacies study of the studied limestone is achieved following the schemes of Dunham (1962).

The algal limestone in the studied core is classified as grainstone with dolomite grains, it characterized by dark to brown color, soft to moderately hard, medium grained, isopacheous calcite cement, The sample also characterize by presence of rich algal and shell fragments (Fig. 2.37).

Dolomitization is a process by which dolomite is formed when magnesium ions replace calcium ions in calcite. It is common for this mineral alteration into dolomite to take place due to evaporation of water in the sabkha area (Tucker, 2001), In the most of algal limestone in the core samples contains dolomite grains, because the magnesium ratio in sea water more than calcium and concentrated by evaporation the magnesium for dolomitization is supplied by seawater.

The nodular gypsum sample characterized by yellowish to dark color, soft to moderately hard, coarse grains with presence of anhydrite. This sample is also characterized by gypsum cross anhydrite plate (Fig. 2.38).

Dehydration of gypsum occurs with increasing salinity and temperature; hydration of anhydrite occurs with decreasing salinity and temperature (Selley, 2000). From the study area changes in temperature between seasons make changes some gypsum to anhydrite.

The blocky halite sample characterized by whitish to gray color, moderately hard, coarse grains, This sample is also characterized by polyhalite such as potassium and magnesium with fluid inclusions and anhydrite (Fig. 2.39).

seawater in the world's contains has a salinity of about 3.5% ((35 g/L), the most of ions between sodium and chlorine deposited halite and anther ions such as potassium and magnesium deposited polyhalite.

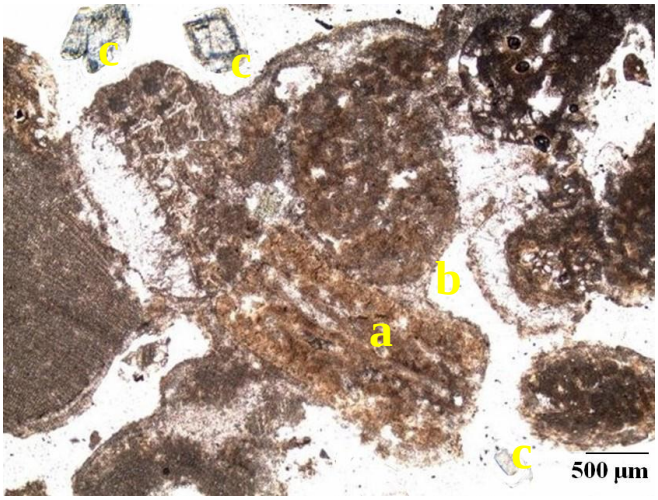

Fig. 2.37: Photomicrograph of the algal limestone (grainstone texture) shows; a) algal grain, b) isopachous cement, c) *dolomite grains (sample 1a).*

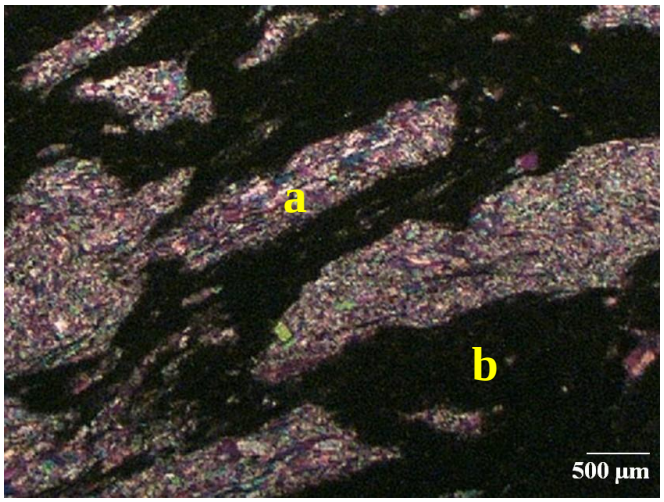

Fig. 2.38: Photomicrograph showing nodules of gypsum shows; a) *gypsum,* b) *anhydrite (sample 1d).*

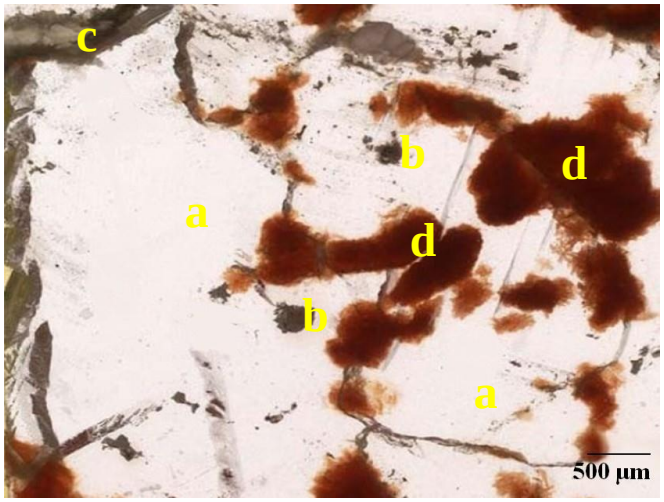

Fig. 2.39: Photomicrograph of large blocky halite shows; a) *blocky halite grains,* b) *few fluid inclusions,* c) *patches of grey anhydrite, d) patches of brown polyhalite,(sample 1e).*

CHAPTER THREE
GEOCHEMISTRY

3.1. Introduction

The present geochemical study is based on complete chemical analysis data of 31 samples of the sabkha sediments and 5 samples from the sabkha brines along the Mediterranean Coast from Surman to Ras Jdeir, Jifarah Plain, NW Libya. Analysis of major ions was done by Inductively Coupled Plasma-Association Emission Spectrometer (ICP-AES) technique, while analysis of major oxides and trace elements was done by inductively coupled plasma-mass spectrometry (ICP-MS) technique. The data include 7 major ions, 12 major oxides and 15 trace elements, as quoted in tables (3.1 to 3.6).

3.2. Statistical Treatment

The statistical treatment of the obtained data of the studied sabkha sediments involves descriptive statistics and correlation matrix using the SPSS© program. The correlation matrix (Table 4.7) suggests that the heavy metals are possibly of different sources. The Th and U are essentially related to terrestrial inputs. Table (4.8) indicates that the studied sediments may contain high concentrations of some elements such as Sr (4423 ppm), Ba, (293.94 ppm), Br (545.36 ppm), Ni (326.58 ppm), Co (340.5 ppm), Cu (317.42 ppm), Zn (326.25 ppm), V (354.27 ppm), Cr (359.91 ppm), Cd (1.94 ppm), Zr (392.17 ppm), Hf (351.65 ppm), Th (365.91 ppm), and U (350.74 ppm). These maximum values, besides the high standard deviation values represent derivation from multi-sources and possible contribution from mineralized sources at the hinterland in addition to enhanced anthropogenic input.

Table 3.1: Chemical analysis data (major ions in ppm) of the studied sabkha brines.

Location	Surman	Zuwarah	Abu Kammash	South Abu Kammash	Ras Jdeir
Sample No.	**1w**	**2w**	**3w**	**4w**	**5w**
Salinity	148.55	160.00	196.12	222.50	206.18
Ca^{2+}	1240.00	1180.09	1240.00	1140.18	1200.00
Mg^{2+}	5822.40	6600.00	8000.16	8600.00	5000.17
Na^{+}	44919.00	48198.81	60467.08	69388.62	68659.59
K^{+}	1650.12	1800.00	1680.00	2400.13	1800.00
Cl^{-}	79938.91	87773.72	110152.90	128550.00	113955.09
SO_4^{2-}	13996.80	13000.00	15500.10	12200.22	15000.15
HCO_3^{-}	120.15	140.08	160.00	160.00	120.15

Table 3.2: Chemical analysis data (major oxides in wt%, trace elements in ppm) of the studied sabkha sediments at the station no.1 (Surman).

Location	**Surman**				
Lithology	**Algal limestone**	**Soil**	**Calcareous sand**	**Gypsum**	**Halite**
Sample No.	**1a**	**1b**	**1c**	**1d**	**1e**
SiO_2	1.29	49.49	13.26	0.93	1.06
TiO_2	0.01	0.88	0.12	0.08	0.06
Al_2O_3	0.40	13.91	1.12	0.80	0.93
Fe_2O_3	0.49	5.53	1.33	0.71	0.33
MgO	1.38	0.88	0.94	0.65	0.19
CaO	55.70	12.80	42.43	32.18	2.66
Na_2O	0.03	0.11	0.09	0.22	44.67
K_2O	0.08	3.48	0.45	0.26	0.39
SO_3	0.19	0.20	0.05	45.12	0.03
Cl	0.03	0.13	0.09	0.23	45.00
P_2O_5	0.01	0.00	0.00	0.00	0.00
LOI	40.26	12.56	39.77	18.11	4.40
Total	99.87	99.97	99.65	99.29	99.72
Sr	4423.37	1012.91	3375.71	997.80	997.93
Ba	293.81	213.91	254.57	175.58	175.71
Br	20.12	9.18	30.21	90.00	544.67
Ni	23.14	58.34	20.31	14.70	326.06
Co	37.06	72.26	34.23	28.62	339.98
Cu	13.98	49.18	11.15	5.54	316.90
Zn	22.81	58.01	19.98	14.37	325.73
V	50.83	86.03	48.00	42.39	353.75
Cr	56.47	91.67	53.64	48.03	359.39
Pb	91.15	67.44	78.69	13.57	13.70
Cd	1.78	0.69	1.13	1.05	0.74
Zr	83.63	389.87	69.16	47.44	48.11
Hf	43.11	349.35	28.64	6.92	7.59
Th	57.37	363.61	42.90	21.18	21.85
U	42.20	348.44	27.73	6.01	6.68

Table 3.3: Chemical analysis data (major oxides in wt%, trace elements in ppm) of the studied sabkha sediments at the station no.2 (Zuwarah).

Location	**Zuwarah**						
Lithology	**Algal limestone**	**Calcareous sand**	**Soil**	**Gypsum**	**Calcareous sand**	**Gypsum**	**Halite**
Sample No.	**2a**	**2b**	**2c**	**2d**	**2e**	**2f**	**2g**
SiO_2	1.47	12.97	49.90	0.88	13.84	1.35	1.58
TiO_2	0.01	0.11	0.91	0.06	0.10	0.06	0.06
Al_2O_3	0.58	0.83	14.32	0.75	1.70	1.22	1.45
Fe_2O_3	0.44	1.45	5.66	0.80	1.51	0.94	0.49
MgO	1.19	1.23	0.41	1.04	0.36	0.53	0.22
CaO	55.51	42.72	12.33	32.57	41.85	32.06	2.70
Na_2O	0.03	0.09	0.09	0.19	0.09	0.36	44.00
K_2O	0.26	0.16	3.89	0.21	1.03	0.68	0.91
SO_3	0.22	0.05	0.18	45.51	0.05	45.00	0.03
Cl	0.03	0.09	0.10	0.21	0.09	0.38	44.33
P_2O_5	0.01	0.002	0.003	0.001	0.002	0.001	0.002
LOI	40.07	40.06	12.15	17.72	39.19	17.22	3.88
Total	99.82	99.76	99.94	99.94	99.81	99.80	99.65
Sr	4423.18	3376.00	1013.32	997.75	3375.13	998.22	998.45
Ba	293.62	254.86	214.32	175.53	253.99	176.00	176.23
Br	20.23	29.29	10.23	93.22	28.32	88.88	544.00
Ni	23.32	20.02	58.75	14.65	20.89	15.12	326.58
Co	37.24	33.94	72.67	28.57	34.81	29.04	340.50
Cu	14.16	10.86	49.59	5.49	11.73	5.96	317.42
Zn	22.99	19.69	58.42	14.32	20.56	14.79	326.25
V	51.01	47.71	86.44	42.34	48.58	42.81	354.27
Cr	56.65	53.35	92.08	47.98	54.22	48.45	359.91
Pb	90.96	78.98	67.85	13.52	78.11	13.99	14.22
Cd	1.59	1.42	0.22	1.44	0.55	0.93	0.78
Zr	84.76	70.29	391.00	48.57	65.95	44.23	41.57
Hf	44.24	29.77	350.48	8.05	25.43	3.71	1.05
Th	58.50	44.03	364.74	22.31	39.69	17.97	15.31
U	43.33	28.86	349.57	7.14	24.52	2.80	0.14

Table 3.4: Chemical analysis data (major oxides in wt%, trace elements in ppm) of the studied sabkha sediments at the station no.3 (Abu Kammash).

Location	**Abu Kammash**						
Lithology	**Algal limestone**	**Calcareous sand**	**Soil**	**Calcareous sand**	**Gypsum**	**Algal limestone**	**Halite**
Sample No.	**3a**	**3b**	**3c**	**3d**	**3e**	**3f**	**3g**
SiO_2	1.56	14.00	50.13	13.09	0.97	0.97	1.45
TiO_2	0.01	0.10	0.83	0.11	0.06	0.01	0.06
Al_2O_3	0.67	1.86	14.55	0.95	0.84	0.08	1.32
Fe_2O_3	0.44	1.55	5.58	1.38	0.90	0.61	0.52
MgO	1.12	0.20	0.24	1.11	0.91	1.51	0.35
CaO	55.44	41.69	12.16	42.60	32.44	55.83	2.83
Na_2O	0.03	0.09	0.10	0.09	0.15	0.03	44.11
K_2O	0.35	1.19	4.12	0.28	0.08	0.04	0.78
SO_3	0.20	0.05	0.17	0.05	45.38	0.20	0.03
Cl	0.03	0.09	0.10	0.09	0.16	0.03	44.42
P_2O_5	0.01	0.002	0.003	0.002	0.001	0.01	0.002
LOI	40.00	39.00	11.98	39.90	17.60	40.39	4.00
Total	99.86	99.82	99.96	99.65	99.49	99.71	99.87
Sr	4423.11	3374.97	1013.55	3375.88	997.84	4423.50	998.32
Ba	293.55	253.83	214.55	254.74	175.62	293.94	176.10
Br	20.09	30.00	9.91	25.27	87.94	19.54	544.11
Ni	23.41	21.05	58.98	20.14	14.74	22.82	326.45
Co	37.33	34.97	72.90	34.06	28.66	36.74	340.37
Cu	14.25	11.89	49.82	10.98	5.58	13.66	317.29
Zn	23.08	20.72	58.65	19.81	14.41	22.49	326.12
V	51.10	48.74	86.67	47.83	42.43	50.51	354.14
Cr	56.74	54.38	92.31	53.47	48.07	56.15	359.78
Pb	90.89	77.95	68.08	78.86	13.61	91.28	14.09
Cd	1.52	0.39	0.05	1.30	1.31	1.91	0.91
Zr	80.42	64.03	386.66	71.46	42.31	78.50	48.69
Hf	39.90	23.51	346.14	30.94	1.79	37.98	8.17
Th	54.16	37.77	360.40	45.20	16.05	52.24	22.43
U	38.99	22.60	345.23	30.03	0.88	37.07	7.26

Table 3.5: Chemical analysis data (major oxides in wt%, trace elements in ppm) of the studied sabkha sediments at the station no.4 (South Abu Kammash).

Location	**South Abu Kammash**				
Lithology	**Calcareous sand**	**Algal limestone**	**Soil**	**Gypsum**	**Halite**
Sample No.	**4a**	**4b**	**4c**	**4d**	**4e**
SiO_2	12.98	1.18	49.85	1.21	0.84
TiO_2	0.11	0.01	0.96	0.06	0.04
Al_2O_3	0.84	0.29	14.27	1.08	0.71
Fe_2O_3	1.44	0.53	5.73	0.77	0.47
MgO	1.23	1.30	0.36	0.67	0.14
CaO	42.72	55.62	12.28	32.20	2.62
Na_2O	0.09	0.03	0.10	0.10	45.36
K_2O	0.17	0.25	3.84	0.32	0.17
SO_3	0.05	0.20	0.21	45.14	0.03
Cl	0.09	0.03	0.11	0.10	45.67
P_2O_5	0.002	0.01	0.003	0.001	0.002
LOI	40.00	40.18	12.10	17.36	3.79
Total	99.72	99.63	99.81	99.01	99.84
Sr	3376.00	4423.29	1013.27	998.08	997.71
Ba	254.86	293.73	214.27	175.86	175.49
Br	30.00	18.96	8.73	90.09	545.36
Ni	20.03	23.03	58.70	14.98	325.84
Co	33.95	36.95	72.62	28.90	339.76
Cu	10.87	13.87	49.54	5.82	316.68
Zn	19.70	22.70	58.37	14.65	325.51
V	47.72	50.72	86.39	42.67	353.53
Cr	53.36	56.36	92.03	48.31	359.17
Pb	78.98	91.07	67.80	13.85	13.48
Cd	1.42	1.70	0.17	1.07	0.70
Zr	68.29	85.93	384.74	49.74	47.45
Hf	27.77	45.41	344.22	9.22	6.93
Th	42.03	59.67	358.48	23.48	21.19
U	26.86	44.50	343.31	8.31	6.02

Table 3.6: Chemical analysis data (major oxides in wt%, trace elements in ppm) of the studied sabkha sediments at the station no.5 (Ras Jdeir).

Location	**Ras Jdeir**						
Lithology	**Algal limestone**	**Calcareous sand**	**Soil**	**Algal limestone**	**Soil**	**Gypsum**	**Halite**
Sample No.	**5a**	**5b**	**5c**	**5d**	**5e**	**5f**	**5g**
SiO_2	1.41	13.22	47.72	1.83	48.60	0.58	0.72
TiO_2	0.01	0.10	0.98	0.01	0.97	0.07	0.05
Al_2O_3	0.52	1.08	12.14	0.94	13.00	0.45	0.59
Fe_2O_3	0.66	1.40	6.13	0.63	6.00	0.84	0.55
MgO	1.07	1.00	2.13	0.65	1.25	1.20	0.27
CaO	55.39	42.49	14.05	54.97	13.17	32.73	2.75
Na_2O	0.03	0.09	0.20	0.03	0.21	0.22	45.17
K_2O	0.27	0.41	1.71	0.69	2.59	0.05	0.05
SO_3	0.20	0.05	0.35	0.20	0.24	45.68	0.03
Cl	0.03	0.09	0.25	0.03	0.24	0.24	45.48
P_2O_5	0.01	0.002	0.003	0.01	0.003	0.001	0.002
LOI	39.95	39.77	13.87	39.53	13.00	17.87	3.92
Total	99.55	99.70	99.53	99.52	99.27	99.93	99.58
Sr	4423.06	3375.77	1011.14	4422.64	1012.00	997.45	997.59
Ba	293.50	254.63	212.14	293.08	213.00	175.23	175.37
Br	17.57	22.31	9.55	21.00	9.61	85.63	545.17
Ni	23.26	20.27	56.57	23.68	57.43	14.35	325.72
Co	37.18	34.19	70.49	37.60	71.35	28.27	339.64
Cu	14.10	11.11	47.41	14.52	48.27	5.19	316.56
Zn	22.93	19.94	56.24	23.35	57.10	14.02	325.39
V	50.95	47.96	84.26	51.37	85.12	42.04	353.41
Cr	56.59	53.60	89.90	57.01	90.76	47.68	359.05
Pb	90.84	78.75	65.67	90.42	66.53	13.22	13.36
Cd	1.47	1.19	1.94	1.05	1.06	1.60	0.83
Zr	82.76	69.83	392.17	84.30	389.00	46.57	45.66
Hf	42.24	29.31	351.65	43.78	348.48	6.05	5.14
Th	56.50	43.57	365.91	58.04	362.74	20.31	19.40
U	41.33	28.40	350.74	42.87	347.57	5.14	4.23

Table 3.7: Correlation matrix of the studied samples

Oxides and Elements	SiO_2	TiO_2	Al_2O_3	Fe_2O_3	MgO	CaO	Na_2O	K_2O	SO_3	Cl	P_2O_5	LOI	Sr	Ba	Br	Ni	Co	Cu	Zn	V	Cr	Pb	Cd	Zr	Hf	Th	U
SiO_2	1.00																									
TiO_2	0.98	1.00																								
Al_2O_3	0.97	0.99	1.00																							
Fe_2O_3	0.99	0.99	0.98	1.00																						
MgO	0.05	0.06	-0.03	0.09	1.00																					
CaO	-0.40	-0.49	-0.50	-0.43	0.52	1.00																				
Na_2O	-0.29	-0.22	-0.20	-0.29	-0.55	-0.66	1.00																			
K_2O	0.92	0.91	0.96	0.91	-0.25	-0.47	-0.17	1.00																		
SO_3	-0.33	-0.23	-0.24	-0.24	0.01	0.03	-0.21	-0.27	1.00																	
Cl	-0.29	-0.22	-0.20	-0.29	-0.55	-0.66	0.99	-0.17	-0.21	1.00																
P_2O_5	-0.19	-0.19	-0.16	-0.20	0.39	0.62	-0.24	-0.15	-0.40	-0.24	1.00															
LOI	-0.26	-0.40	-0.41	-0.32	0.48	0.94	-0.62	-0.38	-0.23	-0.62	0.55	1.00														
Sr	-0.33	-0.45	-0.44	-0.39	0.40	0.88	-0.39	-0.40	-0.43	-0.39	0.76	0.93	1.00													
Ba	-0.06	-0.17	-0.16	-0.12	0.46	0.81	-0.49	-0.14	-0.55	-0.49	0.81	0.88	0.96	1.00												
Br	-0.36	-0.28	-0.27	-0.36	-0.56	-0.66	0.99	-0.24	-0.08	0.99	-0.30	-0.65	-0.44	-0.57	1.00											
Ni	-0.16	-0.09	-0.07	-0.17	-0.55	-0.73	0.99	-0.05	-0.28	0.99	-0.23	-0.67	-0.44	-0.50	0.97	1.00										
Co	-0.16	-0.09	-0.07	-0.17	-0.55	-0.73	0.99	-0.05	-0.28	0.99	-0.23	-0.67	-0.44	-0.50	0.97	0.98	1.00									
Cu	-0.16	-0.09	-0.07	-0.17	-0.55	-0.73	0.99	-0.05	-0.28	0.99	-0.23	-0.67	-0.44	-0.50	0.97	0.98	0.98	1.00								
Zn	-0.16	-0.09	-0.07	-0.17	-0.55	-0.73	0.99	-0.05	-0.28	0.99	-0.23	-0.67	-0.44	-0.50	0.97	0.98	0.98	0.98	1.00							
V	-0.16	-0.09	-0.07	-0.17	-0.55	-0.73	0.99	-0.05	-0.28	0.99	-0.23	-0.67	-0.44	-0.50	0.97	0.98	0.98	0.98	0.98	1.00						
Cr	-0.16	-0.09	-0.07	-0.17	-0.55	-0.73	0.99	-0.05	-0.28	0.99	-0.23	-0.67	-0.44	-0.50	0.97	0.98	0.98	0.98	0.98	0.98	1.00					
Pb	0.28	0.15	0.15	0.22	0.45	0.64	-0.58	0.17	-0.64	-0.58	0.66	0.79	0.81	0.94	-0.68	-0.54	-0.54	-0.54	-0.54	-0.54	-0.54	1.00				
Cd	-0.44	-0.40	-0.48	-0.39	0.87	0.59	-0.27	-0.66	0.14	-0.27	0.45	0.48	0.48	0.40	-0.25	-0.33	-0.33	-0.33	-0.33	-0.33	-0.33	0.22	1.00			
Zr	0.96	0.98	0.99	0.98	0.11	-0.40	-0.27	0.92	-0.30	-0.27	-0.03	-0.31	-0.33	-0.04	-0.34	-0.14	-0.14	-0.14	-0.14	-0.14	-0.14	0.27	-0.35	1.00		
Hf	0.96	0.98	0.99	0.98	0.11	-0.40	-0.27	0.92	-0.30	-0.27	-0.03	-0.31	-0.33	-0.04	-0.34	-0.14	-0.14	-0.14	-0.14	-0.14	-0.14	0.27	-0.35	0.98	1.00	
Th	0.96	0.98	0.99	0.98	0.11	-0.40	-0.27	0.92	-0.30	-0.27	-0.03	-0.31	-0.33	-0.04	-0.34	-0.14	-0.14	-0.14	-0.14	-0.14	-0.14	0.27	-0.35	0.98	0.98	1.00
U	0.96	0.98	0.99	0.98	0.11	-0.40	-0.27	0.92	-0.30	-0.27	-0.03	-0.31	-0.33	-0.04	-0.34	-0.14	-0.14	-0.14	-0.14	-0.14	-0.14	0.27	-0.35	0.98	0.98	0.98

Table 3.8: Descriptive statistics of the studied sabkha samples (major oxides in wt%, trace elements in ppm).

Oxides and Elements	N	Minimum	Maximum	Mean	Std. Deviation
SiO_2	31	0.58	50.13	13.97	18.64
TiO_2	31	0.01	0.98	0.24	0.35
Al_2O_3	31	0.08	14.55	3.60	5.18
Fe_2O_3	31	0.33	6.13	1.89	2.01
MgO	31	0.14	2.13	0.85	0.49
CaO	31	2.62	55.83	31.15	19.24
Na_2O	31	0.03	45.36	8.23	16.66
K_2O	31	0.04	4.12	1.01	1.26
SO_3	31	0.03	45.68	9.72	18.14
Cl	31	0.03	45.67	8.29	16.77
P_2O_5	31	0.001	0.01	0.006	0.004
LOI	31	3.79	40.39	24.36	14.77
Sr	31	997.45	4423.50	2335.33	1508.22
Ba	31	175.23	293.94	227.90	47.03
Br	31	8.73	545.36	127.37	192.38
Ni	31	14.35	326.58	82.25	112.12
Co	31	28.27	340.50	96.17	112.31
Cu	31	5.19	317.42	73.09	112.55
Zn	31	14.02	326.25	81.92	112.40
V	31	42.04	354.27	109.94	122.09
Cr	31	47.68	359.91	115.58	112.17
Pb	31	13.22	91.28	55.92	32.95
Cd	31	0.05	1.94	1.09	0.51
Zr	31	41.57	392.17	131.42	131.31
Hf	31	1.05	351.65	90.90	131.57
Th	31	15.31	365.91	105.16	131.88
U	31	0.14	350.74	89.99	131.76

3.3. Geochemistry of brines

According to El-Omla and Aboulela (2012), there are three main origins for dissolved solids in brines: marine, anthropogenic and terrigenic. The most important anthropogenic sources in the study area include petroleum contamination and combustion of garbage. Na is generally considered as a tracer of the marine source; although a small contribution of terrigenic origin arises due to the input of crustal aerosols (Negrel and Roy, 1998; Han *et al.*, 2010). Differences in chemical composition of the studied water samples suggest different sources of the major ions.

The studied brine water samples were analyzed for Na^+, K^+, Ca^{2+}, Mg^{2+}, Cl^-, SO_4^{2-} and HCO_3^- (*see* Table 4.1). The salinity of the studied brines ranges from 148.55 to 222.5 ppm, reflecting, in agreement with Carpenter and Miller (1969), hypersaline water. The high salinity and rate of evaporation caused the precipitation of halite and the other less soluble evaporites. Shaheen (2006) related the high salinity of sabkha brines to old marine origin. In the present study, the increase in salinities is accompanied by rise in concentration of Na^+ and Cl^- ions and high concentration of Ca^{2+} and Mg^{2+}. This indicates that the studied brines reached saturated with NaCl, favoring halite precipitation.

The molar Na/(Na+Cl) and Ca/(Ca+SO_4) ratios are imperative to relate the genetic relationship (Hounslow, 1995). The majority of the studied brines are in the seawater (Fig. 4.1). The influence of evaporation in the study area shows compatibility with Jones *et al.*, (2009) work, indicating high ionic Cl+SO_4 balance (ranges from 93935 to 140750 ppm) in contrast to HCO_3 (ranges from 120.15 to 160 ppm) in the studied brines.

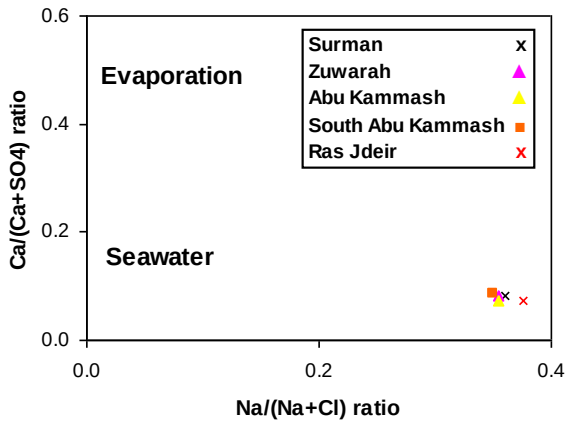

Fig. 3.1: Molar Ca/(Ca+SO_4) and Na/(Na+Cl) to differentiate water of different origin (fields after Hounslow, 1995).

Water having more HCO_3 and less Cl ions is the indication of natural water with no influx of pollution (Gholami and Srikantaswamy, 2009). The average HCO_3/Cl ratio is valuable to discriminate either seawater intrusion or rock weathering (El-Fiky, 2010). In the present study, the estimated average value of HCO_3/Cl ratio is 0.01,

which is slightly lower than the average seawater ratio (0.004). Probably the low ratio is due to the weathering of carbonate rocks, exposed in the study area.

The Cl^-/Na^+ ratios in the studied waters range from 1.66 to 1.85, all slightly higher than the average seawater value (Cl^-/Na^+=1.17), suggesting, in agreement with Shaltami (2014), that the studied brines may have not only marine but also terrigenic and anthropogenic origins. According to Tucker (2001) the NaCl for many halite deposits is derived from the evaporation of seawater. NaCl can also be concentrated from fresh continental waters, as in many salt lakes, or derived from the solution and recycling of older evaporites.

The SO_4^{2-} content ranges from 12200 to 15500 ppm. In agreement with Shaheen (2006), the author believes that the increase of sulfate content in the studied brines may be explained by a partial dissolution of some pre-existing gypsum.

The studied brine water samples show high concentration of K^+ (ranges from 1650 to 2400 ppm). It appears higher than that of average seawater value (11400 ppm, by Hunt, 1981). This may be attributed to partial dissolution of detrital illite which constitutes part of the clay mineral assemblages of the studied sabkha (*see* Fig. 3.19).

In the studied water samples, Ca^{2+} content ranges from 1140 to 1240 ppm, while Mg^{2+} content ranges from 5000 to 8600 ppm. In agreement with El-Omla and Aboulela (2012), the author believes that the depletion of Ca^{2+} in the studied brines is due to precipitation of gypsum (precipitation of calcium ions as $CaSO_4.2H_2O$), and the relative increase of Mg^{2+} is mainly due to the depletion of Ca^{2+}.

The Ca and Mg ions are significant to appraise the magnitude of seawater contribution. In the present study, the estimated average value of Ca/Mg ratio is 0.18, which may indicate, in agreement with Hem (1989), seawater influence.

3.4. Geochemistry of sabkha sediments

3.4.1. Major oxides

The major elements are generally considered somewhat mobile during weathering, transportation, and post-depositional processes (McLennan *et al.*, 1993). The

geochemistry of the major elements is mostly controlled by the mineral composition, which in its turn, strongly affected by the physico-chemical conditions prevailed during deposition. The concentration levels of major oxides in the studied sabkha sediments are represented in Figure (3.2).

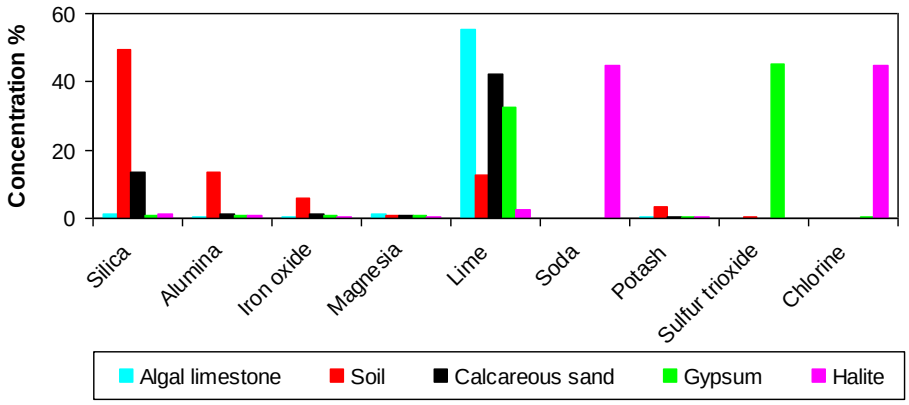

Fig. 3.2: Concentrations of major oxides from all analysis in the studied sabkha sediments.

Lime is, of course, the main constituent in all the studied sabkha sediments. Its average concentrations are 55.49, 12.80, 42.36, 32.36 and 2.71 % for the algal limestone, soil, calcareous sand, gypsum and halite, respectively. CaO displays weak negative correlations with SiO_2, Al_2O_3, K_2O, Fe_2O_3 and TiO_2 (r = -0.40, -0.50, -0.47, -0.43 and -0.49, respectively). Lime displays strong relation with SO_3 only in the gypsum samples (Fig. 3.3), suggesting that gypsum is the main carrier of CaO in the gypsum samples, while in the other samples CaO is contained in the carbonate minerals (calcite and aragonite).

CaO is weakly correlated with MgO (r = 0.52, Fig. 3.4). This relationship means that carbonate minerals are not the sole carrier of MgO. According to Tucker (2001), the requisite Mg/Ca ratios are < 1.2 for low-Mg calcite (< 4 mole % Mg substituting for Ca); 1.2 to 5.5 for high-Mg calcite, and > 2 for aragonite. Generally, high-Mg calcite and aragonite are the predominant mineralogies of organisms in modern seas (Mg/Ca ratio=5.2, Zankl, 1993). The present data shows that the detected calcite is low-Mg calcite (Mg/Ca ratio ranges from 0.01 to 0.15). Kitano and Furutsu (1959) showed that Mg, the major impurity in marine carbonates, exists in the calcite crystal structure as a solid solution series between calcite and dolomite, and that as the

Mg content increases in the solid solution series, the solubility of the calcite increases and eventually becomes greater than that of aragonite. As Mg exists in calcite and is incompatible with aragonite, the crystal type of calcium carbonate exerts a major control on the solution of natural carbonates.

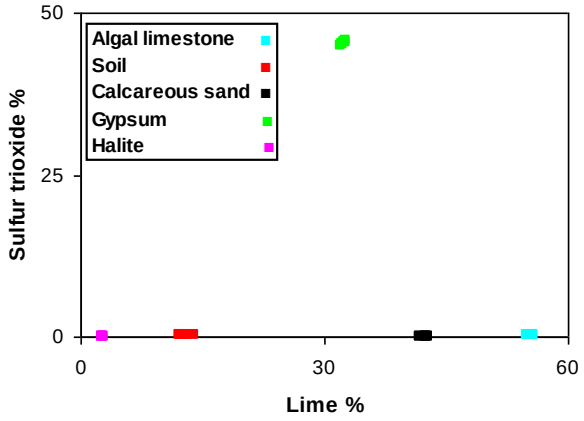

Fig. 3.3: Relationship between lime and sulfur trioxide in the studied sabkha sediments.

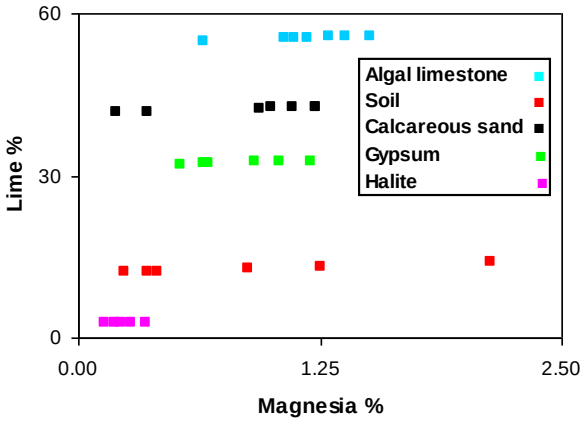

Fig. 3.4: Relationship between lime and magnesia in the studied sabkha sediments.

Silica is the second main constituent in the studied sabkha samples. It is averages are 1.39, 49.28, 13.34, 0.99 and 1.13 % in the algal limestone, soil, calcareous sand, gypsum and halite, respectively. The plot of silica versus alumina suggests that silica and alumina are strongly correlated in the studied samples (r = 0.97, Fig. 3.5). This reflects the occurrence of silica in both silicate and free silica modes.

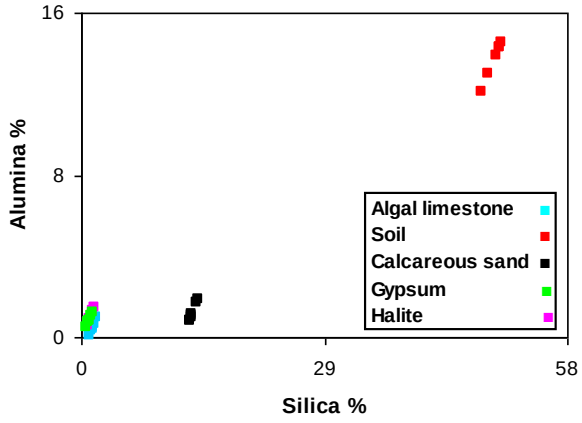

Fig. 3.5: Relationship between silica and alumina in the studied sabkha sediments.

The strong positive correlations between SiO_2 and the major oxides; TiO_2, K_2O and Fe_2O_3 (r = 0.99, 0.92 and 0.99, respectively) can be considered as indirect correlation as a result of intimate coherence between SiO_2 and Al_2O_3.

Aluminum concentration is a reasonably good measure of detrital flux. The studied algal limestone samples show lower concentrations of Al_2O_3 than the siliciclastic contaminated carbonates (Al_2O_3 concentration of 1.59 %, in Veizer, 1983). The strong correlation between K_2O and Al_2O_3 (r = 0.96, Fig. 3.6) suggests in agreement with Zhang (2004) and Nagarajan *et al.*, (2007) that they are bound to alumino-silicate minerals and associated phases and, therefore, they have been concentrated during weathering processes.

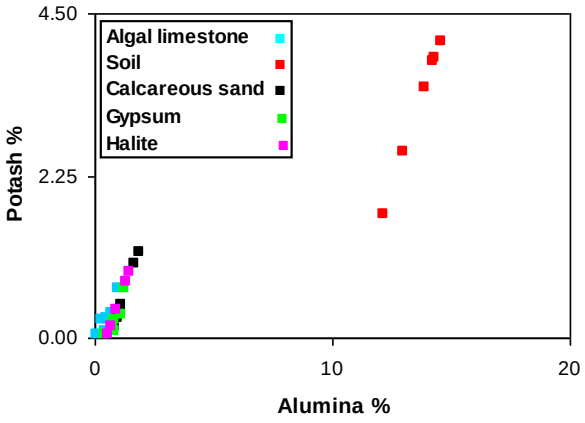

Fig. 3.6: Relationship between alumina and potash in the studied sabkha sediments.

The K_2O/Al_2O_3 ratio is important in sedimentary rocks in understanding the source of aluminum and its distribution between clay and feldspars minerals (Katongo *et al.*, 2004). The K_2O/Al_2O_3 ratios for clay minerals and feldspars are different (0.0 to 0.3, 0.3 to 0.9, respectively; Cox *et al.*, 1995). In the studied sabkha samples, the K_2O/Al_2O_3 ratio ranges from 0.08 to 0.86, indicating that both clay minerals and feldspars have a major role in the distribution of aluminum in the study area.

Froelich *et al.*, (1982) stated that there is an increasing amount of phosphorus, both organic and inorganic, supplied from the terrestrial to the marine environment, resulting in undesirable consequences for coastal ecosystems. Most of this increase can be traced to human activities. Information about the behavior of P in coastal regions is urgently needed in order to understand the impact of human activities on the coastal marine environment (Suzumural and Kamatani, 1995). The studied sabkha sediments show very low P_2O_5 content (ranges from 0.001 to 0.01 %).

Many authors (e.g., Gandhi and Raja, 2014) suggest that Na present in the original carbonate sediments can be modified greatly during diagenesis. The strong correlation between Na_2O and Cl (r = 0.99, Fig. 3.7) supports their accommodation in the form of halite. The author believes that the clay fraction may also contain a quotient of Na_2O. According to Lorenz and Gwosdz (2003) illite contains from 0.05 to 0.5 % Na_2O.

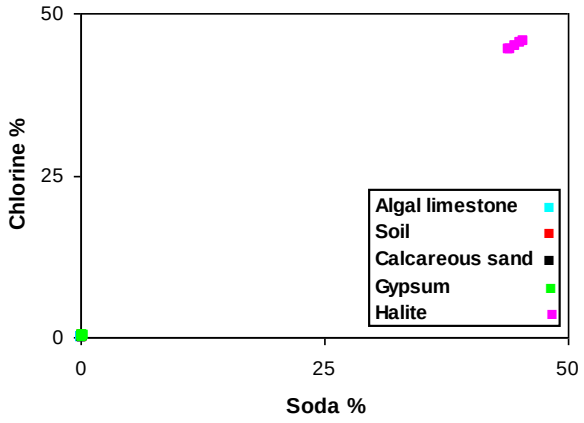

Fig. 3.7: Relationship between soda and chlorine in the studied sabkha sediments.

Titanium is mainly concentrated in phyllosilicates (Condie *et al.*, 1992) and is relatively immobile compared to other elements during various sedimentary processes and may strongly represent the source rocks (McLennan *et al.*, 1993). The studied sabkha samples, except the soil samples, have low TiO_2 contents. Figs (4.8-9) show that TiO_2 is positively correlated with Al_2O_3 and Fe_2O_3, suggesting in agreement with Condie *et al.*, (1992) and Carranza-Edwards *et al.*, (2009) that Ti is contained in both iron minerals and alumino-silicates. In agreement with Shaltami (2012) this assumption seems to be eligible for the studied samples as confirmed by the positive correlation between TiO_2 and the traditional terrigenous elements such as Zr (r = 0.98, Fig. 3.10).

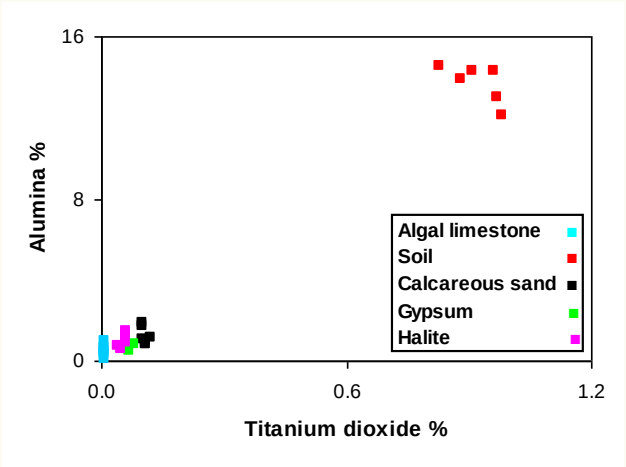

Fig. 3.8: Relationship between titanium dioxide and alumina in the studied sediments.

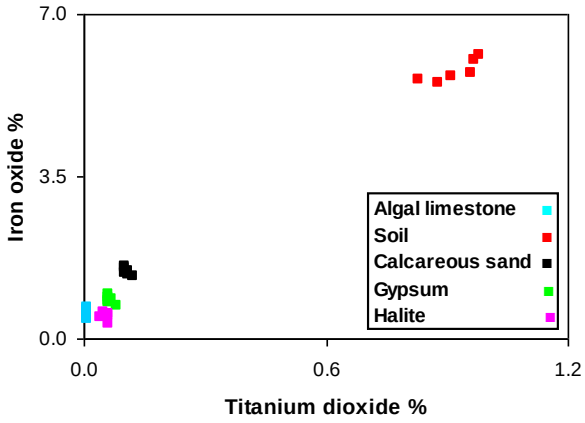

Fig. 3.9: Relationship between titanium dioxide and iron oxide in the studied sabkha sediments.

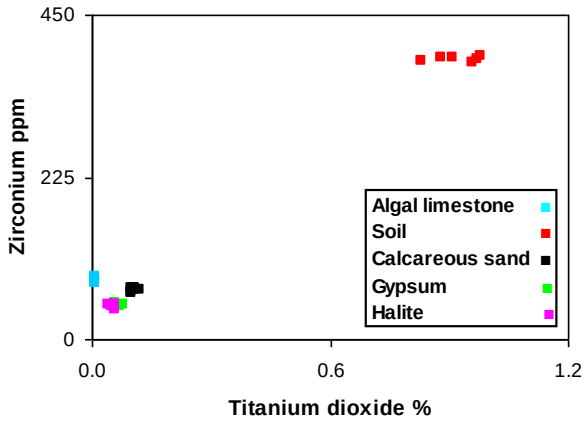

Fig. 3.10: Relationship between titanium dioxide and zirconium in the studied sabkha sediments.

The TiO_2/Zr ratio ranges from 1.16 to 1.27, 21.47 to 24.98, 14.32 to 17.35, 12.06 to 16.86 and 8.43 to 14.43 in the algal limestone, soil, calcareous sand, gypsum and halite, respectively. According to Garcia *et al.*, (1994), Asiedu *et al.*, (2000) and Malick and Ishiga (2015), mature sediments show a wide range of TiO_2/Zr variations whereas immature sediments show a more limited range of TiO_2/Zr variations.

The above arguments suggest that the major oxides CaO and MgO are the main constituents of the carbonate minerals; calcite and aragonite. SiO_2 is mainly in the form of quartz. Sometimes a high quotient of SiO_2 together with the oxides; Al_2O_3, K_2O and partly of Na_2O and Fe_2O_3 are essentially allocated within the structure of the alumino-silicate minerals. Part of Na_2O and the content of chlorine belong mainly to halite. Part of iron may be accommodated as oxides and hydroxides, such as ilmenite, magnetite, hematite and goethite. Part of CaO and the content of SO_3 are allotted within the gypsum structure. However, in summary, it can be stated that the geochemistry of the studied sabkha sediments is mainly controlled by the carbonate, silicate and sulfate components which represent a mixture of marine and continental sedimentation system.

3.4.2. Trace elements

The study of trace elements have become a vital part in modern petrology and more capable for discrimination between petrological processes than the major elements. The behavior of trace elements during sedimentary processes is complex due to many

factors including weathering, physical sorting, adsorption, provenance, diagenesis, and metamorphism (Papadopoulos *et al.,* 2015). The differences in trace elements content in the beach environment is probably due to sorting effect of the sediments or differences in source rocks (Shaltami, 2012).

3.4.2.1. Large Ion Lithophile Elements (LILE) or Low field strength elements (LFSE)

The term large ion lithophile element is frequently used, but poorly defined in the geochemical literature. LILE or LFSE are large cations of small charge and tend to be compatible with major elements. The low ionic potential (ratio of charge to ionic radius) makes these elements relatively soluble in aqueous solution. Because of their solubility, they are quite mobile during metamorphism and weathering (White, 2001). By this definition, LILE are Rb, Cs, Sr and Ba.

In the studied sabkha samples, two LILE, namely, Sr and Ba are analyzed. The ionic radius of Ba ion in its typical valence state (Ba^{2+}) makes isomorphous substitution possible only with Sr and generally not with the other members of the alkaline earth elements. Sr and Ba are known to be relatively mobile in natural oxic and aqueous environments (Dupre *et al*., 1996; Gaillardet *et al*., 1999). The correlation matrix indicates that Ba and Sr are mutual (r = 0.96), but they do not demonstrate any confident coherence to any of the analyzed major oxides.

Sr resides mainly in carbonate and feldspar (Yang *et al*., 2003). The Sr content in carbonate minerals may be used as an important chemical characteristic to identify their genesis. The aragonitic carbonate sediments are better accumulator of Sr than the calcitic ones, essentially because the higher co-ordination of Ca^{2+} ion in the former. On calcite, Sr^{2+} sorption occurs by electrostatic attraction as hydrated ions. However, at higher concentrations, precipitation of strontianite ($SrCO_3$) occurs, and Sr is likely to be less mobile (Parkman *et al.,* 1998). During an X-ray spectroscopic study of coral skeletons, Greegor *et al.,* (1997) found that 40% of Sr present as strontianite and 60% Sr substituted for Ca in aragonite structures. The geochemistry of Sr in calcium sulfate minerals has been extensively studied. Investigation has focused on various aspects: e.g., the strontium distribution in the gypsiferous sediments of coastal salt works (e.g., Rosell *et al.,* 1998); the interpretation of the characteristics of the mother

brines based on the strontium contents of the gypsum rocks (e.g., Peryt and Anczkiewicz, 2015) In marine evaporites the sulfate zones carry Sr, Ba and F (Denison *et al.*, 1998).

Ba, an alkaline earth element that lies in the same group with Ca, is conceived as a heavy metal. Ba^{2+} ions possess relatively low hydration energy, the property that yields more mobility in aqueous systems. According to Bancroft *et al*., (1977), literature resources indicate a scarcity of works addressing the topic of Ba^{2+} uptake by calcite and aragonite, in particular investigation of the kinetic aspects at the stage of surface precipitation. An earlier study of Ba^{2+} uptake on calcite using Electron Spectroscopy for Chemical Analysis (ESCA) reported that adsorption proceeds relatively slowly and that ion exchange of Ba^{2+} - Ca^{2+} is the prevailing mechanism, within the studied range of concentrations. There are a number of studies that focused on the mechanistic details of Ba^{2+} interaction with calcite and aragonite during the stage of crystal growth or dissolution for a specific set of experimental conditions (e.g., Reeder, 1996; Terakado and Taniguchi, 2006). According to Shahwan *et al*., (2002), the association of $CaCO_3$ (a mixture of calcite and aragonite) with montmorillonite clay enhanced the removal of aqueous Ba^{2+} ions by virtue of surface precipitation of $BaCO_3$. Aragonite showed higher removal capacity of Ba^{2+} and faster uptake kinetics than did calcite (Tunusoglu *et al.*, 2007).

The high Sr and Ba contents in the studied sabkha sediments indicate that Sr and Ba may be associated with carbonate minerals (calcite and aragonite) and gypsum. This assumption is confirmed by the strong correlation between Sr and Ba with CaO (r = 0.88 and 0.81, respectively, (Figures 3.11 to 3.12).

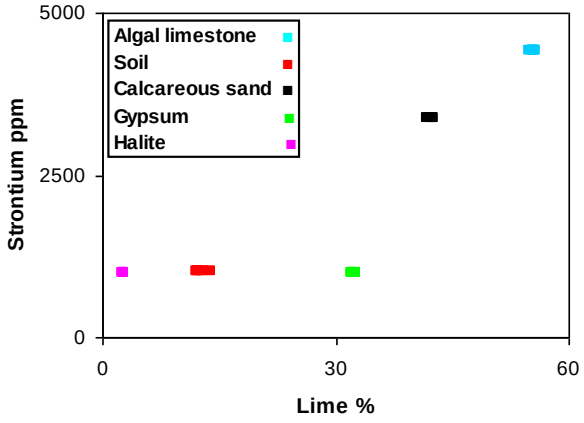

Fig. 3.11: Relationship between Lime and strontium in the studied sabkha sediments.

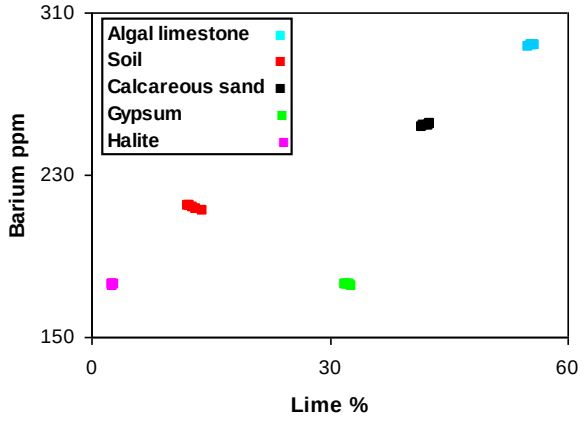

Fig. 3.12: Relationship between Lime and barium in the studied sabkha sediments.

3.4.2.2. High field strength elements (HFSE)

They are highly charged cations and often have appropriate size for many cation sites in minerals. Their charge is too high and requires one or more coupled substitution to maintain charge balance; this is generally energetically unfavorable (White, 2001). Thus HFSE are incompatible elements as they have high ionic potential, they are insoluble and tend to be very immobile during weathering and metamorphism. HFSE include six elements namely, Zr, Hf, Nb, Ta, Th and U. Lopez *et al.*, (2005) reported that the highest abundance of HFSE associates the silts which imply that accessory minerals, such as zircon and Nb-bearing phases are mainly concentrated in silt lithology. The high silica rocks tend to contain higher concentrations of HFSE than the basic rocks (Chandrajith, *et al.*, 2000). The HFSE provide a series of the

geochemical isovalents (Zr-Hf, Nb-Ta and Th-U). The mutual abundance and distribution of these isovalents in most geologic environments follow the popularly known Goldschmidt`s rule which is based on the charge and radius control (i.e., CHARAC). The non-CHARAC behavior of the isovalents is important in interpreting geological environments. The ratios between isovalents have the advantage that they do not change with time as isotopic ratios do (Condie, 2005). In the studied sabkha sediments, four HFSE, namely, Zr, Hf, Th and U are analyzed. The concentration of Zr in sandstone is typically higher than that in both mudrocks and limestone. Zr is generally transported with terrigenous influx in the form of heavy mineral (zircon). The two elements; Zr and Hf with atomic numbers 40 and 72, respectively, form an excellent example of a pair of elements having almost complete chemical similarity in spite of very different total electron numbers and atomic weights. In the present study, Zr and Hf are strongly correlated (r = 0.98, Fig. 3.13), suggesting that these elements are controlled by zircon.

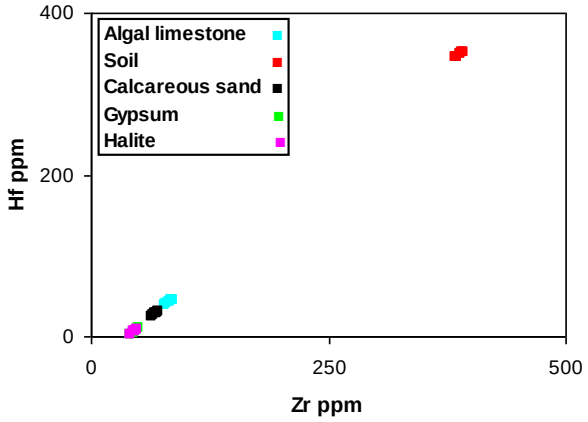

Fig. 3.13: Relationship between zirconium and hafnium in the studied sabkha sediments.

Ahrnes and Erlank (1969) concluded that the Zr/Hf ratio of detrital zircon varies depending on its provenance, with an increase in Hf content from basic to acidic rocks. According to Weyer *et al.*, (2002) the chondritic value of the Zr/Hf ratio is about 35. Table (3.9) shows that the gypsum and halite samples contain more Zr/Hf ratio than those of the algal limestone, soil and calcareous sand samples. The former shows limited range of Zr/Hf variations, while the gypsum and halite samples show a wide range of Zr/Hf variations (from 5.39 to 23.64 and 5.96 to 39.59, respectively).

Table 3.9: Ratios of selected isovalents in the studied sabkha sediments.

Location	Lithology	Sample No.	Zr/Hf	Th/U
Surman	Algal limestone	1a	1.94	1.36
	Soil	1b	1.12	1.04
	Calcareous sand	1c	2.41	1.55
	Gypsum	1d	6.86	3.52
	Halite	1e	6.34	3.27
Zuwarah	Algal limestone	2a	1.92	1.35
	Calcareous sand	2b	2.36	1.53
	Soil	2c	1.12	1.04
	Gypsum	2d	6.03	3.12
	Calcareous sand	2e	2.59	1.62
	Gypsum	2f	11.92	6.42
	Halite	2g	39.59	109.36
Abu Kammash	Algal limestone	3a	2.02	1.39
	Calcareous sand	3b	2.72	1.67
	Soil	3c	1.12	1.04
	Calcareous sand	3d	2.31	1.51
	Gypsum	3e	23.64	18.24
	Algal limestone	3f	2.07	1.41
	Halite	3g	5.96	3.09
South Abu Kammash	Calcareous sand	4a	2.46	1.56
	Algal limestone	4b	1.89	1.34
	Soil	4c	1.12	1.04
	Gypsum	4d	5.39	2.83
	Halite	4e	6.85	3.52
Ras Jdeir	Algal limestone	5a	1.96	1.37
	Calcareous sand	5b	2.38	1.53
	Soil	5c	1.12	1.04
	Algal limestone	5d	1.93	1.35
	Soil	5e	1.12	1.04
	Gypsum	5f	7.70	3.95
	Halite	5g	8.88	4.59

Under the prevailing surface conditions, U is mobile due to its oxidation to the soluble hexavalent state, as compared to the relatively immobile Th, which is concentrated in residual materials. Thus, the intensively weathered sediments display high Th/U ratios. In the present study, Th always dominates over U and they are mutually correlated (r = 0.98, Fig. 3.14). The author believes that Th and U in the studied samples are basically controlled by zircon. This assumption is confirmed by the strong correlation between Zr and both Th and U (Figs 3.15 to 3.16).

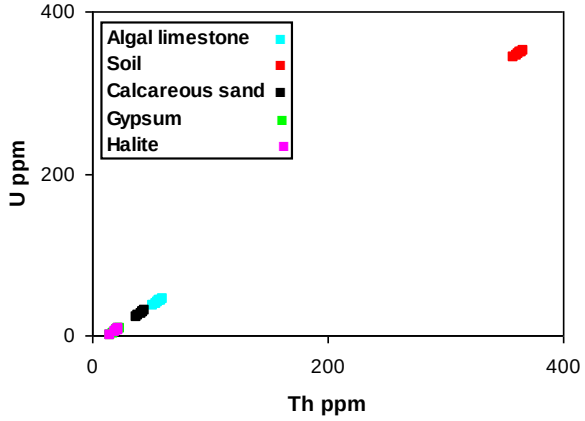

Fig. 3.14: Relationship between thorium and uranium in the studied sabkha sediments.

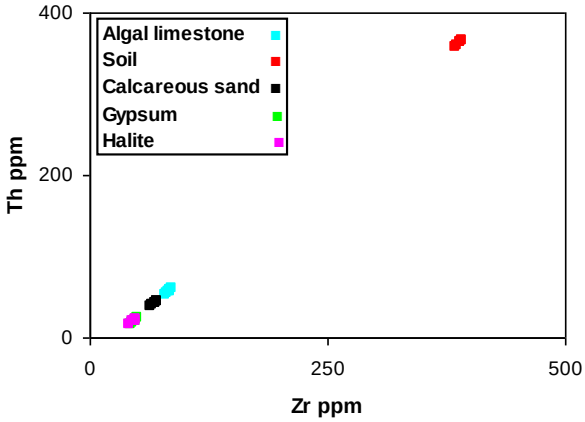

Fig. 3.15: Relationship between zirconium and thorium in the studied sabkha sediments.

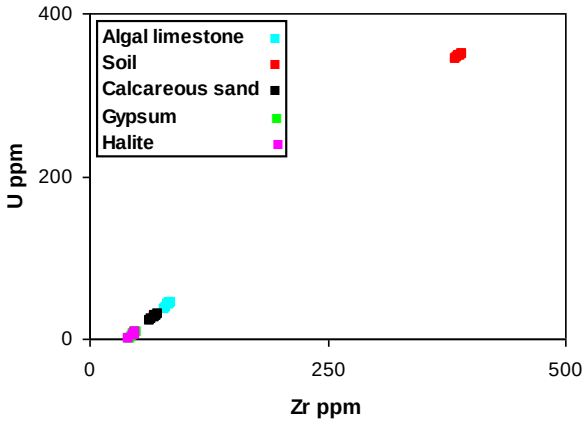

Fig. 3.16: Relationship between zirconium and uranium in the studied sabkha sediments.

The Th/U ratio is 3/1 in the endogenic rocks, while it is 1/1700 in the oceanic water (Faure, 1992), suggesting extreme relative enrichment of U in seawater. Table (3.9) shows that the algal limestone, soil and calcareous sand samples contain less Th/U ratio than those of the gypsum and halite samples. The halite at Zuwarah (sample no. 2g) and the gypsum at Abu Kammash (sample no. 3e) show very high Th/U ratio (109.36 and 18.24, respectively). In most cases, weathering and sedimentary recycling typically result in loss of U, leading to an elevation in the Th/U ratio. According to Asiedu *et al.,* (2000), in sedimentary rocks, Th/U values higher than 4 may indicate intense weathering in source areas or sediment recycling (i.e., derivation from older sedimentary rocks).

The U/Th ratio is used as a redox parameter in many studies (e.g., Jones and Manning, 1994; Nagarajan *et al.,* 2007; Shaltami, 2012). U/Th ratios below 1.25 suggest oxic conditions of deposition, whereas values above 1.25 indicate suboxic and anoxic conditions (Nath *et al*., 1997). According to Nagarajan *et al.,* (2007), in the Arabian Sea, sediments below the oxygen minimum zone (OMZ) show high U/Th (>1.25) ratios, whereas the sediments above the OMZ exhibit low U/Th (<1.25) ratios. The studied sabkha sediments show low values of U/Th ratio (from 0.01 to 0.96), which indicate that these sediments were deposited in oxic conditions.

3.4.2.3. Heavy metals

According to Anderson (2003), heavy metals are stable metals or metalloids and cannot be degraded or destroyed. Therefore, they tend to accumulate in soils and sediments. However, anthropogenic activities have drastically altered the biochemical and geochemical cycles and the balance of some heavy metals. The analyzed heavy metals in the studied sabkha sediments are Br, Ni, Co, Cu, Zn, V, Cr, Pb and Cd.

In the present study, Br, Ni, Co, Cu, Zn, V and Cr are mutually correlated. These elements are strongly correlated with Na_2O and Cl, suggesting, in agreement with Leri *et al*., (2010), that halite and alumino silicates are the sole carriers of Br, Ni, Co, Cu, Zn, V and Cr.

According to Leri and Myneni (2012) the chemistry of bromine in the environment has been presumed altogether unreactive. In seawater, bromine has long been

classified as a conservative element and thought to exist in the form of inorganic bromide. In terrestrial soils, bromide is believed to be so unreactive that it is routinely used as a hydrological tracer. Halite of marine origin can be distinguished by its high Br values (> 50 ppm) compared with non-marine and recycled halite which has much lower Br concentrations (Holser, 1966). The studied halite samples show higher concentrations of Br (544.66 ppm, in average) than the other sediments.

The Cu/Zn, V/Cr, V/Ni and Ni/Co ratios are used as a redox parameter in many studies (e.g., Jones and Manning, 1994; El-Kammar *et al.*, 2007; Shaltami, 2015). According to Hallberg, (1976) the increasing value of the Cu/Zn ratio indicates a reducing depositional condition while decreasing Cu/Zn values suggest increased oxidizing conditions. Ratio of V/Cr above 2 indicates anoxic conditions, whereas values below 2 suggest more oxidizing conditions (Jones and Manning, 1994). According to El-Kammar *et al.*, (2007), weathering will lead to dissolution of V rather than Ni and the ratio (V/Ni) will, accordingly, decrease. The reducing condition causes reduction and reprecipitation of V, i.e. increasing V/Ni ratio. Ni/Co ratios below 5 indicate oxic environments, whereas ratios above 5 suggest suboxic and anoxic environments (Jones and Manning, 1994). Thus, the prevailing well oxidizing coastal environments are well expresses by the low Cu/Zn, V/Cr, V/Ni and Ni/Co ratios (0.66, 0.92, 2.05 and 0.69 in average, respectively).

According to Callahan *et al.*, (1979) Cd precipitates with carbonate minerals, as stable solid compounds or co-precipitates with hydrous iron oxides, is less likely to be mobilized by resuspension of sediments or biological activity. According to Chada *et al.*, (2005) the uptake of Cd^{2+} by calcite was determined to be greater than that of Pb^{2+} under similar experimental conditions. In the studied sabkha sediments, Pb and Cd are positively correlated with CaO (except in the soil samples, Figs. 3.17 to 3.18) and they do not demonstrate any confident coherence to any of the analyzed major oxides. These relationships mean that Pb and Cd may be contained in carbonate minerals and gypsum.

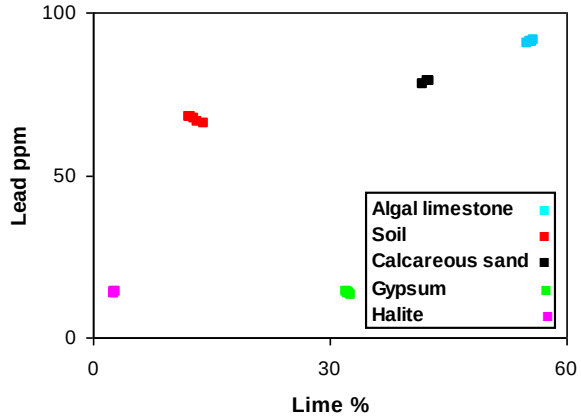

Fig. 3.17: Relationship between lime and lead in the studied sabkha sediments.

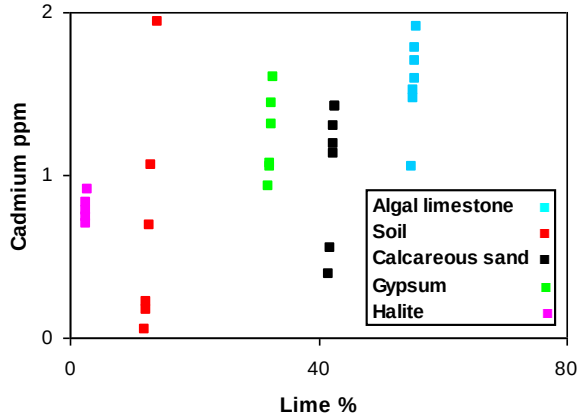

Fig. 3.18: Relationship between lime and cadmium in the studied sabkha sediments.

CHAPTER FOUR
SUMMARY AND CONCLUSIONS

The present work attempts to characterize the mineralogy and geochemistry of the sabkha brines and sediments along the Mediterranean Coast from Surman to Ras Jdeir, Jifarah plain, NW Libya. Based on the geomorphological characteristics, the studied coastal area is submerged shore. It is characterized by low relief or almost flat coastal area with nearly straight shorelines. It extends from Marsa Zuwaghah to the territorial boundary of Tunisia for about 75 km long. This coastal area is characterized by sandy beach, coastal dunes, thin sand sheets, sabkha deposits and scattered patches of Jifarah and Gargaresh formations.

Minerallogically, the mineral composition for the studied sabkha sediments is chiefly composed of variable proportions of carbonates (calcite and aragonite), quartz, feldspars (microcline and orthoclase), evaporites (gypsum and halite), clay minerals (kaolinite and illite) and heavy minerals. Quartz is mostly monocrystalline with uniform and undulatory extinction. It occurs either in the form of angular grains or as rounded grains. Gypsum occurs as colorless irregular grains, while halite occurs as cubic grains.

The detected heavy minerals are opaques (ilmenite, magnetite, hematite and goethite) and non-opaques (zircon, augite, tourmaline, rutile, biotite, garnet, monazite, hornblende, staurolite and pistachite). The opaque minerals constitute the major part of the heavy fraction. Tourmaline is the most abundant non-opaque mineral. It displays pink color. Tourmaline has strong and distinctive pleochrism mainly from pink to brown. Most of the tourmaline grains are subrounded to well rounded. Garnet is the second common non-opaque mineral. It occurs as cubic and rounded grains. The EDX microanalysis data of garnet indicates a variety of andradite. Pinkish zircon is predominant and the colorless variety is occasional. It generally contains different amounts of inclusions as well as vacuoles or bubbles. Pistachite is the only detected epidote mineral. It is characterized by yellowish green color. It forms subrounded to rounded grains. Rutile is present as elongated rounded or irregular grains. It is characterized by reddish brown color. The EDX microanalysis data indicates that

rutile is always impure, where Si, Al, Ca and Fe are common dilutants. The content of Ti represents up to about 83% of the total cations. Brownish green hornblende is the most common abundant amphibole. Mica is represented by biotite. It displays platy shape with rounded nature. It is characterized by brown color. Staurolite occurs in the form of irregular subrounded grains characterized by their orange yellow color, straight extinction and moderate pleochrism. Augite is the only detected pyroxene mineral. It occurs as prismatic grains with pale green color.

Petrographically, the studied algal limestone contains dolomite grains, the nodular gypsum and anhydrite is the most common form and the halite crust contains blocky halite grains with anhydrite, polyhalite and fluid inclusions.

Geochemically, the salinity of the studied brines ranges from 148.55 to 222.5 ppm, reflecting hypersaline water. The molar Na/(Na+Cl) and Ca/(Ca+SO_4) ratios are imperative to relate the genetic relationship. The majority of the studied brines are in the seawater. The estimated average value of HCO_3/Cl ratio is 0.01, which is slightly lower than the average seawater ratio (0.004). Probably the low ratio is due to the weathering of carbonate rocks, exposed in the study area.

The Cl^-/Na^+ ratios in the studied waters range from 1.66 to 1.85, all slightly higher than the average seawater value (Cl^-/Na^+=1.17), suggesting that the studied brines may have not only marine but also terrigenic and anthropogenic origins.

The SO_4^{2-} content ranges from 12200 to 15500 ppm in the studied brines. The author believes that the increase of sulfate content in the studied brines may be explained by a partial dissolution of some pre-existing gypsum.

The studied brine water samples show high concentration of K^+ (ranges from 1650 to 2400 ppm). It appears higher than that of average seawater value (11400 ppm). This may be attributed to partial dissolution of detrital illite which constitutes part of the clay mineral assemblages of the studied sabkha.

In the studied water samples, Ca^{2+} content ranges from 1140 to 1240 ppm, while Mg^{2+} content ranges from 5000 to 8600 ppm. The author believes that the

depletion of Ca^{2+} in the studied brines is due to precipitation of gypsum (precipitation of calcium ions as $CaSO_4.2H_2O$), and the relative increase of Mg^{2+} is mainly due to the depletion of Ca^{2+}.

In the studied sabkha sediments, CaO displays weak negative correlations with SiO_2, Al_2O_3, K_2O, Fe_2O_3 and TiO_2. CaO displays strong relation with SO_3 only in the gypsum samples, suggesting that gypsum is the main carrier of CaO in the gypsum samples, while in the other sabkha sediments CaO is contained in the carbonate minerals (calcite and aragonite).

Cao is strongly correlated with Ba, Sr, Pb and Cd. This relationship means that carbonate minerals and gypsum are the sole carriers of Ba, Sr, Pb and Cd.

In the studied sediments, Br, Ni, Co, Cu, Zn, V and Cr are mutually correlated. These elements are strongly correlated with Na_2O and Cl, suggesting that halite and alumino silicates are the sole carriers of Br, Ni, Co, Cu, Zn, V and Cr.

The studied gypsum and halite samples contain more Zr/Hf ratio than those of the algal limestone, soil and calcareous sand samples. The former shows limited range of Zr/Hf variations, while the gypsum and halite samples show a wide range of Zr/Hf variations (from 5.39 to 23.64 and 5.96 to 39.59, respectively). The author believes that Th and U in the studied samples are basically controlled by zircon. This assumption is confirmed by the strong correlation between Zr and both Th and U. The algal limestone, soil and calcareous sand samples contain less Th/U ratio than those of the gypsum and halite samples. The halite at Zuwarah (sample no. 2g) and the gypsum at Abu Kammash (sample no. 3e) show very high Th/U ratio (109.36 and 18.24, respectively). In most cases, weathering and sedimentary recycling typically result in loss of U, leading to an elevation in the Th/U ratio. In sedimentary rocks, Th/U values higher than 4 may indicate intense weathering in source areas or sediment recycling (i.e., derivation from older sedimentary rocks).

The studied sabkha sediments show low Cu/Zn, V/Cr, V/Ni and Ni/Co and U/Th ratios which suggest that these sediments were deposited in a well oxygenated environment.

Recommendations

This project it may needs further study, especially the comparison between periods of dry and humidity in different seasons and its impact on content mineralogy and geochemistry in sabkha and comparison between seawater and brines in sabkha.

References

Abdel Galil, M. and El-Fergany, E. (2011): Sedimentological significance and brine chemistry of Recent coastal sabkha, Northwest Libya. JKAU: Mar. Sci.; 22(2): 135-158.

Ahrens, L.H. and Erlank, A.J. (1969): Hafnium, Section B-O, in Wedephol, K.H., ed., Handbook of Geochemistry (Vol. 11/5): New York, Springer-Verlag.

Al Bakri, D.H. (1980): The sediments of the Hamber Estuary and the adjacent coastline. PH.D. Thesis. University of Sheffield. England.

Al Farrah, N.; Martens, K. and Walraevens, K. (2011): Hydrochemistry of the Upper Miocene-Pliocene-Quaternary aquifer complex of Jifarah plain, NW-Libya. Geologica Belgica; 14(3-4): 159-174.

Allan, J.A. (1989): Water resource evaluation and development in Libya 1969–1989. Libyan Studies; 20: 235-242

Allbed, A. and Kumar, L. (2013): Soil salinity mapping and monitoring in arid and semi-arid regions using remote sensing technology: A review. Advances in Remote Sensing; 2: 373-385.

Al-Yafei, K. and Al-Bakri, D. H. (2014): Geology of Qatar. Publication of The Environmental Studies Center, Doha, Qatar.

Anketell, J. M. and Ghellali, S. M. (1991): The Jifarah Formation – Aeolian and fluvial deposits of Quaternary age, Jifarah plain. In (Salem, M. J. and Belaid, M. N. editors): The Geology of Libya, V: 1967-2013.

Anderson, D. (2003): Introduction to heavy metal monitoring. Natural Environmental Research Council. CEH. 1p.

Asiedu, D.K.; Suzuki, S.; Nogami, K. and Shibata, T. (2000): Geochemistry of Lower Cretaceous sediments, Inner Zone of Southwest Japan: Constraints on provenance and tectonic environment. Geochemical Journal; 34: 155-173.

Bancroft, G.M.; Brown, J.R. and Fyfe, W.S. (1977): Quantitative X-ray photoelectron spectroscopy (ESCA): Studies of Ba^{2+} sorption on calcite. Chem. Geol.; 19: 131–144.

Basu, A. (1985): Reading provenance from detrital quartz, in Zuffa G.G.I., Provenance of Arenites: Nato Series C.; 148: 231-247.

Basu, A. Young, S. W. Suttner, L. J.; James, W. C. and Mack, G. H. (1975): Reevaluation of the use of undulatory extinction and polycrystallinity in detrital quartz foe provenance interpretation: Journal of Sedimentary Petrology; 45: 873-882.

Blatt, H. Middleton, G. and Murray, R. (1972): Origin of sedimentary rocks, Prentice Hall Inc., Englewood Cliffs, New Jersey; 634p.

Callahan, M. A.; Slimak, M. W. and Gable, N. W. (1979): Water-related fate of 129 priority pollutants. Washington, DC: U.S. Environmental Protection Agency, Office of Water Planning and Standards. EPA-440/4-79-029a.

Carpenter, A.B. and Miller, J. C. (1969): Geochemistry of saline subsurface water, saline country (Missouri). Chemical Geology; 14: 135-167.

Carranza-Edwards, A.; Kasper-Zubillaga, J.J.; Rosales-Hoz, L.; Morales-de la Garza, E.A. and Lozano-Santa Cruz, R. (2009): Beach sand composition and provenance in a sector of the southwestern Mexican Pacific. Revista Mexicana de Ciencias Geológicas; 26(2): 433-447.

Carver, R. E. (1971): Procedures in sedimentary petrology: John Wiley and Sons, Inc. New York, 653pp.

Chada, V.G.; Hausner, D.B.; Strongin, D.R.; Rouff, A.A. and Reeder, R.J. (2005): Divalent Cd and Pb uptake on calcite cleavage faces: an XPS and AFM study. J. Colloid Interface Sci.; 288(2): 350-60.

Chandrajiath, R.; Dissanayake, C.B. and Tobschall, H.J. (2000): Enrichment of high-field strength elements in stream sediments of a granulite terrain in Sri Lanka-evidence for a mineralized belt. Chem. Geol; 175: 259-271.

Chang, L.L.Y.; Howie, R.A. and Zussman, J. (1996): Rock-forming minerals. Non-silicates. vol 5B. Longman, London.

Cherian, A.; Chandrasekar, N. and Rajamanickam, V. (2004): Light minerals of beach sediments from Southern Tamilnadu, south east coast of India. Oceanologia; 46 (2): 233–252.

Condie, K.C. (2005): High field strength element ratios in Archean basalts: a window to evolving sources of mantle plumes. Lithos; 79: 491-504.

Condie, K.C.; Boryta, M.D.; Liu, J. and Quian, X., (1992): The origin of khondalites: geochemical evidence from the Archean to Early Proterozoic granulitic belt in the North China Craton: Precambrian Research; 59(3-4), 207-223.

Cox, R.; Low, D.R. and Cullers, R.L. (1995): The influence of sediment recycling and basement composition on evolution of mudrock chemistry in the southwestern United States. Geochimica et CosmochimicaActa; 59: 2919–2940.

Curtis, R.; Evans, G.; Kinsman, D. J. J. and Shearman, D.J. (1963): Association of dolomite and anhydrite in the Recent sediment of the Persian Gulf. Nature; 197: 669-680.

Deer, W.A.; Howie, R.A. and Zussman, J. (1997): Rock-Forming Minerals. 1A. Orthosilicates (2nd ed.). The Geological Society, London, U.K. (418-442).

De Meijer, R.J.; James, I.R.; Jennings, P.J. and Koeyers, J.E. (2001): Cluster analysis of radionuclide concentrations in beach sand. Applied Radiation and Isotopes; 54(3): 535-542.

Denison, R.E.; Kirkland, D.W. and Evans, R. (1998): Using Strontium Isotopes to Determine the Age and Origin of Gypsum and Anhydrite Beds. Geology; 106(1): 1-18.

Dunham, R.J. (1962): Classification of Carbonate Rocks According to Depositional Texture. In, W.E. Hamm (Ed.), Classification of Carbonate Rocks. American Association of Petroleum Geologists, p. 108-121.

Dupre, B.; Gaillardet, J.; Rousseau, D. and Allegre, C.J. (1996): Major and trace element of river-born material: the Congo basin. Geochim. Cosmochim. Acta; 60: 1301–1321.

Eastman, J. (2001): Guide to GIS and image processing. Clark University, USA.

El-Tantawi, A.M.M. (2005): Climate change in Libya and desertification of Jifarah Plain using geographical information system and remote sensing techniques. PHD. Thesis. Der Johannes Gutenberg University, Mainz, Germany.

El-Fiky, A.A. (2010): Hydrogeochemical characteristics and evolution of groundwater at the Ras Sudr-Abu Zenima area, Southwest Sinai, Egypt. Journal of King Abdul Aziz University, Earth Sciences; 21(1): 79-109.

El Hinnawy, M. and Cheshitev G. (1975): Geological Map of Libya; 1:250 000 Sheet: Tarabulus NI 33-13. Explanatory Booklet. Ind. Res. Cent.,Tripoli, 65p.

El Hinnawy, M. and Chesthitev, G. (1975): Geologic map of Libya, 1:250000 sheet Al Khums NI 33-14. Explanatory Booklet. Ind. Res. Cent.,Tripoli, 65p.

El-Kammar, A.M.; Arafa, I.H. and El-Sheltami, O.R. (2007): Mineral composition and environmental geochemistry of the beach sediments along the eastern side of the Gulf of Suez, Egypt. Journal of African Earth Sciences; 49: 103–114.

El-Omla, M.M. and Aboulela, H.A. (2012): Environmental and mineralogical studies of the sabkhas soil at Ismailia-Suez Roadbed, Southern of Suez Canal District, Egypt. Open Journal of Geology; 2: 165-181.

Faure, G. (1992): Principles and Applications of Inorganic Geochemistry. Macmillan Pub. Co., New York, 626p.

Folk, R. L. (1978): Petrology of Sedimentary Rocks: Austin Texas, Hemphil Public. 182p.

Folk, R.L. (1980): Petrology of sedimentary rocks. Univ. of Texas, Hemiplli's, Austin, Texas, 170p.

Force, E.R. (1980): The Provenance of Rutile. Sedimentary Petrology; 50(2): 485-488.

Frihy, O.E. and Komar, P.D. (1993): Long-term shoreline changes and the concentration of heavy minerals in beach sands of the Nile Delta, Egypt. Mar. Geol; 115: 253-261.

Froelich, P.N.; Bender, M.L; Luedtke, N.A.; Heath, G.R. and Devries, T. (1982): The marine phosphorus cycle. Am. J. Sci.; 282: 474-511.

Fuchtbauer, H. and Muller, G. (1970): Sediments and sedimentgestin. Springer Verlag, Stuttgart, 726 pp.

Gaillardet, J.; Dupre, B. and Allegre, C.J. (1999): Global silicate weathering and CO_2 consumption rates deduced from the chemistry of large rivers. Chem. Geol.; 159: 3–30.

Gandhi, M.S. and Raja, M. (2014): Heavy mineral distribution and geochemical studies of coastal sediments between Besant Nagar and Marakkanam, Tamil Nadu, India.Journal of Radiation Research and Applied Sciences; 7: 256-268.

Garcia, D.; Fonteilles, M. and Moutte, J. (1994): Sedimentary fractionations between Al, Ti, and Zr and the genesis of strongly peraluminous granites. J. Geol.; 102: 411–422.

Garzanti, E.; Vermeesch, P.; Ando,S.; Lustrino, M.; Padoan, M. and Vezzoli, G. (2014): Ultra-long distance littoral transport of Orange sand and provenance of the Skeleton Coast Erg (Namibia). Marine Geology; 357: 25-36.

Gavish, E. (1974): Geochemistry and mineralogy of a Recent sabkha along the coast of Sinia, Gulf of Suez. Sedimentology; 21: 397-414.

Gholami, S. and Srikantaswamy, S. (2009): Analysis of agricultural impact on the Cauvery River water around KRS Dam. World Applied Sciences Journal; 6 (8): 1157-1169.

Ghoneim, E. Benedetti, M. M. and El-Baz, F. (2012): An integrated remote sensing and GIS analysis of the Kufrah Paleoriver, Eastern Sahara, Libya. Geomorphology; 139: 242 – 257.

Greegor, R.B.; Pingitore, N.J. and Lytle, F. (1997): Strontianite in coral skeletal aragonite. Science; 275: 1452–1454.

Hallberg, R.O. (1976): A geochemical method for investigation of palaeoredox conditions in sediments: Ambio, Special Report; 4: 139-147.

Hallett, D. (2002): Petroleum Geology of Libya, first edition, Elsevier, Amsterdam.

Han, G.; Tang, Y.; Wu, Q. and Tan, Q. (2010): Chemical and strontium isotope characterization of rainwater in karst virgin forest, Southwest China. Atmospheric Environment; 44: 174–181.

Hammuda, O. S. (2000): Mesozoic and Cenozoic history of the Jifarah Arch, NE Libya and SE Tunisia. The geology of north west Libya .Volume 1. Second Symposium on the Sedimentary Basins of Libya, held in Tripoli; pp. 41, 42, 44.

Hem, J.M. (1989): Study and interpretation of the chemical characteristics of natural water, 3rd ed. US Geological Survey, Water Supply Paper 2254, USGS Washington DC.

Holser, W.T. (1966): Bromine geochemistry of salt rocks. In: Second Symposium on Salt (Ed. by J.L. Rau); 1: 248-275. Northern Ohio Geol. Soc., Cleveland, Ohio.

Hunt, T.S. (1981): Potassium Salts in Sea-Water. Nature; 43: 463-464.

Hounslow, A.W. (1995): Water quality data: analysis and interpretation, Lewis Pub., New York, 397p. IFS (Irrigation Fact Sheet), 1995. Using irrigation for tree fruit cooling, Agdex: 753, British Columbia, Minestry of Agriculture and Food, 7p.

Jones, B. and Manning, D.C. (1994): Comparison of geochemical indices used for the interpretation of paleo-redox conditions in Ancient mudstones: Chemical Geology; 111(1-4): 111-129.

Jones, B.F.; Naftz, D.L.; Spencer, R.J. and Oviatt, C.G. (2009): Geochemical evolution of Great Salt Lake, Utah, USA. Aquat Geochem; 15: 95-121.

Kasper-Zubillaga, J. J. (2009): Roundness in quartz grains from inland and coastal dune sands, Altar Desert, Sonora, Mexico. Boletin de la Sociedad GeoloGica Mexicana; 61(1): 1-12.

Kasper-Zubillaga, J. J. Dickinson, W. W. Carranza-Edwards, A. and Hornelas-Orozco, Y. (2005): Petrography of quartz grains in beach and dune sands of

Northland, North Island, New Zealand: Journal of Geology and Geophysics; 48: 649-660.

Katongo, C.; Koeberl, C.; Witzke, B.J.; Hammond, R.H. and Anderson, R.R. (2004): Geochemistry and shock petrography of the Crow Creek Member, South Dakota, USA: Ejecta from the 74-Ma Manson impact structure. Meteoritics and Planetary Science; 39(1): 31–51.

Kendall, A. C. (1979): Continental and supratidal (sabkha) evaporites. Subaqueous evaporites. In: Facies Models Geoscience Canada (Ed. By R.G. Walker), pp. 145-174.

Kitano, Y. and Furutsu, T. (1959): The state of magnesium contained in calcareous shells. Bull. Chem. Soc. Japan; 33: 1-4.

Kloss, W.S and Roy, P.D. (2010): Evaporite mineralogy and major element geochemistry as tools for palaeoclimatic investigations in arid regions: A synthesis. Boletin De La Sociedad Geologica Mexicana; 62: 370-390.

Leri, A.; Hakala, J.; Marcus, M.; Lanzirotti, A.; Reddy, C. and Myneni, S. (2010): Natural organobromine in marine sediments: New evidence of biogeochemical Br cycling. Global Biogeochemical Cycles; 24, GB4017.

Leri, A. and Myneni, S. (2012): Natural organobromine in terrestrial ecosystems. Geochimica et Cosmochimica Acta; 77: 1-10.

Lopez, J.M.G.; Bauluz, B.; Fernández-Nieto, C. and Oliete, A.Y. (2005): Factors controlling the trace-element distribution in fine-grained rocks: the Albian kaolinite-rich deposits of the Oliete Basin (NE Spain). Chemical Geology; 214 (1-2, 3): 1-19.

Lorenz. W. and Gwosdz, W. (2003): Manual on the geological-technical assessment of mineral construction materials. SH 15, Hanover, 498 p.

Madhavaraju, J. and Ramasamy, S. (1999): Rare earth elements in limestones of Kallankurichchi Formation of Ariyalur Group, Tiruchirapalli Cretaceous, Tamil Nadu: Journal of the Geological Society of India; 54: 291-301.

Malick, B.M.L. and Ishiga, H. (2015): Geochemical maturity of pocket beach sands from the Sanin region of southwest Japan. Earth Science Research; 4(2): 45-61.

Mange, M.A. and Maurer, H.F.W. (1992): Heavy Minerals in Colour. Chapman and Hall, London, 147 p.

Margineanu, R.M.; Blebea-Apostu, A.M.; Celarel, A.; Gomoiu, C.M.; Costea, C.; Dumitras, D.; Ion, A. and Duliu, O.G. (2014): Radiometric, SEM and XRD investigation of the Chituc black sands, southern Danube Delta, Romania. Journal of Environmental Radioactivity; 138: 72–79.

McLennan, S.M.; Hemming, S.; McDaniel, D.K. and Hanson, G.N. (1993): Geochemical approaches to sedimentation, provenance, and tectonics, in Johnson, M.J., Basu, A. (eds.), Processes Controlling the Composition of Clastic Sediments: Geological Society of America, Special Paper; 284: 21-40.

Mohamed, F.N. (2013): Fuzzy-GIS Development of Land Evaluation System for Agricultural Production in North West Libya. PHD. Thesis. Heriot-Watt University, Scotland.

Morton, A.C. (1984): Stability of Detrital Heavy Minerals in Tertiary Sandstones from the North-Sea Basin. Clay Minerals; 19(3): 287-308.

Morton, A.C. and Hallsworth, C.R. (1994): Identifying provenance-specific features of detrital heavy mineral assemblages in sandstones. Sedimentary Geology; 90: 241-256.

Morton, A.C. and Hallsworth, C.R. (1999): Processes controlling the composition of heavy mineral assemblages in sandstones. Sediment Geology; 124: 3–29.

Nagarajan, R.; Madhavaraju, J.; Nagendra, R.; Armstrong-Altrin, J.S. and Moutte, J. (2007): Geochemistry of Neoproterozoic shales of the Rabanpalli Formation, Bhima Basin, Northern Karnataka, southern India: implications for provenance and paleoredox conditions. Revista Mexicana de Ciencias Geológicas; 24 (2): 150-160.

Nath, B.N.; Bau, M.; Ramlingeswara-Rao, B. and Rao, C.M., (1997): Trace and rare earth elemental variation in Arabian Sea sediments through a transect across the oxygen minimum zone. Geochimica et CosmochimicaActa; 61: 2375-2388.

Negrel, P. and Roy, S. (1998): Chemistry of rainwater in the Massif Central (France): a strontium isotope and major element study. Applied Geochemistry; 13: 941–952.

Nesrine, N; Rachida, B and Ahmed, R. (2015): Multivariate Statistical Analysis of Saline Water: A Case Study: Sabkha Oum LeKhialate (Tunisia). International Journal of Environmental Science and Development; 69(1): 40-43.

Nilgun, O. and Betel, E. (2005): Source of the basinal sediments in the Marmara Sea investigated using heavy minerals in the modern beach sands. Marine geology; 216(1-2): 1-15.

Nwer, B.; Zurqani, H. and Rhoma, E, (2013): The Use of Remote Sensing and Geographic Information System for Soil Salinity Monitoring in Libya. Journal of Global Science and Technology Forum (GSTF).

Overstreet, W.C. (1967): The geological occurrence of monazite. US Geol Surv Prof Paper; 530:1–327.

Ozdemir, O. and Dunlop, D.J. (2000): Intermediate magnetite formation during dehydration of goethite. Earth and Planetary Science Letters; 177: 59-67.

Paine, M. (2005): Sedimentology of the Bondi Main heavy mineral beach placer deposit, Murray Basin, southeastern Australia. Sedimentary Geology; 174: 117–195.

Papadopoulos, A.; Christofides, G.; Pe-Piper, G.; Koroneos, A. and Papadopoulou, L. (2015): Geochemistry of beach sands from Sithonia Peninsula (Chalkidiki, Northern Greece). Mineralogy and Petrology; 109: 53-66.

Parkman, R.H.; Charnock, J.M. and Livens, F.R. (1998): A study of the interaction of strontium ions in aqueous solution with the surfaces of calcite and kaolinite. Geochim Cosmochim Acta; 62(9): 1481-1492.

Parra, J.G.; Marsaglia, K.M.; Rivera, K.S.; Dawson, S.T. and Walsh, J.P. (2012): Provenance of sand on the Poverty Bay shelf, the link between source and sink sectors of the Waipaoa River sedimentary system. Sedimentary Geology; 280: 208-233.

Pavicic, L.; Babic, L.; Crnjakovic, M. and Zupanic, J. (2000): The provenance of sands on North Dalmatian beaches: Between ignorance and the need for coastal zone management. Periodicum Biologorum; 102: 349-354.

Peryt, T.M. and Anczkiewicz, R. (2015): Strontium isotope composition of Middle Miocene primary gypsum (Badenian of the Polish Carpathian Foredeep Basin): evidence for continual non-marine inflow of radiogenic strontium into evaporite basin. Terra Nova; 27: 54–61.

Peterson, C.D.; Komar, P.D. and Schneidegger, K.F. (1986): Distribution, geometry and origin of heavy mineral placer deposits on Oregon beaches. Journal of Sedimentary Petrology; 56: 67-77.

Pilkey, O.H. (1963): Heavy minerals of the U.S. South Atlantic shelf and slope. Geol. Soc. Am. Bull; 74:641-648.

Polozek, K. (2000): Distribution of heavy minerals in CRP-2/2A, Victoria Land Basin, Antarctica. Terra Antartica; 7(4): 567-573.

Polozek, K. and Ehrmann, W. (1998): Distribution of heavy minerals in CRP- 1. Terra Antartica; 5(3): 633-638.

Prost, G. (2014): Remote sensing for geoscientists, third edition, CRC Press, USA.

Rahman, M.A.; Alam, M.S. and Shine, F.M.M. (2004): Roundness and Sphericity of Calstic Sediments of Apical Part of the Tista Fan in Panchagarh District, Bangladesh. Rajshahi University Studies, Part-B.

Rasmussen, B. and Muhling, J.R. (2007): Monazite begets monazite: evidence for dissolution of detrital monazite and reprecipitation of syntectonic monazite during low-grade regional metamorphism. Contrib Mineral Petrol; 154:675–689.

Reeder, R.J. (1996): Interaction of divalent cobalt, zinc, cadmium, and barium with the calcite surface during layer growth. Geochim. Cosmochim. Acta; 60: 1543–1552.

Rosell, L.; Orti, F.; Kasprzyk, A.; Playa, E. and Peryt, T.M. (1998): Strontium geochemistry of Miocene primary gypsum: Messinian of SE Spain and Sicily and Badenian of Poland. Sedimentray Research; 68(1): 63–79.

Saadi, N. M.; Aboud, E. and Watanabe, K. (2013): Integration of DEM, ETM+, geologic, and magnetic data for geological investigations in the Jifarah Plain, Libya. Geoscience and Remote Sensing, IEEE Transactions; 47 (10): 3389-3398.

Sagga, A. M. S. (1993): Roundness of sand grains of longitudinal dunes in Saudi Arabia: Sedimentary Geology; 87: 63-68.

Selley, R. C. (2000): Applied sedimentology, second edition, Academic Press, USA.

Shaheen, S.E.M. (2006): Mineralogy and sedimentology studies on Recent coastal sabkha, northwestern Mediterranean Coast, Egypt. Sedimentology of Egypt; 14: 65-82.

Shahwan, T.; Atesin, A.C.; Erten, H.N. and Zararsiz, A. (2002): Uptake of Ba^{2+} ions by natural bentonite and $CaCO_3$: A radiotracer, EDXRF and PXRD study. Journal of Radioanalytical and Nuclear Chemistry; 254: 563–568.

Shaltami, O.R. (2012): Mineral composition and environmental geochemistry of the beach sediments along the Mediterranean Coast from Benghazi to Bin Jawwad, Northeast Libya. PH.D. Thesis. Cairo Univ. Cairo, Egypt.

Shaltami, O.R. (2014): Major ion and rare earth element concentrations in rainwaters from Ajdabiya, Benghazi and Al Marj, NE Libya: Natural and anthropogenic sources. Scientific Benghazi University Journal; 1: 41-56.

Shaltami, O.R. (2015): Geochemistry of the Shahat Marl Member, Wadi Az Zad, Al Jabal Al Akhdar, NE Libya. Arabian Journal of Earth Sciences; 2(3): 23-39.

Shearman, D. J. (1970): Recent halite rock, Baja California, Mexico. Trans. Inst. Min. Metall; 79(B): 155-162.

Shine, F. M. M. (2006): Shape Analysis of Detrital Quartz Grains and its Environment of Deposition in Holocene Sediments along the Karotoya River, Bogra, Bangladesh. Journal of Geo-Environment; 6: 54-63.

Stivaletta, N; Barbieri, R; Picard, C and Bosco, M. (2009): Astrobiological significance of the sabkha life and environments of southern Tunisia. Planetary and Space Science; 57: 597–605.

Suzumural, M. and Kamatani, A. (1995): Origin and distribution of inositol hexaphosphate in estuarine and coastal sediments. Limnol. Oceanogr; 40(7): 1254-1261.

Terakado, Y. and Taniguchi, M. (2006): Method for the study of trace element partitioning between calcium carbonate and aqueous solution: A test case for Sr and Ba incorporation into calcite. Geochem. J.; 40: 161–170.

Tucker, M.E. (2001): Sedimentary petrology: an introduction to the origin of sedimentary rocks. Oxford: Blackwell.

Tunusoglu, O.; Shahwan, T. and Eroglu, A.E. (2007): Retention of aqueous Ba^{2+} ions by calcite and aragonite over a wide range of concentrations: Characterization of the uptake capacity, and kinetics of sorption and precipitate formation. Geochemical Journal; 41: 379-389.

Veizer, J. (1983): Trace elements and isotopes in sedimentary carbonates, in Reeder, R.J. (ed.), Carbonates: Mineralogy and Chemistry: U.S.A, Mineralogical Society of America, Reviews of Mineralogy; 11: 265-299.

Warren, J. K. (1989): Evaporite Sedimentology, Prentice Hall, New York, 285 p.

Warren, J. K. (2006): Evaporites: Sediments, Resources and Hydrocarbons. Berlin, Springer, 1036 p.

Weibel, R. (1998): Diagenesis in oxidising and locally reducing conditions-an example from the Triassic Skagerrak Formation, Denmark. Sedimentary Geology; 121: 259–276.

Weibel, R. and Friis, H. (2004): Opaque minerals as keys for distinguishing oxidising and reducing diagenetic conditions in the Lower Triassic Bunter Sandstone, North German Basin. Sedimentary Geology; 169: 129-149.

Weyer, S.; Munker, C.; Rehkomper, M.; and Mezger, K. (2002): Determination of ultra-low Nb, Ta, Zr and Hf concentrations and the chondritic Zr/Hf and Nb/Ta ratios by isotope dilution analyses with multiple collector ICP-MS,Chem, Geol.; 187(3-4): 295-313.

White, W. M. (2001): Geochemistry: An on-line textbook. John-Hopkins University Press, 700 p.

Yang, S.; Jung, H.S. and Li, C. (2003): Two unique weathering regimes in the Changjiang and Huanghe drainage basins: geochemical evidence from river sediments. Sedimentary Geology; 164(1-2): 1-178.

Zankl, H. (1993): The origin of High-Mg-Calcite microbialites in cryptic habitats of Caribbean coral reefs—Their dependence on light and turbulence. Facies; 29: 55-59.

Zhang, K.J. (2004): Secular geochemical variations of the Lower Cretaceous siliciclastic rocks from central Tibet (China) indicate a tectonic transition from continental collision to back-arc rifting. Earth and Planetary Science Letters; 229: 73-89.